Applying microdroplets as label-free sensors for reactions inside the droplets

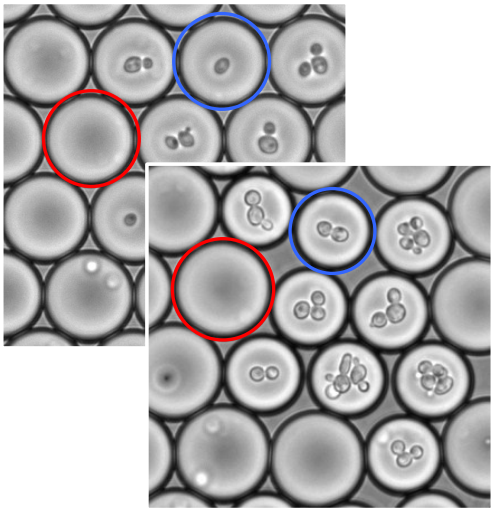

Tobias Wolfgang Hofmann

Heidelberg, December 10, 2012

Dissertation

SUBMITTED TO THE

Combined Faculties of the Natural Sciences
and Mathematics
of the Ruperto-Carola-University of Heidelberg, Germany

FOR THE DEGREE OF

Doctor of Natural Sciences

PUT FORWARD BY
Dipl.-Phys. Tobias Hofmann
born in Berkeley, California, USA

Oral examination: February 8, 2012

Applying microdroplets as label-free sensors for reactions inside the droplets

Referees: **Prof. Dr. Joachim P. Spatz**
Prof. Dr. Rainer H. A. Fink

Abstract Droplet-based microfluidics offers tremendous capabilities for high-throughput-screening systems, but so far, the dearth of appropriate analytical assays has limited its widespread application.

Here, we present a novel, label-free sensor method for the detection of biochemical reactions inside of micron-sized droplets. The method exploits the osmotically driven change in droplet size as a quantitative marker of the total osmolarity. Changes in osmolarity, which originate, for example, from the metabolic activity of cells, can be detected down to a few mOsm/l.

We characterize the sensor system by investigating mixtures of two types of monodisperse aqueous droplets in oil, containing various, fixed amounts of solute. Differing concentrations of solute induce water flow between the droplets through the oil, compensating for the osmotic pressure until equilibrium is reached. The flux is mediated by the diffusion of reverse micelles and increases with increasing differences in solute concentration.

We apply the method to monitor and quantify the metabolic activity of encapsulated yeast at the single cell level and demonstrate its use for live/dead assays.

Due to its simple and broadly applicable principle, our novel sensor method provides a powerful analytical tool for screening applications, and advances the evolution of high-throughput-screening systems with droplet-microfluidics.

Kurzfassung Die tropfenbasierte Mikrofluidik bietet einzigartige Möglichkeiten für die Durchführung von Hochdurchsatz-Analyseverfahren. Bisher wird ihre weitreichende Anwendung allerdings vom Mangel an geeigneten Verfahren zur Analyse der Tropfeninhalte verhindert.

In dieser Arbeit stellen wir eine neue, markerfreie Methode zur Detektion biochemischer Reaktionen innerhalb von Mikrotropfen vor. Diese nutzt die Größenänderung von Tropfen durch Osmose als Maß für die Gesamtosmolarität eines Tropfens und erlaubt die Detektion von Änderungen der Gesamtosmolarität um wenige mOsm/l. Derartige Änderungen werden beispielsweise durch den Stoffwechsel von Zellen hervorgerufen.

Wir charakterisieren die Größenänderungen mit Hilfe einer Mischung zweier monodisperser Tropfenarten, die jeweils eine konstante Stoffmenge an Sucrose enthalten. Unterscheiden sich die Sucrose-Konzentrationen der Tropfen, wird der damit einhergehende osmotische Druck durch Wassertransport zwischen den Tropfen ausgeglichen. Der Wassertransport wird durch die Diffusion reverser Mizellen vermittelt und steigt mit steigendem Konzentrationsunterschied der Tropfen.

Schließlich verwenden wir die Methode, um den Stoffwechsel einzelner Hefezellen in Tropfen zu beobachten und zu quantifizieren. Insbesondere können Tropfen die lebende Zellen enthalten anhand ihrer Größenabnahme zuverlässig von anderen Tropfen getrennt werden.

Durch ihr einfaches und allgemeines Prinzip deckt unsere Sensormethode einen großen Anwendungsbereich ab und erweitert insbesondere die Anwendbarkeit von tropfenbasierter Mikrofluidik in Hochdurchsatzanalyseverfahren.

Contents

Preface

Progress in modern life sciences as well as in pharmaceutical science is more and more driven by the analysis of large amounts of experimental data. In biomedicine, blood samples of cancer patients containing billions of cells are screened for few tumor cells and biomarkers [1, 2], which permit detection, diagnosis and monitoring of cancer. Biologists investigate the heterogeneity of cell populations[3] and analyze the whole genome of organisms[4]. In search for bioactive substances for development of new drugs, pharmaceutical companies measure the dose-response curves of thousands of compounds[5].

Hence, there is an increased demand for HTS (high-throughput screening) methods, which allow for fully automated execution of more than 100.000 experiments a day[6]. Miniaturization and parallelization of systems and reactions of interest are key to cost-efficient and rapid HTS.

Consequently, microfluidics, the science and technology of handling small amounts of fluids, takes a leading role in HTS technology, offering a multitude of advantages. In particular, droplet-based microfluidics provides unique capabilities for the simultaneous conduction of millions of independent experiments as well as their rapid analysis[7]. Two immiscible fluids are used to generate monodisperse droplets[1] of micrometer dimensions (1 - 100 µm), commonly aqueous droplets dispersed in oil. Those compartments serve as biocompatible, spatially isolated microreactors, comprising very small amounts of compounds down to single cells or molecules in picoliter-sized volumes. Due to generation rates of several kHz, a multitude of experiments can be conducted simultaneously (about 10^8 experiments a day[8]) with minimal expense of reagents, and therefore, costs. Finally, a broad range of techniques for the manipulation of droplets allows for quantitative and rapid analysis of droplet contents, rendering droplet microfluidics ideal for high throughput assays.

HTS has already profited considerably from new droplet-based platforms. For example, Agresti et al. [8] performed directed evolution of enzymes, a process in which the yield of an enzyme is optimized, with a thousand-fold increase in speed and a 1-million-fold reduction in cost compared to existing methods (state-of-the-art robot screening). Another example is the high resolution dose-response screening published by Miller

[1] monodisperse = of equal size

et al. [9] which allows for the measurement of 10,000 instead of about 10 data-points per dose-response curve, simultaneously using less quantities of reagents compared to existing methods.

However, a huge hurdle towards widespread application of droplet microfluidics is the limited availability of assays for analyzing the droplets' contents and the subsequent processing. Most existing methods rely on markers, commonly fluorescent ones, whose specific Moreover, markers usually have to be added to the dispersed phase prior to encapsulation, since the washing steps involved in more complex assays are difficult to adapt to droplet microfluidics. Therefore, additional, ideally label-free methods for analyzing the droplets contents are needed.

In this thesis, a novel, label-free sensor method is presented, which facilitates simple analysis by coupling the biochemistry inside a droplet to a (easily measurable) physical property of the droplet. More specifically, the operating principle is based on the osmotically driven size change of droplets differing in their composition.

Hence, the reader will be introduced to the research topic by two chapters: one comprising a brief overview of droplet microfluidics (chapter 1), and one giving a detailed introduction to mass transfer in microdroplet systems, focusing on osmosis (chapter 2). Subsequent to description of materials and methods used (chapters 3 and 4), the operating principle and theory of the sensor method is presented (chapter 5). Parts of the results were already published in Hofmann et al. [10] and are presented more elaborately within this thesis. An experimental characterization of the sensor system, including the verification of osmosis being the driving force, is provided in chapter 6. Finally, the application of the sensor method to detect cellular activity is demonstrated (chapter 7), and a conclusive discussion as well as an outlook on future research are provided (chapter 8 and 9).

Part I

Introduction

1 Droplet microfluidics

Little more than one decade ago, droplet microfluidics emerged from the interdisciplinary research field of microfluidics[11], the science and technology of manipulating small amounts of liquids using micron-sized geometries, and has rapidly grown since. Droplet based microfluidics, or in short, droplet microfluidics, deals with immiscible two-phase systems comprising droplets (or bubbles) with dimensions ranging from a few to hundreds of micrometers in diameter (Figure 1.1). Simple microfluidic devices

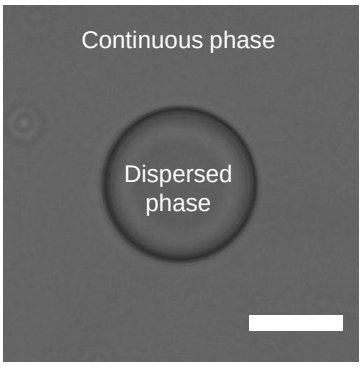

Figure 1.1: *Aqueous droplet (dispersed phase) in oil (continuous phase) measuring 50 µm in diameter. Scale is 30 µm.*

are used to generate very well-defined microdroplet emulsions, which offer several attractive properties for miniaturized assays in diverse research fields: Monodisperse aqueous droplets dispersed in oil can be easily produced at very high rates (up to several kHz), forming thousands of identical, isolated microreactors[12]. This allows for a high degree of parallization of experiments and makes microdroplet systems perfectly suited for quantitative and statistical analysis. Simultaneously, the picoliter volumes of the droplets greatly reduce the amount of reagents needed, minimizing the costs. Since the droplets' interfaces can be rendered biocompatible, droplets containing very small amounts of cells or molecules are particularly useful for biological assays[13].

These advantages have stimulated a multitude of applications in various disciplines of academic and industrial research, ranging from bioreactors comprising living cells to diagnostic or analytical high-throughput systems and the synthesis of advanced materials[14, 15, 16]. In this thesis, a sensor method is presented which allows for the detection of biochemical reactions in droplets.

For the abundance of reviews on droplet microfluidics, only a brief overview over the fundamentals of droplet microfluidics will be given in this chapter, addressing materials of microfluidic devices, as well as the generation, stability, and manipulation of droplets in separate sections. In a final section, existing methods for the detection of droplet contents will be presented. More detailed discussions can be found in the cited literature, including the selected reviews given in References [17],[18], and [19] which provide a broad overview of microfluidics.

1.1 Materials for droplet microfluidics

Although several materials including glass[20, 21], silicon[22] and Teflon[23] have been successfully used to fabricate microfluidic devices, an abundant amount of applications relies on PDMS (Polydimethylsiloxane) as basic material, a transparent polymer (Figure 1.2 A). PDMS offers great advantages for microfluidic device fabrication, as diverse channel geometries are rapidly fabricated by a simple lithographic process, so-called soft-lithography. This method uses a photosensitive resist to form a master mold, from which microstructured PDMS blocks (Figure 1.2 B) are replicated and tightly sealed to glass or other PDMS pieces by oxygen plasma treatment. For fabrication of the replica, a mixture of the monomer and a crosslinker is casted onto the master mold. After curing, the microstructured PDMS block is detached. Since PDMS is a soft material (with a Young's modulus of about 750 kPa[24]), it is effortless to handle, and can e.g. be cut to fit or punched through, forming connections for tubings. The soft nature also allows for an easy implementation of valves[24]. Combined with low fabrication costs, the easy manufacturing allows for rapid prototyping of all kinds of devices.

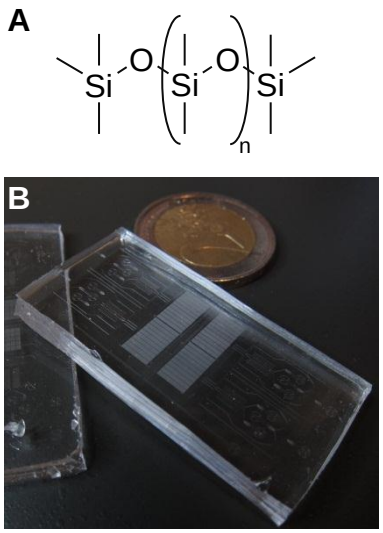

Figure 1.2: *(A) Chemical structure of PDMS. (B) Photograph of a microstructured PDMS block.*

PDMS offers numerous further advantages for microfluidic devices. It is nontoxic and inherently hydrophobic but can be easily rendered hydrophilic[25, 26]. Thus, generation of water-in-oil droplets as well as oil-in-water droplets is possible. Furthermore, PDMS is highly gas permeable, which is very useful for culturing cells and sustaining microorganisms inside of microchannels[27]. Some liquids like water or ethanol, and other small molecules penetrate PDMS as well[28], which can be exploited for the formation of membranes. However, in many cases concerning droplet microfluidics, this perme-

ability also bears disadvantages, as PDMS leads to high dissolution rate of droplets[29]. Consequently, PDMS geometries are *per se* not well-suited for long-term storage and incubation of droplets. This issue can in some cases be addressed by saturating the PDMS with water, rendering droplet sizes stable for several days[30].

Another serious drawback is the massive swelling of PDMS in most organic solvents, which makes them ill-suited for PDMS devices[29]. Other materials with a higher solvent resistance, like glass, however, suffer from an expensive and time-consuming device fabrication process[21]. As a consequence, both liquids used for droplet generation are required to be compatible with PDMS, which severely restricts the range of liquids. Silicone oil, for example, has a very bad compatibility with PDMS[13]. For water-in-oil droplets, typically fluorocarbon or hydrocarbon oils are used as continuous phase. However, the range of applications of hydrocarbon oils is limited due to the high solubility of hydrophobic molecules in these oils[13]. Contrariwise, most organic compounds are highly insoluble in fluorinated oils, since they are both, hydrophobic and lipophobic[31]. In addition, fluorinated oils are biocompatible and allow for gas exchange, rendering them well-suited for droplet-based microfluidics[32, 33, 34, 35].

1.2 Droplet generation devices

Monodisperse droplets are commonly generated by flowing two immiscible liquids through channel geometries of predefined dimensions. In these geometries, microdroplets are formed by breakup of the dispersed phase in a very well-defined way.

The most widely used geometries are T-junctions[11] (Figure 1.3 A) and various kinds of flow-focusing geometries[36] (Figure 1.3 B). A T-junction consists of two orthogonal channels, each comprising a flow of one liquid phase. At the intersection an interface forms and droplets of the dispersed phase are generated due to the shear force exerted by the continuous phase[37]. In a flow-focusing geometry, the dispersed phase flows

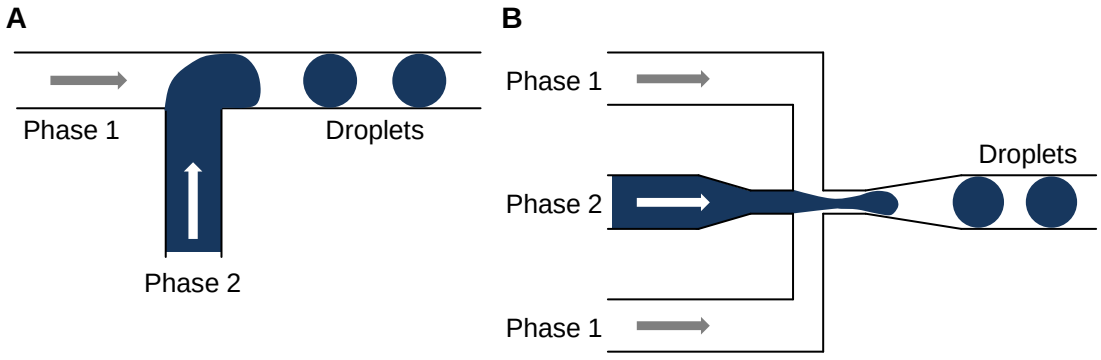

Figure 1.3: *Schemes of droplet generation by a T-junction (A) and a flow-focusing geometry (B). In both cases, droplets of the dispersed phase are sheared off by flows of the continuous phase.*

through an orifice and is subsequently sheared off from both sides by a co-flowing flow of the continuous phase. Since flow rates of each phase can be tuned separately, easy control over the generation rate as well as the size of the droplets is provided. Rates and sizes range from few hertz to more than 10 kHz, and from 1 µm to several hundreds of microns, respectively[8, 12]. Also, special channel geometries can be used to facilitate the deterministic encapsulation of single cells or beads in droplets[38, 39].

Other geometric methods for droplet generation are capillaries[40, 20] or step emulsification[41], in which droplets are formed at an abruptly expanding channel. Besides continuous droplet generation by flows of liquid phases, methods permitting on-demand production of single droplets exist, using for example laser pulses[42] or microvalves[43]. The stability of generated droplets can be considerably improved by addition of tensides, as will be described in the next section.

1.3 Stability and biocompatibility of microdroplets

In most cases, amphiphilic molecules, so-called surfactants are added to the continuous phase (Figure 1.4). The term surfactant, a contraction of SURFace ACTive AgeNT, was chosen since these molecules aggregate at the interface between the two phases and alter its properties, for instance decreasing the surface tension.

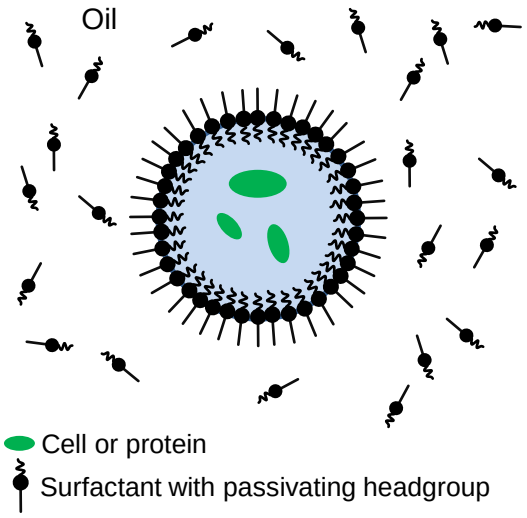

Figure 1.4: *Schematic view of an aqueous droplet in oil stabilized by surfactant. Surfactants dissolved in the continuous phase aggregate at the droplet interface and stabilize it. A passivating hydrophilic head group of the surfactant renders the inner side of the interface biocompatible.*

Surfactants are an essential part of droplet microfluidics for two reasons: First, they stabilize microdroplet emulsions against coalescence by providing an additional energy barrier, for example by steric repulsion. Even densely-packed emulsions can be stable

for weeks to months, depending on the types of continuous phase and surfactant used, increasing the lifetime of an emulsion by several orders of magnitude[13]. Moreover, surfactants can promote adhesion and bilayer formation between droplets without causing coalescence, generating model systems for probing membrane properties[44, 45]. As a consequence of the permeability of the membrane, chemical reactions in adjacent droplets can be coupled[44]. It is noteworthy that emulsions may be highly stable without the addition of any surfactants under certain circumstances. An example is the so-called "ouzo effect"[1], a phenomenon describing the formation of a highly stable oil-in-water emulsion upon addition of water to ouzo, which comprises the essential oil anise[46].

The second reason which makes surfactants indispensable for many microfluidic applications is the possibility to render the inner interface of droplets biocompatible, e.g. by adding PEG[2] groups to the hydrophilic head of the surfactant[47, 48] (Figure 1.4). This allows for the encapsulation of cells and molecules without affecting their viability or causing denaturation. Besides passivation, surfactants may be functionalized to provide binding sites for adherent cells[48].

1.4 Droplet manipulation

Besides the capability of generating monodisperse, stable droplets, the reliable manipulation of droplets, that is fusion, splitting, sorting, as well as mixing, is a crucial prerequisite for useful microfluidic applications. Since the advent of droplet microfluidics in the early 2000s, an abundance of methods for manipulation of droplets using channel geometries, tweezers, acoustics, electric and magnetic fields, temperature (among others) has been published[12, 17].

Droplets can be fused and split either passively, by flowing them through certain channel geometries[49], or actively, for instance by applying electric fields[50]. Electrocoalescence can also be used to directly dispense liquid and reagents into droplets passing through a channel[51].

Common methods for the active sorting of droplets by size or content are based on electric fields which are applied locally in a channel and allow for a dielectrophoretic manipulation of droplets[8, 52] (Figure 1.5 A). Furthermore, droplets can be easily sorted by size passively by means of certain channel geometries, exploiting flow profiles[53, 54] and hydrodynamic resistance[55]. For example, droplets can be separated by flowing them through pillar fields, a method called DLD (deterministic lateral displacement)[53, 54]. If spacing and diameter of the pillars are adjusted correctly, the

[1] also called spontaneous emulsification or louche effect
[2] Polyethylene glycol

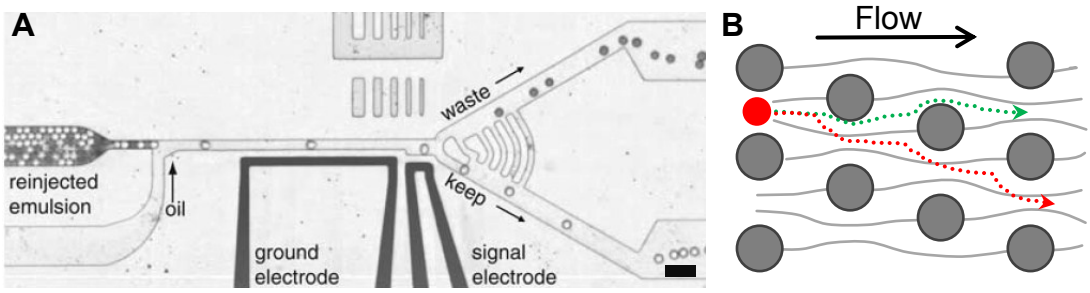

Figure 1.5: *(A) Separation of droplets by their content with the help of electrodes. Voltage is applied based on a fluorescent signal. Image adapted from Ref. [8]. Scale is 80 µm. (B) Separation of droplets by their size in a continuous flow by means of deterministic lateral displacement. The deflection of the droplet by the pillar field depends on its size. Image created on basis of Ref. [53].*

path of the droplets depends on their size, as they either follow the direction of the flow or the rows of pillars (Figure 1.5 B). Other methods include the use of magnetic fields, thermocapillary effect or surface acoustic waves[12]. Rapid mixing inside of a droplets can be performed by flowing droplets through meandering channel geometries, which induce a circulating flow pattern within the droplet due to friction with the channel wall[56]. Finally, the contents of microdroplets can be extracted from the emulsion and incorporated into a continuous stream, for example by methods based on electrocoalescence[57]. The continuous stream may be collected at an outlet of the microfluidic device and used for further experiments.

1.5 Analysis of the droplets

The analysis of the content of individual droplets (which prerequires its definite identification among other droplets) is one of the most essential functionalities for droplet-based assays. Therefore, considerable effort has been put into the development and automatization of detection processes.

Since most of the microfluidic devices are transparent, the majority of detection methods is based on optical measurements, either relying on microscopes equipped with cameras or photodiodes placed besides or beneath a channel[30, 8, 52]. Bright field microscopy can be used to track individual droplets and monitor contents like cells or beads, and allows for an automated analysis by image processing[30]. A more sophisticated approach which is widely-used in high-throughput systems is the addition of fluorescent markers to droplets. The fluorescence intensities of droplets passing through a channel trigger a dielectrophoretic sorting process, which allows for very high detection rates[8, 52] (Figure 1.5 A). However, the scope of applications is limited by the need and specificity of fluorescent labels. Another interesting method is the

use of droplets as optical microcavities, from whose resonances (so-called Whispering Gallery Modes) size and certain contents can be inferred[58].

Alternative detection techniques include electrical methods, e.g. based on the impedance signal of a droplet[59], or mass spectrometry of single droplets[60]. However, the integration of those techniques with microdroplets is challenging. Furthermore, contents of individual droplets can be extracted and subsequently separated by electrophoresis or analyzed by mass spectroscopy[61].

2 Mass transfer in microdroplet systems

Per definition, microdroplet emulsions and emulsions in general consist of two immiscible fluids, with the dispersed phase forming spatially isolated compartments, i.e. droplets. However, due to residual solubilities of molecules in the continuous phase and transport mechanisms involving surfactants, this isolation does not necessarily prevent the exchange of molecules between compartments or leakage into the continuous phase[62, 63]. Therefore, cross-contamination is generally not negligible for microdroplet systems and has to be quantified in every single case. The majority of microfluidic applications comprises droplets differing from each other in composition, e.g. in droplet libraries[64]. In almost all of them, it is crucial to prevent cross-contamination for proper functioning. However, some microfluidic applications, including the one presented in this thesis, rely on the transfer of compounds between droplets.

In this chapter, various processes mediating the transfer of solvent and solutes between droplets or the partitioning of compounds into the continuous phase will be discussed. Of paramount importance for this work is the transfer of solvent between droplets. Hence, a detailed discussion of the underlying mechanisms will be provided in the first section, focussing in particular on solvent transfer that results from differences in the droplet composition. In a second section, transfer of solutes between droplets will be covered.

The transfer of solutes and solvent by coalescence of droplets or breakdown of the emulsion is of no importance for this work and therefore won't be covered at all. A review on coalescence in emulsions can be found in Reference [65].

As only water-in-oil microdroplets were used in this work, the main focus of this chapter is placed on transport processes in emulsions consisting of oil as continuous phase and aqueous solutions as dispersed phase, which are also called inverse emulsions.

2.1 Solvent transfer in microdroplet systems

Two major mechanisms facilitating solvent transfer between droplets in an emulsion exist. One the one hand, heterogeneities of droplet compositions may give rise to a volume flux between the droplets. The driving force of the transfer is an osmotic pressure across the continuous phase, which serves as a liquid semipermeable membrane

between the droplets. Since osmosis in emulsions is an essential mechanism of the work presented in this thesis, first, a general introduction to osmosis will be given. Then, a critical review of the current state-of-the-art literature on osmosis in emulsions will be provided.

On the other hand, volume flux between droplets is caused by heterogeneities of droplet sizes, a process called Ostwald ripening[66, 67]. Ostwald ripening and other processes mediating only an efflux of solvent out of droplets are of minor importance for this work and will be summarized in a third subsection.

2.1.1 Introduction to osmosis

When two binary solutions differing solute concentration are divided by a semipermeable membrane, a membrane permeable to the solvent but not to the solute, a net flow of solvent from the dilute to the more concentrated side arises until equilibrium is reached (Figure 2.1). This phenomenon is called osmosis, an expression which originates from greek "o-smós", meaning to push or thrust. The equilibrium state is not necessarily reached when solute concentrations are similar[1], but usually due to the build-up of hydrostatic pressure (as in the case of the U-shaped tube shown in Figure 2.1). Osmosis plays a crucial role in biological systems and, in the form of reverse osmosis, has gained great impact on separating processes in chemistry, e.g. the desalination of water. Examples of the biological relevance of osmosis are the turgor pressure in cells and the water uptake by plant roots, which are both osmotically driven processes. Furthermore, many organisms living in an aqueous environment require some kind of osmoregulation to maintain the desired water content of their body. For example, saltwater fishes have to actively drink to compensate for osmotic water loss, as the salt concentration in water is higher than in their body, while freshwater fishes don't[68, 69].

No uniform definition of osmosis exists, as authors from various research fields use the term in different ways, or avoid a definition at all. For example, just a few take the existence of osmosis of gases into account[70]. However, osmotic pressure is well-defined as the pressure difference which has to be applied across a semipermeable membrane to establish equilibrium state with respect to the solute. In particular, osmotic pressure as experimentally determined is a pressure difference and not an absolute pressure, and consequently, an "osmotic pressure of a solution" does not exist[71], contrary to the frequent, inaccurate use in literature[72, 73, 74]. The total concentration of osmotically active solutes of a solution is referred to as osmolarity and can be measured, for instance, by measuring the osmotic pressure exerted in a membrane system (Pfeffer cell) or the freezing point depression. Unlike diffusion in a single-phase system, osmosis is a reversible process[75]. It is important to note that osmotic pressure is a colligative

[1] Especially in the case pure solvent *versus* a solution that's an impossibility.

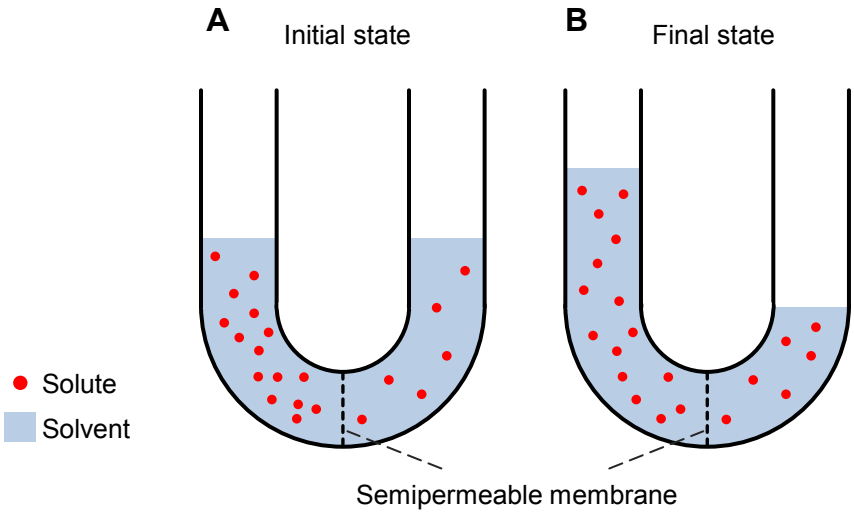

Figure 2.1: *In initial state (A), two binary solutions of different concentrations are separated by a semipermeable membrane. Subsequently, a net flow of water through the membrane arises until the osmotic pressure is compensated by the build-up of hydrostatic pressure (B).*

property of two phases, i.e. solutions, depending only on the ratio of solute to solvent molecules and not on the nature of the particles[2].

For dilute solutions the empirical van't Hoff equation holds, which van't Hoff proposed in 1887[75] based on the experiments of Pfeffer[76]:

$$\Pi = RT\Delta c \tag{2.1}$$

Here, R is the ideal gas constant, T the absolute Temperature and Δc the concentration difference of nonpermeable solutes across the membrane. Despite the analogy of van't Hoff's relation to the ideal gas law does not require the mechanisms to be similar, it was[75] and in popular science often still is incorrectly assumed that the underlying mechanism of osmosis was diffusion. In 1957, Mauro ended the debate by showing "that any pressure difference applied (across the membrane, osmotic as well as hydrostatic) gives rise to a transfer of water which is predominantly nondiffusional in nature"[77].

More than 120 years of research on osmosis have passed since van't Hoff proposed his relation, but despite osmosis being well understood thermodynamically by now, the molecular mechanisms causing osmosis remain unclear[78, 79, 80]. In 1991, Guell[81] listed more than a dozen proposals for kinetic models, which were only partially discarded (e.g. the "Solute bombardment theory"[71]), and partially still are subject to an ongoing discussion[78, 79, 80]. Two of the most prominent and controversially discussed ideas for kinetic model are those of negative pressure imparted by solutes ("negative

[2] In the limit of infinite dilution.

pressure model"[82]) and the decrease in water concentration upon addition of solutes inducing the osmotic flow[83, 84].

By contrast, various undisputed thermodynamic descriptions of osmosis have been given, which all originate from the entropy of mixing between solvent and solute. Van't Hoff's law can be derived e.g. by making use of Gibbs' concept of chemical potentials[3][71, 85]. According to Gibbs, the chemical potential of a substance in a mixture may be defined by $\mu = \mu_0 + RT\ln(a)$, where R is the gas constant, T the absolute temperature, a the activity and μ_0 a constant standard potential for any given temperature and pressure[71]. The activity $a = x\gamma$ is the product of the mole fraction x and the fraction coefficient γ, which equals unity in an ideal mixtures. As the molal fraction of the solvent decreases with increasing molal fraction of the solute, the activity of the solvent a_s, and therefore its chemical potential μ_s decreases as well, at least for an ideal mixture. Consequently, in a membrane system comprising two ideal binary solution of differing solute concentrations, a difference in chemical potential between the solutions prevails. In most cases, this is also true for dilute non-ideal solutions, as γ approximately constant at low solute concentrations. The difference in chemical potential corresponds to an osmotic pressure of $\Pi = -RT/V \ln a_s$ where V is the partial molal volume of the solvent, which can be simplified to the well-known van't Hoff relation[71]. Thus, a gradient in chemical potential is the driving force of osmotic flux, and equilibrium is reached when chemical potentials of solvents on both sides are equal[4]. As theoretically expected, Czihak and coworkers experimentally verified that the equilibrium is a dynamic equilibrium[86].

To take the dissociation (or association) of a compound in an ideal dilute solution into account, an additional factor is introduced to van't Hoffs law, the van't Hoff factor ν. The van't Hoff factor is defined as the number of ions produced per dissolved molecule. For instance, for sodium chloride $\nu = 2$, as it dissociates in sodium and chloride ions in solution. Most non-electrolytes exhibit a van't Hoff factor of unity.

However, in non-ideal solutions and concentrated ideal solutions, interactions between dissolved particles, e.g. ion pairing, affect the activity of solutes and solvent, leading to a deviation from the osmolarity of an ideal solution. This deviation is quantified by the osmotic coefficient Φ[87, 88], which allows for the calculation of the actual osmolarity of a (binary) solution $c_{\mathrm{Osm}} = \Phi\nu c$ with the solute concentration c.

Consequently, the osmotic pressure Π between two non-ideal binary solutions is

$$\Pi = \nu RT|\Phi_1 c_1 - \Phi_2 c_2| \ , \tag{2.2}$$

[3] A nice collection of derivations of van't Hoff's relation can be found in Reference [80].

[4] Since only the solvent may permeate through the membrane, only the chemical potential of the solvent is of importance.

where c_1 and c_2 are the molar concentrations of the solute and Φ_1 and Φ_2 the respective osmotic coefficients.

For water as solvent, Φ relates to the activity of water a_w by

$$\ln a_w = -\frac{\nu m}{55.51}\Phi \ , \tag{2.3}$$

where m is the molal concentration of the solute in water, and 55.51 represents the molal concentration of water.

The osmotic coefficient of aqueous solutions can be calculated theoretically, for example by the Pitzer equations[88].

Classical thermodynamic descriptions of osmosis are independent of the kind of particle interactions as well as the nature and geometry of the membrane (as long as it's semipermeable), and only describe the equilibrium state. Thus, the dynamics of the system, the intermediate states, are not accessible. Using irreversible thermodynamics, Kedem and Katchalsky[89] described passive transport in a membrane system driven by hydrostatic pressure differences (Δp) or osmotic pressure ($RT\Delta c$) in case of a binary solution. The derived equations of volume (solvent) flux J_v and solute flux j_s are known as the Kedem-Katchalsky equations and predict the coupling between solute and solvent fluxes for a membrane partially permeable to the solute:

$$J_v = L_p(\Delta p - \sigma RT\Delta c) \tag{2.4}$$

$$j_s = \omega RT\Delta c + (1-\sigma)\bar{c}J_v \ , \tag{2.5}$$

with L_p, σ and ω being the filtration, reflection and permeation coefficients of the membrane, respectively. For an ideally semipermeable membrane, $\sigma = 1$, for a completely permeable to the solute, $\sigma = 0$.

A considerable drawback of models based on irreversible thermodynamics is that no insight into the transport mechanisms within the membrane is provided. The membrane is essentially treated as a "black box"[90], independent of membrane geometry and properties. Consequently, for the description of transport through membranes of specified structure, mechanistic models are used, which are based on either a homogeneous (non-porous) membrane or pore membrane (or a combination of both)[91]. The main difference between those models is that transport in non-porous membranes is exclusively mediated by diffusion, while transport in pore membranes may result from diffusive as well as convective flow[92]. A multitude of detailed models and simulations of osmotic transport has been published which seek to provide insight into the full dynamics of osmosis and its underlying mechanisms, considering particle interactions[78] and specific membrane geometries like carbon nanotubes[93].

Having described osmosis in general, the next section focuses on osmosis in water-

in-oil emulsions, a process which is of particular importance for the sensor method developed in this thesis.

2.1.2 Osmotically driven water transport in microdroplet systems

Osmotically driven water migration across an oil layer has been studied extensively using single and double emulsions. While most literature on mass transfer in emulsions refers to experiments with bulk emulsions, researchers have discovered microfluidics as a tool to characterize emulsion properties using capillary video microscopy[94, 95, 96, 74, 97] or droplet trapping devices[33, 45, 98, 99]. Advantages of those newer approaches are the more well-defined experimental systems compared to bulk emulsions and, in case of trapping devices, the high number of identical experiments, which allows for a detailed and quantitative investigation of molecular mechanisms.

Results from early microscopy studies with bulk double emulsions should be interpreted carefully, since a break-up of the thin oil phase, even a temporary one, can't be excluded (due to the experimental design). For example, Matsumoto et al. [100] found water permeability of the oil layer to decrease with increasing osmotic pressure. On the other hand, Garti and Romano-Pari[101] as well as Kinugasa et al. [102] reported on decreasing water transport rates with decreasing osmotic pressure. Later on, Wen et al. [96] explained the surprising trend observed by Matsumoto et al. with a breakdown of the oil phase, resulting in leakage of water from the inner to the outer aqueous phase which was not taken into account.

The molecular mechanisms by which water transport can be mediated is subject of the next subsection.

Molecular water transport mechanisms in nonadhesive emulsions

Transport rates of water were reported to depend on various parameters of the experimental system, including the magnitude of osmotic pressure, concentration and nature of surfactants (in water or oil phase), nature and specifically viscosity of oil, and temperature[100, 103, 104]. In general, an increase in concentration of oil-soluble surfactant was reported to increase the water transport rates[105, 94], whereas effects of the concentrations of water-soluble surfactants are less pronounced but more complex[94, 105]. Combined with the separation distance between droplets, those parameters dictate the predominant molecular transport mode of water in oil. For example, water transfer rates between visually contacting (but not adhering) and non-contacting droplets were observed to differ considerably, which was attributed to a change of the water transport mechanism[95]. Four main mechanisms facilitating water transport between non-adhering aqueous compartments have been proposed (partially

without being supported by direct evidence): water transport through thin lamella of surfactant[106], and water transfer by diffusion of single molecules[100], reverse micelles[106], or hydrated surfactants[104], respectively.

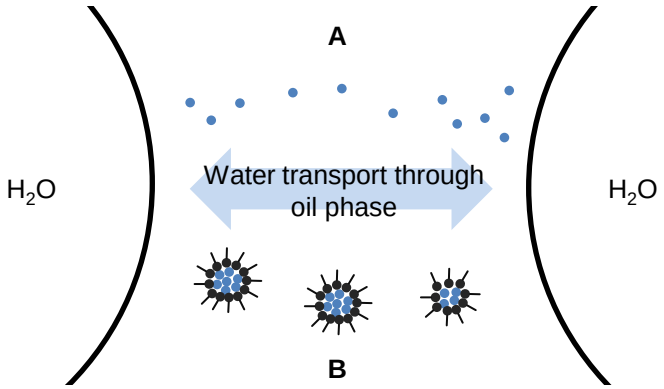

Figure 2.2: *Mechanisms of water transfer between non-contacting droplets. Water transport is mediated either by the diffusion of single water molecules (A) or by the diffusion of reverse micelles comprising many water molecules (B).*

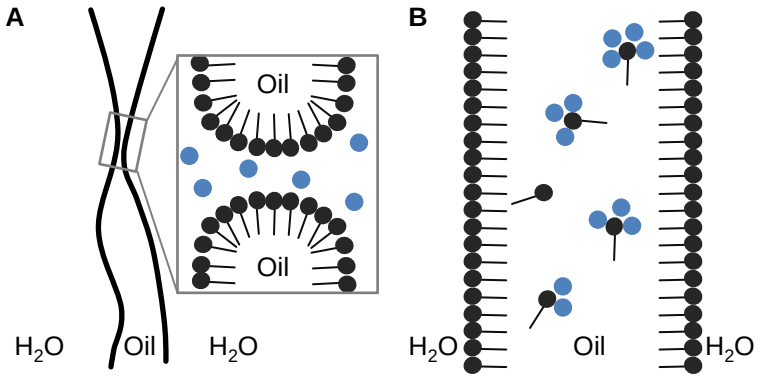

Figure 2.3: *Mechanisms of water transfer between contacting droplets (depicted are the contact zones). (A) Water transport through thin lamella of surfactant. (B) Water transport via the diffusion of hydrated surfactants.*

In the case of the droplets being separated by an oil layer of at least a few microns thickness (non-contacting case), water was reported to be transported either by diffusion of single water molecules or diffusion of water molecules in reverse micelles through the oil (Figure 2.2)[100, 106, 104]. Reverse micelles are small aggregates (up to tens of nanometers) of surfactants, which may include molecules of the dispersed phase or compounds which are soluble in the dispersed phase. Transport of single molecules is easily described by partitioning of the water molecule into the oil phase and subsequent diffusion, whereas the kinetics of the reverse micelle mechanism are still unclear[107, 108]. Various studies investigating the kinetics of solubilization (encapsulation of water in micelles) concluded, that micelles neither form at nor adsorb to the

droplet interfaces[109, 107]. Instead, water molecules were reported to partition into the oil phase prior to the incorporation in micelles or the formation of micelles and *vice versa* for release of the water molecules from reverse micelles. Since experimental results have been equivocal, there is an ongoing discussion on the extent to which reverse micelles affect the solubility of water in oil and the transfer rates of water[110, 111].

When in close contact, two further water transport mechanisms were reported. According to Kita et al. [106], thermal fluctuation of the droplet interfaces might lead to spontaneous formation of "surfactant lamellae" between two aqueous compartments, through which water is transported. This model is similar to a pore flow model with transient pores. Colinart et al. [104] proposed the "hydrated surfactant" model, according to which surfactants hydrate at the droplet's interface, diffuse through the oil, and dehydrate at the opposed oil-water interface. Since the diffusion length of hydrated surfactants is shorter than a few microns[104], the mechanism was expected to be important for thin oil layers. Indeed, most recently, in the longest atomistic simulation of a microemulsion system (simulation time of 1 µs) evidence for the hydrated surfactant mechanism was found[112].

These transfer mechanisms form the basis for the subsequent discussion of current literature on osmotically driven water transport in emulsions. As the surfactant used in this thesis is nonadhesive, i.e. it doesn't promote adhesion between droplets, focus is placed on nonadhesive emulsions.

Osmotically driven water transport in nonadhesive emulsions

About a decade ago, Wen and Papadopoulos were able to form and observe single water droplets (W1) at defined locations in an oil-phase (O) surrounded by a suspending aqueous phase (W2), using microcapillary video microscopy[95] (Figure 2.4). They applied the system to investigate osmotically driven water transport in emulsions with the two aqueous phases W1 and W2 either in visual contact or separated by a "microscopically detectable minimum distance"[95, 94, 96]. Osmotic pressure was generated by using various aqueous solutions of sodium chloride with concentrations ranging from 0.1 M to 5 M. The internal droplet W1 always comprised the lower solute concentration and shrank until equilibrium state was reached (Figure 2.4). The final radii were reported to be in good agreement with the theoretical predictions for every experiment. Up to now, this set of experiments[95, 94, 96] delivers the most quantitative information about osmotically driven water transfer in non-adhesive water-in-oil(-in-water) emulsions. Hence, their results will be critically reviewed in the following section.

For the droplet W1 and the aqueous phase W2 being separated by more than a few micrometer thick oil layer, Wen and Papadopoulos reported diffusion of reverse micelles as well as spontaneous emulsification to be the predominant water transport processes.

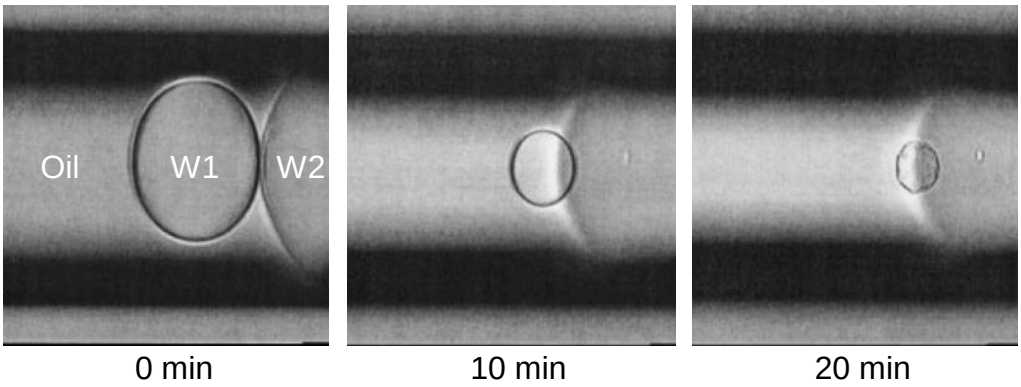

Figure 2.4: *Image sequence taken from an experiment performed by Wen and Papadopoulos, showing the shrinkage of an aqueous droplet (W1) in contact to a second aqueous phase (W2). W1 comprised 0.1 M of sodium chloride, and W2 5 M. Image quality and lack of a scale is due to the original images, which are adapted from Ref. [96].*

However, in visual contact of the aqueous phases, transport *via* hydrated surfactants was suggested.

In non-contacting arrangements, transport rates were about one order of magnitude lower compared to contacting arrangements, and independent of the separation distance between the droplets[95]. Furthermore, transfer rates always remained constant during one experiment until the final concentration was reached, albeit concentration differences decreased due to the droplet's shrinkage[96]. Surprisingly, in the presence of salt in both aqueous phases, transport rates measured in different experiments decreased with an decreasing initial salt concentration difference between the aqueous phases[96]. For the latter observation no explanation was found.

For visually contacting organizations of the aqueous phases and constant osmotic pressure[5], water transport rates remained constant during each experiment [95, 96] and rose linearly with the magnitude of the concentration difference applied. In case of the presence of salt in both aqueous phases, water transport rates were initially constant over a wide range of concentration differences and then dropped asymptotically to zero, thus showing a nonlinear relationship between concentration difference and water transport rate[96].

They concluded that, in their experiments, all water transport mechanisms were controlled by interfacial processes rather than being limited by diffusion within the oil membrane (as suggested by Magdassi et al. [113], Garti[114], and Colinart et al [104]). Similar conclusions had been drawn by Caroll et al. [115] and Chen et al. [116] when studying water transfer in bulk emulsions.

The experiments performed by Wen and Papadopoulos are disputable in two major points.

[5] W1 was composed of pure water and only W2 comprised salt.

First, the salt concentrations used were very high. As a consequence, interactions between sodium ions and chloride ions lead to deviations from van't Hoff's equation for dilute solutions (see section 2.1.1), which can be quantified by the osmotic coefficient Φ (see (2.2), page 16). According to lists published by Pitzer et al. [88] and Hamer and Wu[87], the osmotic activity coefficient of a 5.0 M/kg NaCl solution is $\Phi_5 = 1.19$, and for a 1.0 M/kg NaCl solution $\Phi_1 = 0.93$. Thus, a nonlinear dependence of water transfer rate on solute concentration difference is expected, even though the water transfer rate might depend linearly on the osmotic pressure. In particular, the nonlinear relationship between salt concentration difference and transport rate observed by Wen and Papadopoulos is not surprising and may not be used to justify a switch of water transfer mechanisms.

Second, albeit Wen's and Papadopoulos' results suggested that no ions were transported across the oil phase (e.g. droplets were reported to equilibrate at the theoretically predicted volumes), this conclusion was proven wrong by Cheng et al. in 2007[97][6]. Using an identical experimental set-up as well as similar oil and surfactant types, Cheng and coworkers observed migration of chloride ions across the oil phase from one aqueous phase to the other, where precipitates were formed. However, the transport of ions seemed to stop after few minutes and only unidirectional ion flow in direction of the concentration gradient was observed[97]. Therefore, further experiments are needed to draw definite conclusions, but nevertheless, Wen's and Papadopoulos' results should be carefully interpreted with permeability to chloride ions in mind.

Still, the surprising decrease of transport rates for decreasing initial salt concentration differences in a non-contacting arrangement can't be explained. It may be hypothesized, that the decrease is due to a increasing concentration of salt in W1 rather than a decreasing concentration difference between the aqueous phases, since experiments with constant concentration difference but varying salt concentration in W1 were not performed. In this case, either sodium ions or chloride ions had to permanently influence the transport kinetics of the system, e.g. by interacting with the droplet interfaces. Based on the results of Cheng and coworkers, chloride ions would be best candidate.

Besides transfer of chloride ions, Cheng also observed water flux between the aqueous phases.

Indeed, in most cases, the oil-membrane is permeable to both, water molecules and solutes comprised in the aqueous phase. Hence, the magnitude of the osmotic effect depends on the relative timescales of water and solute transfer processes: if water transfer rates are much higher than rates of solute transfer (caused by diffusion and solute concentration gradient), droplets change sizes[45, 96, 33]. In case solutes migrate

[6] Prior, Sela et al. [117] published a similar results, but swelling-breakdown of the emulsion could not be excluded.

much more rapidly through the oil phase, droplet sizes remain stable[34, 32, 62]. Thiam et al. [45] demonstrated the dependency of transport rates nicely by generating binary adhesive droplet pairs forming a bilayer. One droplet type consisted of pure water (labeled with methylene blue) and the other type contained electrolytes. In less than one minute, the volume of pure water droplets decreased to few percent of its initial size and the droplet comprising electrolytes grew in size and became slightly colored. Hence, the transport rate of water through the bilayer was faster than the one of methylene blue, and both in turn much faster than the transport rate of the electrolytes.

Osmotically driven water transport through bilayer membranes

As described by Thiam et al. adhesion of droplets can mediate a faster exchange of water and solutes, since the neighbouring droplets are separated by very thin membranes of nanometer thickness[44, 45, 118]. In addition, the permeability of a bilayer membrane depends on its fluidity, which was already observed for vesicles by Lande et al. in 1995[119] and verified for droplets by Kato et al. [120] and Thiam et al. [45]: the lower the fluidity, the lower the permeability of the bilayer. The permeation of water molecules through bilayers is most frequently described by the solution-diffusion mechanism[121], according to which water molecules first partition into the hydrophobic phase and then diffuse across[122, 123]. Diffusion within the membrane has to be the rate limiting process, and ideally, water (or solute) transport is exclusively driven by a concentration gradient at constant pressure within the membrane[92]. Then, water flux through the membrane $j(t)$ is proportional to the concentration gradient Δc, $j(t) = -P/l\Delta c$, where l is the membrane thickness, and P the permeability coefficient of the membrane (which may depend not only on the membrane, but also on the nature of the solvent)[92]. The solution-diffusion model has also been successfully applied to describe water transfer in dilute, nonadhesive emulsions by several researchers[124, 125].

Conclusive remarks

Despite all research, and because of contradictory results and a huge amount of different systems, there is still a lack of understanding of the relations between water transport and the system parameters, like osmotic pressure. Nonetheless, some microfluidic systems already exploit osmotic pressure across oil-layers or PDMS-membranes in order to control droplets' volumes and solute concentrations and induce crystallization of proteins and salts [126, 99, 127]. In addition, evidence based on results published by Schmitz et al. [30] and Joensson et al. [53] suggest that osmotic pressure caused by the metabolic activity of cells gives rise to size changes of droplets: Schmitz and coworkers observed a change of droplet sizes while incubating monodisperse droplets, some of them containing yeast cells. After several minutes shrinkage of yeast containing

droplets occurred. Recently, the same system was used by Joensson et al. to demonstrate a method for size separation of microdroplets. While both authors assumed osmosis to be the underlying mechanism, neither direct evidence was given nor further investigations were provided.

2.1.3 Ostwald ripening and other processes

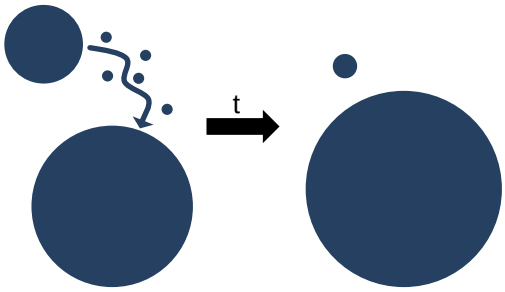

Figure 2.5: *Ostwald ripening of droplets. Due to the difference in Laplace pressure water is transferred from droplets of smaller radii to droplets of larger radii.*

Solvent transfer between droplets may also be induced by a mechanism independent of the droplet compositions. Instead, heterogeneities in chemical potential are caused by dissimilar droplet sizes[128, 111, 129]. These differences in chemical potential are equilibrated by a process called Ostwald ripening[7], which leads to the growth of larger droplets at the expense of smaller ones[130, 67, 111] (Figure 2.5).

Thus, Ostwald ripening causes coarsening of emulsions, i.e. an increase in mean droplet diameter, by transfer of solvent of the dispersed phase between single compartments of dispersed phase. Transport of the dispersed phase is mediated by the same mechanisms as described previously (section 2.1.2), in particular by molecular diffusion or transfer in (reverse) micelles[109]. This ripening process is a consequence of the change in solubility C with the curvature of the droplet, which is approximately described by the Kelvin equation

$$C(r) = C_{\text{inf}} \exp(K/r), \tag{2.6}$$

with C_{inf} being the bulk solubility of water in oil and K a system constant[131, 132]. The cause for this change in solubility, which is equivalent to a change in vapor pressure, is the Laplace pressure $\Delta P = 2\gamma/r$[133, 111, 134, 135]. The Laplace pressure is the pressure difference between the inside and the outside of a droplets caused by the surface tension γ[133]. Lifshitz and Slyozov[136] and, independently, Wagner[137] formulated the first theory of Ostwald ripening, which became known as the LSW

[7] Named after the Nobel laureate Wilhelm Ostwald, who first described this process in 1896[66].

(Lifshitz-Slyozov-Wagner) theory. Since then, it has been revised and further development was achieved[130]. A detailed description of Ostwald ripening, which also appears in all kinds of colloidal systems[138], can be found in the review given in Reference [111].

Contrary to Ostwald ripening and osmosis, other mechanisms like solubilization[108, 107], evaporation[139] and dissolution[140] exclusively lead to an efflux of water out of a droplet into the continuous phase or the environment of a droplet. Microfluidics provides, on the one hand, tools for the investigation of those processes. Huebner and coworkers, for example, characterized the enhanced shrinkage of trapped droplets exposed to oil flowing with different velocities[98]. On the other hand, microfluidic applications make use of these processes: shrinkage of droplets caused by evaporation and dissolution has been used for concentration purposes[141, 140, 98], protein precipitation and crystallization[142, 143, 144], and particle packing[143].

2.2 Solute transport in microdroplet systems

As described previously, heterogeneities in chemical potentials arising from differing compositions of the droplets may lead to the transfer of solute or solvent between the droplets. In most microfluidic applications though, significant size change of droplets, i.e. the transfer of solvent, can be avoided by experimental design and the correct choice of oil and surfactant type[34, 32, 62].

However, because of the diverse nature of solutes comprised in the droplets, preventing cross-contamination of the droplets' contents poses a much more complicated challenge, in particular if long term storage is needed, e.g. in droplet libraries[64]. Hence, considerable effort has been put in the investigation and minimization of solute exchange between droplets. Essentially, three ways of coping with leakage of compounds exist: adaption of surfactant and oil, addition of molecules preventing leakage or increasing solubility within the aqueous phase, and synthesis and use of molecules specifically designed to stay inside the aqueous phase.

Many compounds, for example the fluorescent dye rhodamine 101, are highly soluble in both water and oil and thus instantly diffuse into the continuous oil phase[32]. The addition of 5% BSA (bovine serum albumin) was found to substantially reduce the leakage of fluorescein into the oil[34], probably by increasing its solubility in the aqueous phase. The initial assumption of BSA forming a barrier at the droplets interface[34] was proven wrong by Skhiri and Gruner et al. [32].

Other molecules like coumarin-based fluorogenic substrates, which are widely used in enzymatic assays, transfer very rapidly between the aqueous droplets. Woronoff et al. met this problem by synthesizing a highly water soluble kind of such a substrate specifically for application in microdroplet assays, preventing any leakage from droplets[35].

Furthermore, they reported on a decreasing rate of solute exchange with increasing solubility of solutes in the aqueous phase[35].

For lipophobic solutes, transport is facilitated by mechanisms similar to those reported for water in section 2.1.2. Thus, rates of solute transport have been reported to strongly depend on type of oil, nature and concentration of surfactant used, and, of course, the chemical and physical properties of the compound itself[32, 45, 33, 34, 97, 145, 146]. An increase in surfactant concentration in the continuous phase generally leads to a decrease in the retention of solutes, due to reverse micelles increasing their solubility in the oil phase. Analogous to the case of water, different transfer mechanism of solutes prevail for adhering, contacting, and non-contacting droplets.

In case of adhesion between the droplet interfaces, solute transfer is most frequently described by two permeation models, the solution-diffusion mechanism[121, 92] and the pore-flow mechanism[92]. According to the pore-flow model, compounds traverse the bilayer through transient hydrophilic defects caused by thermal fluctuations (analogously to the "surfactant lamellae mechanism" described in the previous section)[147]. Both models differ in the way the chemical potential gradient within the membrane is expressed: within a perfect solution-diffusion membrane, only a concentration gradient, and within a perfect pore-flow membrane, only a pressure gradient exists[92]. Permeation kinetics of halide anions like bromide, iodide, and chloride, for example, are consistent with the solution-diffusion mechanism, whereas the pore mechanism was reported to become relevant for cations under certain circumstances[117, 148].

Adhesion of droplets generally accelerates the exchange of compounds between the droplets. However, if the oil phase between the droplets gets very thin ($< 1\mu m$) but no adhesion occurs, solute transport may become significantly retarded. This effect was observed by Cheng et al. [97] when investigating transport of chloride and silver ions across an oil phase in a water-in-oil-in-water emulsion, and interpreted in terms of the spatial confinement impeding the formation of micelles.

When aqueous compartments are separated by a distance larger than a few microns, solute transfer is mediated either by partition and diffusion of single molecules or *via* reverse micelles[35, 34, 32, 97, 74, 149].

As reported by Skhiri and Gruner et al. [32], the spatial organization of droplets determines the equilibration time-scale of solutes in an nonadhesive emulsion. Their model emulsion initially comprised monodisperse droplets with two differing concentrations of a fluorophor, whose subsequent transfer between the droplets compensated for the initial concentration differences. Significant volume changes were prevented by buffer osmolarities considerably higher than the osmolarity of the fluorophor. They concluded that, on microscopic level, the equilibration was determined by transport of fluorophores in reverse micelles, whereas on macroscopic level, the arrangement of

droplets relatively to each other dictated the pace of equilibration. As naively expected, computations yielded fastest equilibration for a perfectly alternating droplet configuration, while equilibration time-scales of other arrangements may be several orders of magnitude slower.

Albeit being an undesired property in the majority of microfluidic assays, there are lots of applications exploiting the permeability of interfaces or the continuous phase of emulsions to solutes, in academic research as well as in industry. For example, transfer of solutes in emulsions is a key process in pharmaceutics for drug delivery[150]) and in chemistry for separation processes by means of ELMs (Emulsion Liquid Membranes)[151, 152].

Albeit the sensor method presented in this thesis is based on the osmotically driven transfer of solvent between droplets, solute transport has to be considered as well, due to the non-ideal semipermeability of the oil membrane. For example, solutes which partition significantly faster into the oil and other droplets than water do not contribute to the osmotic pressure between droplets (in ideal case).

Part II

Materials and Methods

3 Experimental set-up

For generation of water-in-oil droplets, microfluidic flow-focusing devices made of the polymer PDMS (Polydimethylsiloxane), a silicone, were used (see also section 1.1). Microstructured PDMS blocks were fabricated in a multi-step process based on a process called soft-lithography[153], which uses photolithographic methods to create a master mold for the PDMS. In most experiments, monodisperse droplets comprising aqueous solutions of sucrose or cell suspensions with a few cells per droplet were produced. Due to its permeability to gases and water[28], PDMS (without any modifications) isn't well-suited for long term storage of droplets. Therefore, droplets were transferred to a gas-tight incubation chamber made of glass for incubation and observation by video microscopy.

3.1 Design and fabrication of microfluidic devices

This section describes the production of the microfluidic devices from the fabrication of a master geometry, to the generation of silicone replica and the assembly of the device. A scheme of the prototyping of PDMS replica is depicted in Figure 3.2.

3.1.1 Fabrication of a SU-8 silicon master by photolithography

Photomasks were designed with the help of QCAD (Ribbonsoft, Andrew Mustun) and printed on a flexible transparency (PMS-12 Super-High Res Mask Film, J. D. Photo-Tools) (Figure 3.1). This was used to create a master of the desired structure on a silicon wafer (type: P/Boron, orientation: 100, thickness: 256-306 µm, diameter: 2" ± 0.015"; Si-Mat Silicon Materials Inc.) by means of contact photolithography[154, 25]. All steps described in the master fabrication procedure were performed under clean room conditions. Prior to their use, silicon wafers were dried for at least 30 minutes in a drying oven at 230 °C and dust was removed with a stream of nitrogen. For photoresist coating, approximately 2 ml of photonegative resist (NANO SU-8 25; Microchem) were pipetted onto a wafer mounted to a Delta 10 coating centrifuge (BLE Laboratory Equipment GmbH).

Then, a two-step spin-coating procedure was performed.Rotation speeds as well as all parameters used later on are listed in Table 3.1. Subsequently, coated wafers (Figure

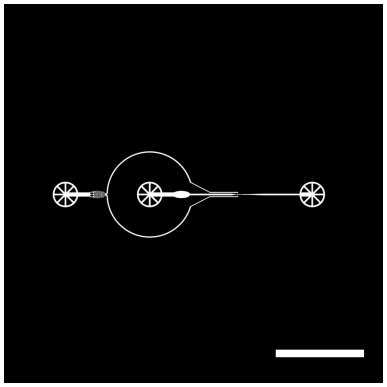

Figure 3.1: *Photomask comprising a geometry for droplet production. White regions are transparent on the transparency (except of the scale). Scale is 5 mm.*

3.2 B) were baked on a hot plate first at 65 °C, and then at 95 °C. In this so-called Soft Bake step the solvent evaporates, with the step-wise heating reducing thermal tensions in the resist. Next, the photomask transparency was cut to fit a 49 mm x 49 mm glass slide and attached to it with a few water drops, with the printed side pointing away from the glass slide (Figure 3.2 A). For exposure, the photomask composite was fixed to a mask aligner with the transparency facing the subjacent wafer and both brought in contact. By illuminating the coated wafer with UV light for 7 s through the mask, uncovered regions of photoresist were selectively cross-linked (Figure 3.2 C). Right after exposure, cross-linking process was completed by another heating cycle on a hot plate ("Post Exposure Bake"). In order to remove the unexposed photoresist, the wafer was then developed in mr-Dev 600 developer (micro resist technology GmbH) under gentle agitation for about 2 minutes (Figure 3.2 D). Subsequently, the wafer was rinsed with fresh developer and then with isopropanol to terminate the development process, and dried in a stream of nitrogen. Finally, the wafer was put in the drying oven for at least 30 min at 170 °C (Hard Bake).

Table 3.1: *Fabrication of SU-8 master molds.*

Step	Parameter
Spin coating	500 rpm: 5s 1800 rpm: 35 s
Soft bake	65°C: 3 min 95°C: 10 min
Exposure	7 s
Post exposure bake	65°C: 1 min 95°C: 3 min
Development	2 min in mrDev-600 developer
	10 s in mrDEV-600 isopropanol

Prior to their first use, the SU-8 masters were passivated with perfluorooctyltrichlorosilane (ABCR GmbH & Co. KG) to allow for an easy removal of PDMS later on. This step wasn't performed in a clean room. For silanization, 500 µl of silane were pipetted in a small petri dish standing in a desiccator comprising the SU-8 masters. After decreasing the pressure down to approximately 10 mbar by a vacuum pump, the pump was removed and the desiccator remained closed for at least 4 h. Subsequently, the wafers were rinsed with ethanol, blow-dried with nitrogen and stored in 2.5" petri dishes.

3.1.2 Fabrication of silicone replica

The SU-8 silicon masters were used as casting molds to fabricate structured PDMS devices. To initiate the polymerisation of the polymer, its two liquid components, a siloxane (the monomer) and a crosslinker (Sylgard 184 Silicone Elastomer Kit, Dow Corning GmbH), were thoroughly mixed in a weight ratio of 10:1. The mixture was evacuated in a desiccator for 15 min until no bubbles were visible. Then, it was casted onto the structured SU-8 masters situated in medium sized petri dishes until a PDMS height of approximately 5 mm was reached (Figure 3.2 E). After another evacuation to remove any remaining bubbles, the petri dish was heated in an oven at 65 °C for at least two hours. The hardened PDMS block was carefully detached from the petri dish with the help of a scalpel and ethanol. Afterwards, the PDMS replica (Figure 3.2 F) could be easily peeled off

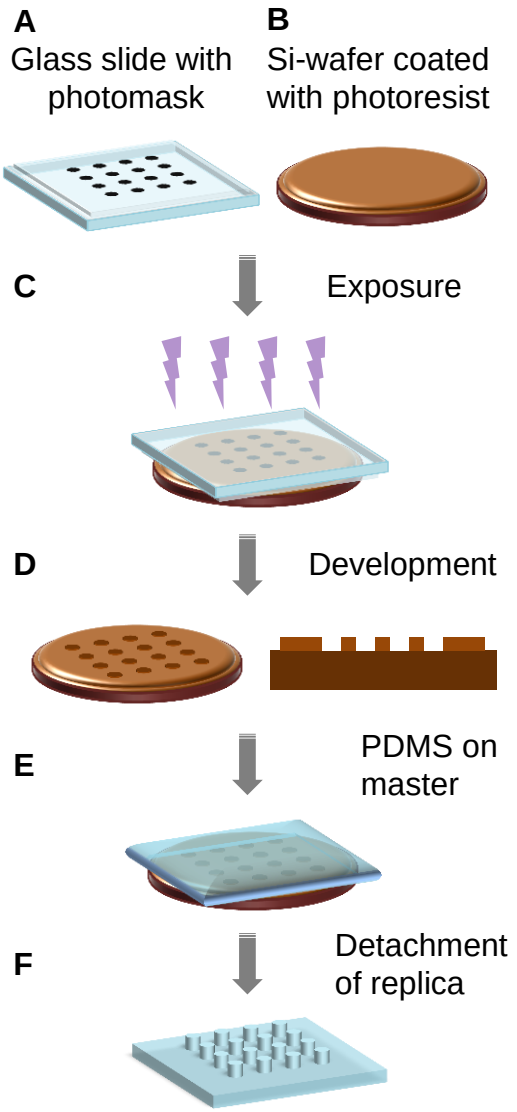

Figure 3.2: *Prototyping of PDMS replica. A silicon wafer coated with photoresist (B) is brought in contact with the photomask (mounted on a glass slide) (A) and exposed to UV light (C). After removal of the unexposed photoresist only illuminated, crosslinked regions remain, yielding a master of the structure (D). Microstructured PDMS replica are generated by casting a mixture of the monomer and the crosslinker onto the SU-8 master (E) and peeling it off after curing (F).*

of the SU-8 master and cut to size. Future inlets and outlets of 0.5 mm diameter were punched using a hand puncher (Harris Uni-Core 0.5 mm, Ted Pella Inc.). For further use, both, PDMS replica and SU-8 master, were rinsed with ethanol and blow dried with nitrogen.

3.1.3 Assembly of microfluidic devices

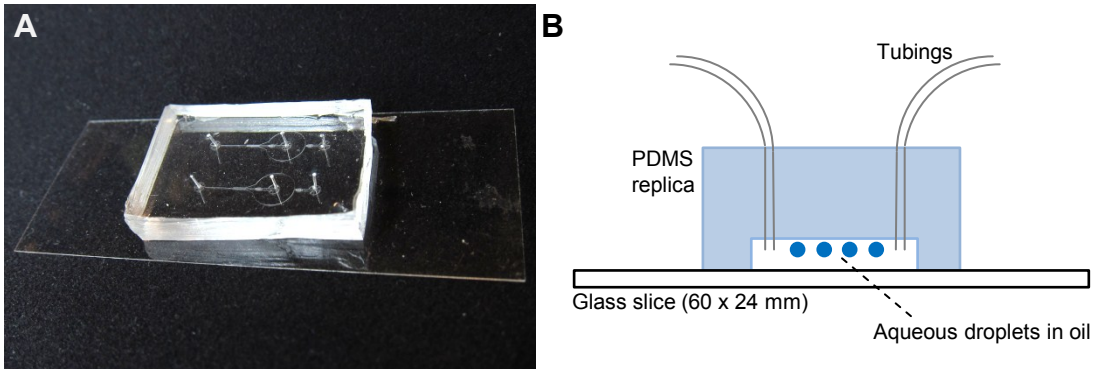

Figure 3.3: *(A) Photograph of the microfluidic device used for droplet generation. It consists of a microstructured PDMS replica covalently bound to a coverslip. (B) Schematic side view of the microfluidic device.*

With the help of coverslips the PDMS replica were sealed tightly, resulting in leakproof microfluidic devices (Figure 3.3 A and B). Coverslips measuring 24 mm x 60 mm were cleaned in a 30% alkaline extran (Extran MA01; Merck) solution in an ultrasonic bath for 15 min. After the ultrasonication was repeated with the coverslips placed in ultrapure water (MilliQ water), they were dried under a stream of nitrogen. For the sealing, coverslip and PDMS replica were subjected to an oxygen plasma (100-E Plasma System, PVA TePla AG) for 17 s at 150 W and 0.5 mbar, and quickly brought into contact, applying slight pressure. The plasma activation introduces Si-OH (silanol) groups on both surfaces which render the surfaces hydrophilic and form covalent Si-O-Si bonds on contact[153, 155]. To strengthen the seal and accelerate the recovery of non-hydrophilic surfaces, the microfluidic device was heated in an oven for 30 min at 65 °C[156].

Hydrophobic channel surfaces needed for the manipulation of water-in-oil emulsions were obtained by rinsing the channels with Ombrello (moton automotive Deutschland). To this a 1 ml syringe (Omnifix-F, B. Braun Melsungen AG) with a cannula (Microlance 3, BD) filled with Ombrello was connected to an inlet of the microfluidic device *via* a polyethylene tubing (Fine Bore Polyethylene Tubing; 0.28 mm ID, 0.61 mm OD; Smiths Medical). Generally, Ombrello was stored in aliquots under argon atmosphere. In a final step, the channels were flushed with air, once again using a syringe.

To increase stability of the microfluidic devices, the coverslips were fixed to standard

26 mm x 67 mm glass slides (Carl Roth) using adhesive tape.

3.2 Droplet generation

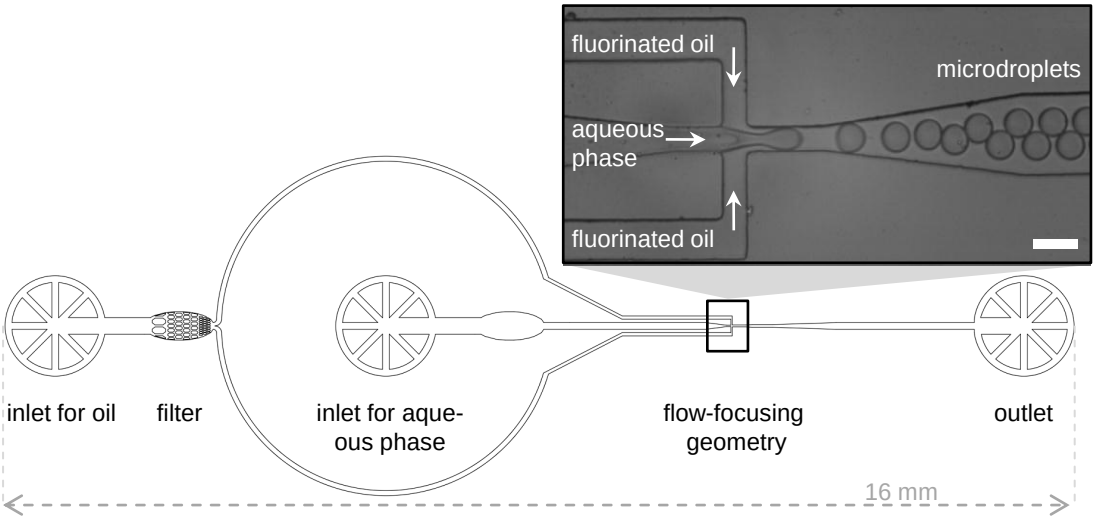

Figure 3.4: *Schematic of a channel geometry used for droplet generation. Tubings are connected to the inlets and the outlet, respectively. The filter structure downstream of the oil inlet prevents larger dirt particles from entering the channels. Droplets are generated by the flow-focusing geometry shown in the micrograph. Scale is 50* µm.

Monodisperse aqueous droplets in a fluorocarbon oil (FC-40, Acros Organics) were generated by microfluidic devices with flow-focusing geometries (Figure 3.4). In these geometries, break-up of an aqueous flow is induced by perpendicular streams of oil (Figure 3.4, micrograph), as already described in section 1.2. Filter structures downstream of the inlets prevented larger dirt particles from clogging the orifice (the end of the aqueous channel, at which droplets are formed). In case the aqueous phase comprised cells, devices lacking the respective filter were used (Figure 3.4), as cells usually got stuck in the filter structure. To stabilize the droplets and prevent unspecific adsorption of biomolecules a PFPE–PEG block-copolymer surfactant (Krytox PEG 600 Diblock, 19 mM) was added to the oil phase, passivating the droplet interfaces. Synthesis of the surfactant was done by Jan-Willi Janiesch as published in Reference [10].He also determined the surface tension between aqueous and oil phases stabilized by 19 mM Krytox PEG 600 surfactant to approximately 30 mN/m.

The aqueous and the oil solutions were put in 1 ml syringes with cannulas, which were connected to the inlets of the PDMS device *via* polyethylene-tubings. Flow control was provided by precision syringe pumps (Aladdin-1000, World Precision Instruments), flowing the aqueous stream at 50 - 100 µl/h and the oil stream at 200 - 300 µl/h through a 20 µm wide orifice (Figure 3.4, micrograph). Droplet generation was microscopically

observed through a 20x objective mounted on an Axiovert 200 microscope (Carl Zeiss MicroImaging GmbH) equipped with an ORCA-ER camera (Hamamatsu). This allowed for the adjustment of flow rates until the desired droplet size and generation rate was reached. Sizes ranged from 15 to 100 µm in diameter. After the adjustment, droplet production was allowed to stabilize for a few minutes.

To transfer the droplets to an incubation chamber, they were collected in a small pipette tip stuck to the outlet hole. When a sufficient amount of droplets was collected (usually after a couple of seconds), the rear of the pipette tip was closed by a gloved fingertip and the tip was pulled out. Droplets were released simply by removing the finger.

Despite a tubing connected to the outlet seems to be the easiest way for the transfer of droplets, it turned out to often lead to coalescence of droplets, presumably caused by electrostatic interactions with the tubing. Using the pipette tip considerably reduced the number of events, but coalescence persisted to occur occasionally, dependent on buffers and channel geometries used. Buffers of high salinity were observed to cause coalescence more frequently than buffers of low salinity.

Unfortunately, the attachment of the pipette tip altered the pressure conditions in the channels, and consequently also the droplet sizes. Since the frame rate of the camera was too slow to capture the droplets flowing through a channel in the microfluidic device, no precise size measurement was possible. Hence, the initial radii of the collected droplets could not be precisely measured upon transfer to the incubation chamber.

3.3 Observation and incubation of droplets

For all experiments, droplets were transferred to self-made observation and incubation chambers (Figure 3.5). The chamber consisted of two glass slides forming bottom and top of the chamber, which were separated by two glass spacers of 130 - 160 µm height, and was sealed air-tight with dentists' glue (twinsil picodent Dental-Produktions- und Vertriebs-GmbH). A schematic of a chamber is depicted in Figure 3.5. Attempts to use incubation devices made of PDMS didn't succeed, since the PDMS is permeable to gas and water[28, 27] and induced droplet shrinkage, even when saturated with water.

The surfaces of all glass slides (Carl Roth, 24 mm x 60 mm, height 0.13-0.16 mm) were rendered hydrophobic by treating them with Ombrello. To accomplish this, 100 µl of Ombrello were put on a coverslip which was then covered by another coverslip. After one minute of incubation, the coverslips were separated, rinsed thoroughly with ultrapure water and dried under a stream of nitrogen. This procedure was repeated with the untreated sides of the coverslips. Spacers of about 5 mm x 10 mm size were cut out of the treated coverslips using a glass cutter. While collecting droplets in the

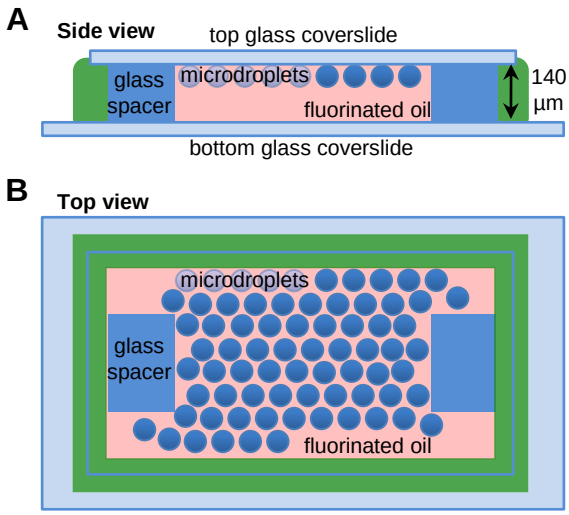

Figure 3.5: *Schematic side view (A) and top view (B) of the chamber used for incubation and observation of the droplets.*

pipette tip, glass spacers were put on the bottom glass slide and the area between them was covered with a thin film of oil, to which subsequently the droplets were transferred. Immediately thereafter, another glass slide was put on top of the glass spacers. Air bubbles were pushed out under application of slight pressure. The interior, exclusively filled with oil and droplets, was then sealed gas-tight with two-component glue and the chamber was directly transferred to a microscope for observation. Typically, time-lapses with imaging intervals ranging from 2 min to 10 min, and total acquisition times up to 48 h were recorded. Lateral drifting of droplets was a common problem, caused by tilted glass slides or the buoyancy-driven reorganization of droplets from a multilayer to monolayer arrangement.

3.4 Static systems - droplets comprising fixed amounts of solutes

Static systems were composed of two types of droplets containing fixed amounts of solutes. Most experiments were performed with droplets of different sucrose concentrations ranging from 10 µM to 800 mM. Furthermore, dilutions of bromphenol blue and YPD medium (Fisher Scientific, YPD-Broth, Molecular Genetics Powder) were used.

Droplets of both types were generated in one microfluidic device comprising two separate flow-focusing geometries (Figure 3.6). Mixing the droplet types in the microfluidic device was found to yield a better degree of mixing than mixing droplets produced in distinct devices, which usually resulted in the formation of regions of one droplet type. The simultaneous production allowed to tune the sizes and production rates of

the droplet types relatively to each other. Usually, initial droplet radii were chosen to differ in size in order to be able to distinguish between the two droplet types optically.

Two syringes filled with oil and the differing aqueous solutions each were attached to the inlets of the device and droplet generation and observation was performed as described in sections 3.2 and 3.3.

For imaging of the mixed droplet ensemble, the observation chamber was mounted on a Zeiss Axiovert 200 Microscope equipped with an 20x objective (ZeissLD A-Plan 0.3 Phase 1) and an Orca ER camera (Hamamatsu Photonics). Image acquisition was done by Wasabi (Hamamatsu Photonics), recording 16 bit images with a resolution of 1344 x 1024 pixels (10 ms exposure time, 0.312 µm per pixel). Unfortunately, image acquisition was severely hampered by large focus drifts, which resulted from a descending objective. Thus, over some periods, no determination of the droplets' radii was possible.

After an experiment, all channels of the microfluidic device were rinsed with ultra pure water to avoid clogging.

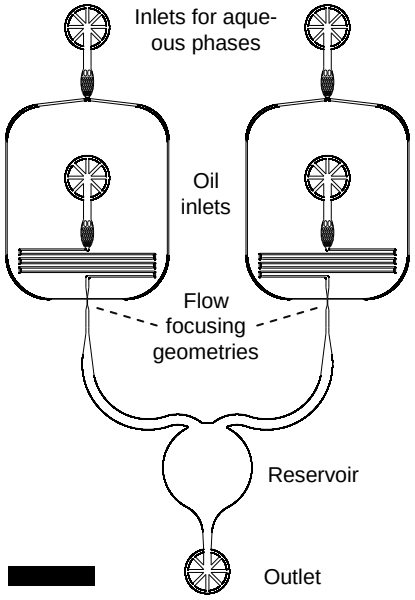

Figure 3.6: *Schematic of a microfluidic device comprising two flow-focusing geometries for simultaneous production of two droplet types, differing in content, size and generation rates. Scale is 2.5 mm.*

3.5 Dynamic systems

Like static systems, dynamic systems were also composed of two droplet types, however one type contained a catalytically active compound, a cell or an enzyme, in addition to just the growth medium or substrate. Therefore, in one droplet type the amount of solutes got altered with time whereas it remained fixed in the other.

3.5.1 Droplets comprising yeast

Yeast cultures (Saccharomyces cerevisiae, Baker's yeast) were grown overnight in YPD[1] medium (Fisher Scientific, YPD-Broth, Molecular Genetics Powder) with shaking at 30 °C. The cell suspension was centrifuged for 2 min at 6000 rpm and resuspended in fresh YPD medium prior to injection into the microfluidic device. Manual agitation of a small magnetic stirrer added to the suspension in the syringe prevented the settlement

[1] Yeast (Extract) Peptone Dextrose

of cells. Both, droplets with and without cells, were produced by a single flow-focusing geometry randomly distributing yeast cells in monodisperse droplets. The distribution of cells in droplets should follow a Poisson distribution[157, 158], provided the cells do not agglutinate.

Droplets were generated and prepared for observation as described in sections 3.2 and 3.3. Flow rates were adjusted so that about half of the droplets were empty. For imaging, the same set-up as in the static system case was used.

Live/dead screening

For the live/dead assay, yeast was cultured as described above. Dead cells were prepared by heating a yeast cell suspension (2 ml) for 5 min at 80 °C. Dead and live cells were washed twice with staining buffer (pH 7.5, 100 mM Tris, 150 mM NaCl, 1 mM $CaCl_2$, 0.5 mM $MgCl_2$). After mixing live and dead cell samples, 4 ml of a 1 mg/ml propidium iodide solution (P3566, Invitrogen) was added to the yeast suspension (2 ml) and incubated for 15 min at room temperature. The suspension was washed twice with staining buffer, resuspended in fresh YPD medium, and then used for droplet generation as described in section 3.2. Fluorescence and bright field images were taken with a Zeiss Axiovert 200M Laser-Scanning-Microscope equipped with an 20x objective (Zeiss LD Plan-Neofluar, 0.4 Korr) and a helium-neon laser (543 nm, LGK 7786 P100, Lasos Lasertechnik GmbH) using the image acquisition software Pascal 5 (Zeiss). Resolutions were 2048 x 2048 pixels (0.57 µs per pixel) for bright field and 512 x 512 pixels (6.4 ms per pixel) for fluorescence images (field of view: 450 µm x 450 µm).

3.5.2 Droplets comprising E. Coli

E.Coli (Strain BL21(DE3), Novabiochem) were plated on an agar plate and incubated overnight at 37 °C. An isolated colony was picked with the tip of a pipette, which was added to a conical flask containing approximately 20 ml of instant LB[2] medium (Sigma-Aldrich Inc.). The flask was incubated at 37 °C and 60 rpm overnight. Both, conical flask as well as LB medium, were autoclaved prior to use. The overnight culture was diluted to an optical density OD600 = 0.01 (absorption of the suspension at λ = 600 nm) with fresh LB medium . For measurement of the optical density by means of a spectrophotometer (Nanodrop ND-1000, Peqlap Biotechnologie GmbH), 3 µl of the suspension were used, and each measurement was repeated four times. Sterile LB medium was used as Blank measurement. For experiments, 1 ml of the diluted suspension containing 100 µg/ml ampicillin trihydrate (Serva Electrophoresis GmbH) was drawn into a syringe. A stock solution of 1 mg ampicillin in 1 ml hydrochloric acid was prepared, which was stored at 4 °C and diluted 1:100 with LB medium prior to use.

[2]LB is short for lysogeny broth.

As in the yeast experiments, a magnetic stirrer was added to the syringe comprising the suspension to prevent the settlement of the bacteria due to gravity. Droplet generation and observation was performed as described in sections 3.2 and 3.3. The remaining suspension of the overnight culture was put in a 50 ml falcon tube and used as a positive growth control. The tube was situated in the incubator of the Axiovert 200 M microscope upon start of microscopic observation at 37 °C and 5 % CO_2.

3.5.3 Enzymatic system

BSA (bovine serum albumin; Sigma-Aldrich) combined with proteinase K (Proteinase K from Tritirachium album; Sigma-Aldrich) was used as model for an enzymatic system. As for the static systems (section 3.4), two different droplet types were produced, one type comprising only the substrate (type *b*) and the other the enzyme in addition (type *a*). Immediately after mixing the enzyme with the substrate, the mixture was drawn into a syringe and droplets were produced, collected, transferred and observed as described previously. The two aqueous phases consisted of a digestion buffer (30 mM Tris-HCl, pH 8, 10 mM $CaCl_2$, 0.02 mM BSA) with and without 10 µg/ml proteinase K, respectively. Activity of proteinase K was verified by a SDS-PAGE[3]-based digestion assay. Upon completion of the enzyme-substrate reaction, i.e. complete digestion of the substrate, whether in the droplet or in the syringe, the osmolarity of type *a* droplets was expected to be at least tenfold higher than the osmolarity of *b* droplets, since proteinase K cleaves BSA at dozens of sites (313 sites are listed in Ref. [159]).

3.6 Osmolarity of solutions

The osmolarities of YPD medium were measured five times each with a cryoscopic osmometer (Osmomat 030, Gonotec). To determine the osmolarity of depleted YPD media, water and ethanol were removed in vacuo at 80° C. The residue was resolved in an equal amount of distilled water.

[3] sodium dodecyl sulfate polyacrylamide gel electrophoresis

4 Image processing and data analysis

Micrographs of droplets were processed and analyzed by self-written routines, which relied on a Hough transform for the tracking of droplets. In this chapter, after a short introduction on the Hough transform in general, the working principle of both, the applied Hough transform and the routines used for droplet detection will be presented. Subsequently, the further processing of the gathered data, including the calculation of mean concentrations and volumes as well as the estimation initial radii, will be described.

4.1 Droplet detection by Hough transform

For the detection of the circular shape of droplets in the recorded micrographs and the determination of their radii, Matlab (MATLAB version 7 and version 8, The MathWorks Inc., 2010, Natick, Massachusetts, equipped with image processing and signal processing toolboxes) routines based on a Hough transform written by Tao Peng[160] were used. This algorithm detects geometric patterns in digital grayscale images by performing a voting procedure in a parameter space, the Hough or accumulator space, in which each point describes an instance of the geometric pattern.

The transform is named after Paul V. C. Hough, who invented the basic method in his patent "methods and means for recognizing complex patterns" in 1962[161], originally to recognize particle tracks in binary pictures obtained from a bubble chamber. He geometrically described a transform which maps colinear points in the image plane to intersecting straight lines in the "plane transform", the parameter space. The first algebraic description of this procedure was given by Azriel Rosenfeld in 1969[162], who also proposed the representation of the transform space as an array of counters, so that pixels lying on a straight line in the image give rise to a high array value. In 1972, Duda and Hart[163] published a modification of the transform for line detection, which circumvented some computational problems by choosing an alternative parametrization, and proposed a method for circle detection. This algorithm got generalized to the detection of lines[164] and circles in gray level images by Kimme, Ballard and Sklansky in 1975 [165], using gradient information to improve and accelerate detection. Since then, various improvements and modifications of the Hough transform have been made, al-

lowing to detect analytical and non-analytical shapes[166, 167] as well as 3-dimensional shapes[168].

The working principle of the method published by Kimme, Ballard and Sklansky[165], which is the basis of the Hough transform used in this work, will be sketched in the following paragraph.

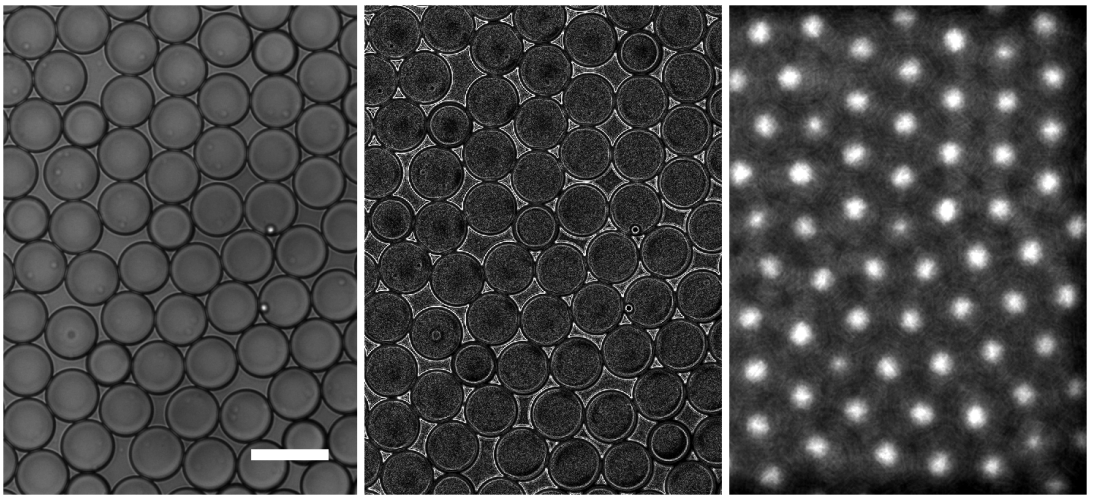

Figure 4.1: *(A) Right half of a micrograph showing a monolayer of droplets. Scale is 50 µm. (B) Absolute value of the gradient of the image shown in (A). (C) Parameter space for the image shown in (A) considering droplet radii from 12 µm to 25 µm. Bright pixels correspond to a high accumulator and indicate a potential candidate for a center of a circle, that is, of a droplet in (A).*

First, in a grayscale image (Figure 4.1 A), edge enhancement followed by thresholding for noise reduction is performed. The result is a black-and-white image with bright edges on dark background. The gradient information (direction and absolute value (Figure 4.1 B)) gained in the procedure of edge detection is used to later on to accelerate the algorithm and to detect the circles' radii.

In the second step, the binary image (Figure 4.2 A) is transformed into parameter space (also called Hough space) to find candidates for centers of circles (a_c, b_c) in the image. Since circles can be parametrized by the center coordinates (a, b) and the radius r, every circle is described by a point (a, b, r) in three-dimensional parameter space $\{a, b, r\}$. The radius r' of the circles searched for, or a range of radii $[r'_{\min}, r'_{\max}]$, has to be known in advance. Around a pixel (x, y) on an edge a (digitized) circle of radius r' is drawn, its circumference comprising the possible centers (a, b) of circles that run through the edge point (x, y) (Figure 4.2 B). For each point (a, b) an accumulator in parameter space at (a, b, r') is increased by unity (voting process) (Figure 4.2 B). This procedure is repeated for each edge pixel (x, y) in the binary image, resulting in high counts in the accumulation array if a circle of radius r' in the grayscale image is located at (a, b) (Figure 4.2 C). The resulting final accumulation array (Figure 4.1 C) is

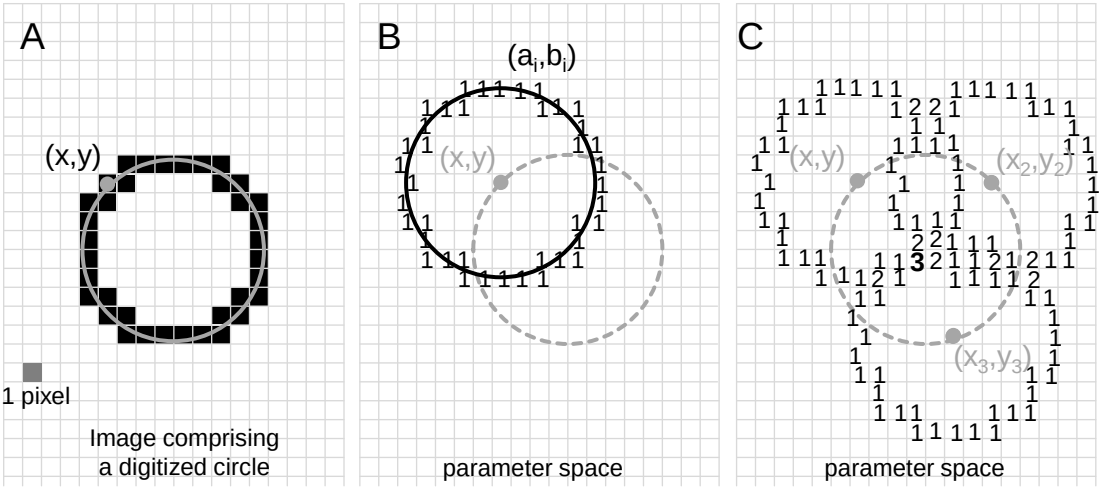

Figure 4.2: *Working principle of the Hough transform. (A) Schematic of a digitized circle of radius r in an binary image comprising an edge point (x, y). (B) Voting process in parameter space for the edge point (x, y) and a searched radius $r' = r$. In the accumulation array $\{a, b, r'\}$, counts of possible centers of circles (a, b) are increased by unity. (C) Repetition of the voting process for other edge points (x_j, y_j) leads to high counts at pixels (a, b) comprising a center of a circle in the grayscale image.*

smoothed and thresholded to obtain the candidates for the centers of circles as maxima of the accumulation array.If a range of radii is given, the procedure is repeated for every (digitized) r' in $[r'_{\min}, r'_{\max}]$. Since more points lie on the circumference of larger circles, accumulators for each r' have to be normalized by multiplying with $1/r'$ for the voting process. Subsequently, the radius of a circle at (a, b) can be estimated by picking the radius r' for which the accumulator at (a, b, r') is highest.

The Hough transform algorithm used in this work differs slightly from the previously described technique, mainly in the process of radius determination: First, a total accumulator array for all radii in $[r'_{\min}, r'_{\max}]$ is computed to find candidates for the centers of circles. Then, the radii for a located center are estimated by computing the maxima of a signature curve $s(r)$ of the radial gradient.

4.2 Tracking of droplets

The previously described Hough transform was embedded into a self-written Matlab routine determining centers and radii of microdroplets and tracking them over time in a sequence of images.

In order to optimize droplet detection, input parameters of the Hough transform were manually adjusted for each experiment. Visual feedback was provided by marking and numbering the detected centers and drawing the respective circles in micrograph.

Typically, values in the ranges of 5 - 8 for gradient threshold, 0.5 - 1 for concentric circles parameter and 20 - 35 for the radius of the smoothing filter were set. Minimum and maximum radii in pixels were chosen according to preliminary size measurements in ImageJ[169], considering droplet dimensions in initial and final state. Since the Hough transform is computationally intensive and a wider range of radii impairs the detection of circles, the radius range was chosen as small as possible, resulting in typical computation times of 20 - 90 s per image.

As shown in Figure 4.1 A, droplets exhibit a distinct boundary in bright field micrographs. The thickness and sharpness of this rim is caused by refractive effects and dependent on the position of the focal plane as well as the solute concentration inside the droplet. For analysis, only the outer radii of the droplets were considered, albeit the inner radii were detected as well (Figure 4.3). If more than two concentric circles per droplet were detected, only the two smallest radii were saved.

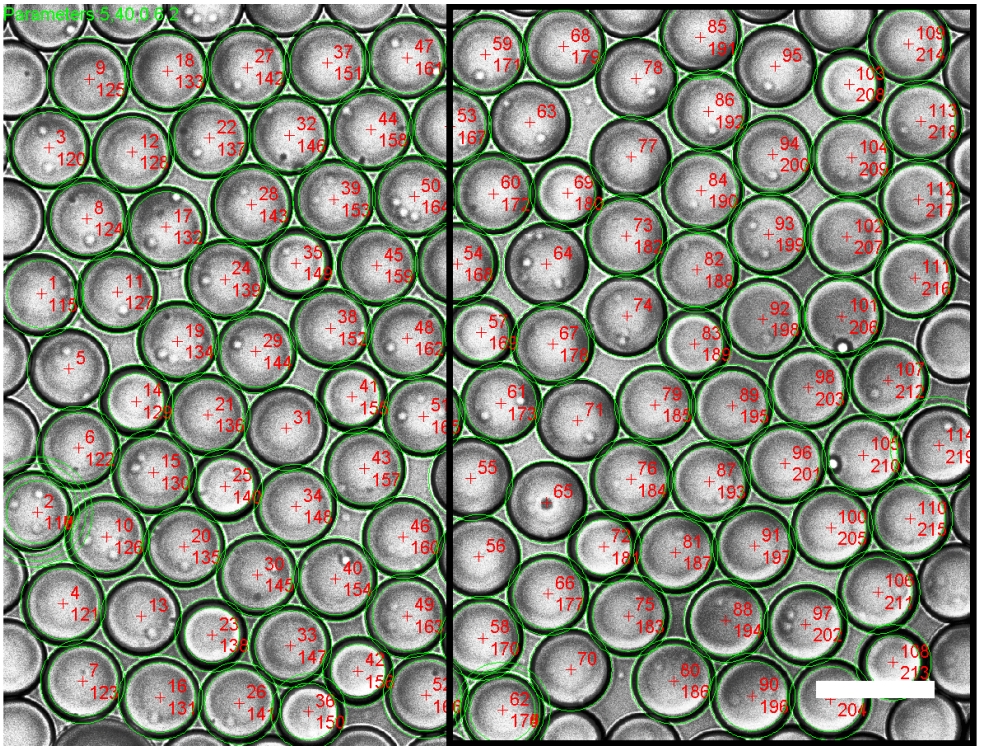

Figure 4.3: *Overlay of a bright field micrograph and the detected centers and radii of the circular shaped droplets. The section on the right is similar to the image shown in Figure 4.1 A. Usually, inner and outer radii of droplets were detected and marked separately. Scale is 50* µm.

To follow the size change of individual droplets over time, i.e. over different images of a time-lapse, a simple tracking technique was applied. Two droplets on images of consecutive points in time were identified with each other, if the center of a droplet lay in a circular droplet area of the previous point in time (or, if this condition was

not met, in the area of a droplet which was formerly detected at this position). This algorithm is capable to track individual droplets exhibiting moderate lateral drifting in a densely-packed monolayers of droplets.

Microdroplets were manually assigned to the different droplet types (high or low solute concentration) by means of their initial size and tracking number. Only droplets showing a minor amount of false radius detections in the course of the time-lapse or at least in initial and final state were selected. Quality of radius detection was verified for each droplet of one type by plotting its radius *versus* time.

An estimation of the relative frequencies of the different droplet types in the emulsion was obtained by counting the droplet numbers within the field of view at the beginning of the time-lapse.

4.3 Calculation of concentrations and data analysis

For droplets without an active entity inside, i.e. static systems, the amount of solute n_i does not change. Hence, the concentration of the solute in one droplet of the type $i \in \{a, b\}$ at the point in time t is given by

$$c^d_{i,t} = n_i / V^d_{i,t} = c^d_{i,0} \cdot V^d_{i,0} / V^d_{i,t} = c^d_{i,0} \cdot (r^d_{i,0} / r^d_{i,t})^3 \ , \tag{4.1}$$

with $r^d_{i,t}$ and $V^d_{i,t}$ being the radius and volume, respectively, of a single droplet at the time point t. The uncertainty of the determined radius was estimated to 0.5 µm, resulting mainly from refraction effects and the focal plane not being the equatorial plane of the droplets.

Hereafter, the droplet type comprising the higher solute concentration is referred to as droplet type a and the lower concentration type as droplet type b.

The mean droplet radii $r_{i,t}$, volumes $V_{i,t} = 4/3\pi\langle r^3\rangle$, and the corresponding mean concentrations $c_{i,t}$ of each droplet species were calculated, as well as the respective standard errors of the mean (s.e.m.). False detections of radii of single droplets which passed a manually set upper or lower radius threshold were not considered for calculation of the mean radius.

As the setup used did not allow for the measurement of droplet sizes immediately after production, a dead time, t_{dead} , of about 10 to 15 minutes from mixing the droplets to the start of a time-lapse had to be taken into account, in which the droplets already changed sizes.

Initial volume growth rates of both droplet types, $\Delta V_i/\Delta t$, were determined by linear regression of data obtained within the first 30 min and ranged from 5 to 300 fl/min, with relative uncertainties of about 10 %. For all type a droplets, the initial radius was calculated *via* linear extrapolation $r_{a,0} = [r^3_{a,0,measured} - 3/(4\pi) * (\Delta V/\Delta t) * t_{dead}]^{(1/3)}$,

resulting in a relative error in the order of 10 %.

Generally, errors of analytically derived parameters are calculated by error propagation, using $\Delta c/c = 0.01$, $\Delta r = 0.5$ µm, and the relative error $\Delta N/N = 0.1$. Latter results from truncated droplets at the boundary of the field of view. If standard errors and the errors of a single measurement were of the same order of magnitude, combined errors (sum of squares) were calculated. Unless mentioned otherwise, errors in Figures are combined errors.

Part III

Results and Discussion

5 Using droplets as sensors

As described previously (in chapter 2), heterogeneities in composition or, more precisely, in total osmolarity of microdroplets may give rise to water flux between droplets, driven by osmotic pressure.

This thesis presents a new method which exploits the associated size change of the droplets as an intrinsic and label-free marker for the total osmolarity of droplets. Thus, the droplets themselves can be applied as sensors for reactions changing the total osmolarity inside the droplets.

In this chapter, the basic principle of this novel, intrinsic sensor method will be presented first, and subsequently, a mathematical description of the volume changes will be given.

5.1 Operating principle of the sensor method

The sensor method basically relies on two kinds of aqueous microdroplets, a and b, in a densely packed water-in-oil emulsion, which, at some point t, differ in their total osmolarity, i.e. the total concentration of osmotically active solutes $c_{a,t}$ and $c_{b,t}$ (Figure 5.1). For simplicity, the total osmolarity, which is also known as osmotic concentration, will be referred to as concentration in this and the following chapters.

Such differences in concentration may be caused by reactions inside the droplets, e.g. metabolism of cells or catalytic activity of enzymes. As a result, an osmotic pressure between type a and b droplets builds up, which may be equilibrated either by diffusion of solutes or exchange of water by osmosis (see section 2.1.2). Depending on the nature of solutes, surfactants, and the continuous phase, solute transport can be inhibited and the interfaces of the droplets and the carrier oil serve as a semipermeable membrane which is only permeable to water, but not to solute molecules.

Consequently, water flows into droplets of higher concentration until the volume change compensates the initial osmotic pressure and equilibrium, $c_{a,e} = c_{b,e} = c_e$, is reached (Figure 5.1, Final state). As long as solute transport is prevented, the mechanism of water transfer (see section 2.1.2) due to osmosis is of no importance for the final state and only affects the dynamics of equilibration.

Finally, the differences in droplet size are exploited as a label-free marker for reactions changing the total solute concentration, and thereby for the activity of the encapsulated

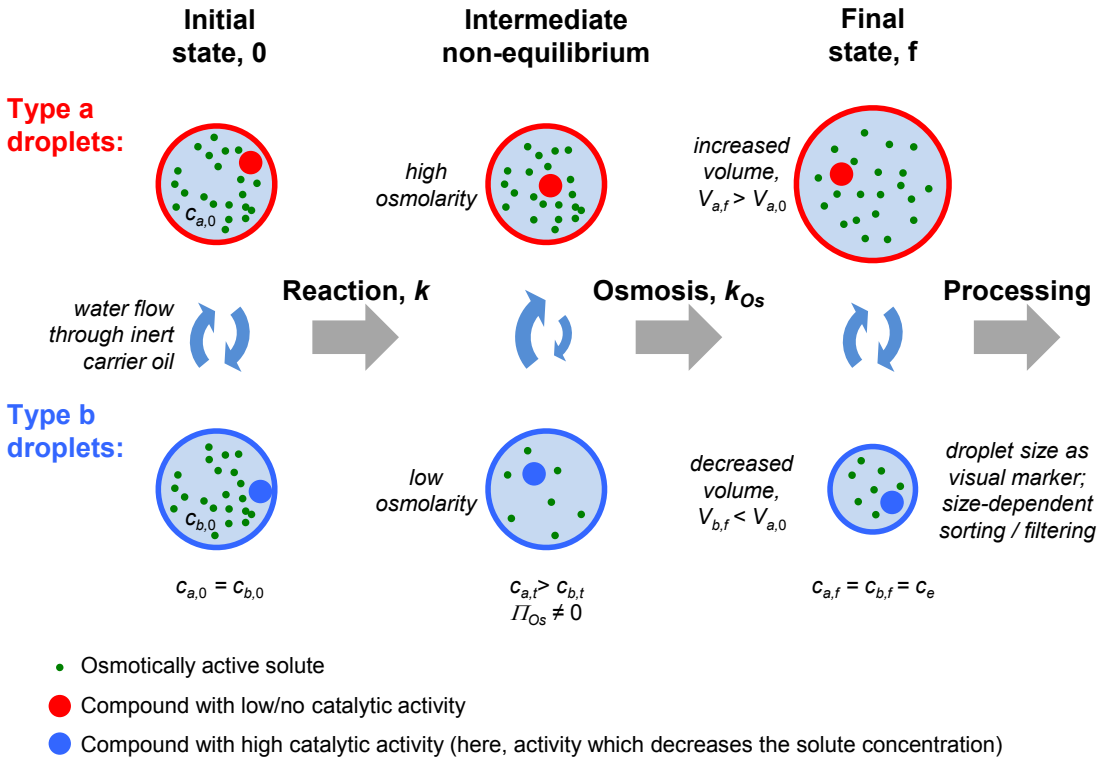

Figure 5.1: *Working principle of the droplet sensor method relying on osmotic pressure differences between two droplets. (Figure as published in Ref. [10])*

entities. A key advantage of the change in droplet size is that it not only acts as a visual marker, but also allows further physical "on-chip" processing, e.g. filtering or hydrodynamic size separation[53, 54, 170].

5.2 The equilibrium state

To calculate the size change of the droplet sub-populations a and b, osmotic pressure is considered the only driving force for mass exchange between the droplets. This assumption is legitimate for systems in which Ostwald ripening is negligible slow, and coalescence as well as transport of solutes is prevented by surfactants. Additionally, water is assumed being the only compound which can permeate from one droplet to the other (Figure 5.1).

Each of the two droplet types $i = a, b$ is characterized by initial concentration, $c_{i,0}$, initial mean droplet volume, $V_{i,0}$, and the number of droplets within field of view, N_i, which are taken as an estimate for the total numbers of droplets in the observation chamber. On the simplifying assumption that all droplets of one species behave similarly, a single droplet is described by the mean concentration $c_{i,t}$ and the mean droplet

volume $V_{i,t}$ of its droplet species at some point t. In the following, both concentration and volume of droplets are understood as the respective mean values.

The osmotic pressure $\Pi_{Os,t}$ between droplets of the two species can be estimated by van't Hoff's law for dilute solutions:

$$\Pi_{Os,t} \approx RT\Delta c_t = RT(c_{a,t} - c_{b,t})\,, \tag{5.1}$$

with R being the ideal gas constant and T the absolute temperature of the system.

To calculate the droplet volumes $V_{i,e}$ in the final equilibrium state in which the equilibrium concentration, $c_e = c_{a,e} = c_{b,e}$ is reached, conservation of mass (5.2) and conservation of the amount of solutes (5.3) have to be taken into account:

$$N_a V_{a,0} + N_b V_{b,0} = N_a V_{a,e} + N_b V_{b,e}\,, \tag{5.2}$$

and

$$V_{i,0} c_{i,0} = V_{i,e} c_e,\ i = a, b\,. \tag{5.3}$$

From (5.3) and the equality of equilibrium concentrations, $c_{a,e} = c_{b,e}$, follows the equivalence of the ratio of the relative equilibrium volumes of the droplet types and the ratio of the initial concentrations

$$\frac{V_{a,e}/V_{a,0}}{V_{b,e}/V_{b,0}} = \frac{c_{a,0}}{c_{b,0}}\,, \tag{5.4}$$

which is independent of N_i. Using equations (5.2) and (5.4), the droplet volumes in equilibrium state can be derived from the initial states:

$$V_{a,e} = \frac{N_a V_{a,0} + N_b V_{b,0}}{N_a + N_b \frac{V_{b,0}}{V_{a,0}} \frac{c_{b,0}}{c_{a,0}}} = \frac{\frac{N_a}{N_b} V_{a,0} + V_{b,0}}{\frac{N_a}{N_b} + \frac{V_{b,0}}{V_{a,0}} \frac{c_{b,0}}{c_{a,0}}}\,, \tag{5.5}$$

$$V_{b,e} = \frac{N_a V_{a,0} + N_b V_{b,0}}{N_a \frac{V_{a,0}}{V_{b,0}} \frac{c_{a,0}}{c_{b,0}} + N_b} \tag{5.6}$$

Hence, equilibrium volumes depend on the initial volumes of the droplet types, the ratio of initial concentrations, and the ratio of droplet numbers. Since the concentration of solutes in equilibrium is given by the ratio of total amount of solutes and total volume, one directly obtains

$$c_e = \frac{n_{tot}}{V_{tot}} = \frac{N_a V_{a,0} c_{a,0} + N_b V_{b,0} c_{b,0}}{N_a V_{a,0} + N_b V_{b,0}}\,, \tag{5.7}$$

independent of the dynamics which lead to equilibrium state.

The equations above provide the theoretical framework for the quantitative analysis of droplet sizes in equilibrium state. As the non-equilibrium states greatly depend

on the experimental system (see section 2.1.2), they will be discussed on basis of the experimental results, which are presented in the following chapter.

6 Characterization of the droplet sensors

Prior to the application of the sensor method to biological systems, consistency of experiments with theory has to be verified to facilitate quantitative analysis of the droplets sizes. To characterize the osmotically driven size change of droplets experimentally, mixtures of monodisperse droplet ensembles comprising various but fixed amounts of solute (sucrose or bromophenol blue) were used. Since fluorinated oils hinder the exchange of solutes between the droplets substantially (see section 1.1), a fluorocarbon oil was selected as continuous phase. The specific choice of both surfactant and oil type was motivated by their very frequent use in all kinds of microdroplet systems [13, 30, 47, 158, 32], rendering this experimental system most promising for future application.

In this chapter, first, stability of the microdroplet emulsion in the absence of osmotic pressure, a necessary condition for the droplet sensors, will be investigated. Subsequently, size change of droplets in the presence of osmotic pressure will be characterized by analyzing droplet sizes in equilibrium state as well as in non-equilibrium states. Finally, the sensitivity of the droplet sensor system will be addressed.

6.1 Stability of droplets

A crucial prerequisite for the application of the droplet sensor method is the stability of droplet sizes when all droplets comprise identical solute concentrations. This condition was difficult to reproducibly meet for droplets incubating in a PDMS device, whether saturated with water or not, since PDMS generally leads to a high dissolution rate of the droplets[28, 33, 142, 171, 172]. Therefore, incubation was performed in a gas-tight incubation chamber made of hydrophobic glass slides. Consequently, in the absence of an osmotic pressure, droplets situated within large, densely-packed droplet monolayers remained stable in size for several days to weeks. Even polydisperse emulsions with droplet radii ranging from 13 to 22 µm were stable in sizes for several days (Figure 6.1). This suggests that the difference in Laplace pressure between small and large droplets, which was in the order of 1 kPa[1], was not sufficient to induce measurable Ostwald ripening rates. These results are consistent with literature reporting that effects of

[1]The surface tension is $\gamma = 30$ mN/m at the oil-water interface (see section 3.2).

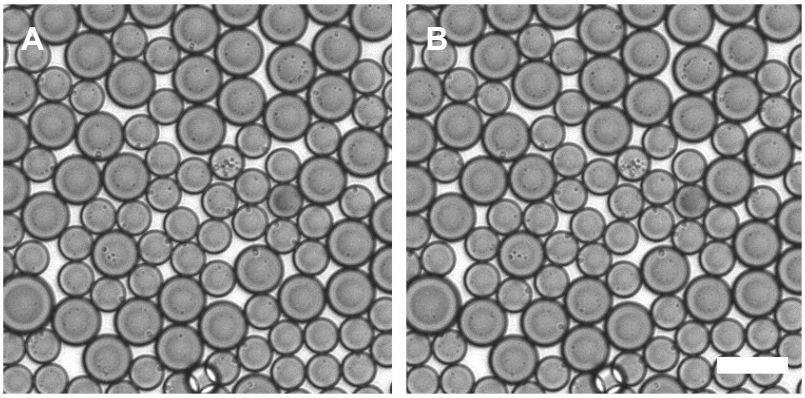

Figure 6.1: *Stability of droplets in absence of osmotic pressure. Polydisperse droplets comprising 20 mM bromophenol blue remain stable in size over 48 h (A: 0 h, B: 48 h). The mean of the relative size change of each droplet is* $\langle \frac{r_f}{r_i} \rangle = 0.996 \pm 0.04$ *(combined error). Scale is 50* μm.

Ostwald ripening in emulsions of this scale are very small[111]. While Ostwald ripening wasn't observed at all due to its slow process, and coalescence of droplets very rarely occurred[2] droplets in all experiments tended to form coherent clusters (Figure 6.2), an effect called flocculation. Within the monolayers, every droplet had at least one contact to another droplet, which only was released upon action of a force, induced e.g. by interaction with another droplet or lateral drifting (caused by buoyancy). Due to the non-adhesive nature of the surfactant, the weak attraction between droplets is suggested to be caused by depletion forces of excess surfactant in the oil, so-called depletion flocculation[173, 174].

In contrast, at the borders of densely-packed regions, droplet sizes rapidly decreased

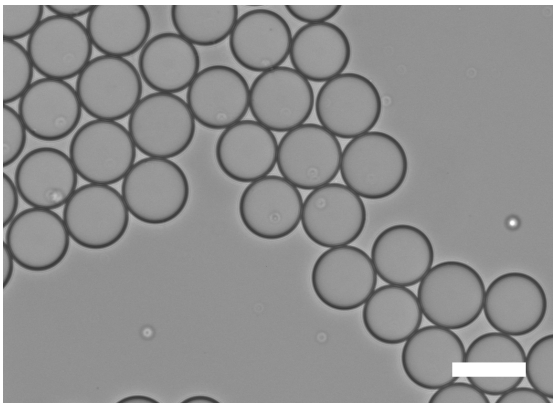

Figure 6.2: *Depletion flocculation of droplets. Within droplet monolayers, droplets without contact to other droplets are rarely observed. Scale is 50* μm.

[2]During incubation, less than 10 incidents were observed taken all experiments together, giving evidence for the good stabilization by the surfactant.

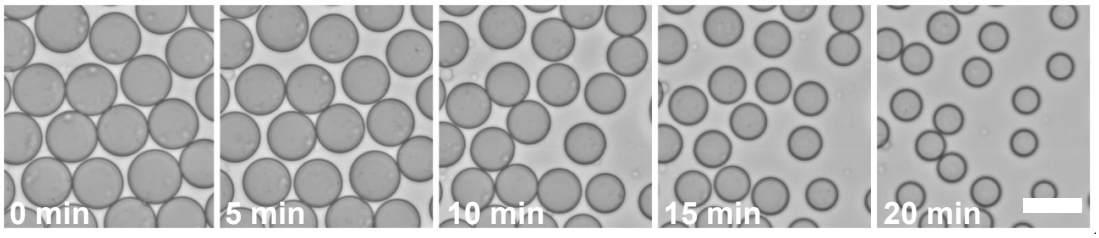

Figure 6.3: *Dissolution of droplets at the border of a droplet monolayer with time. Some droplets get stuck to the glass during dissolution process. Scale is 30 μm.*

with time. This effect was caused by dissolution of water molecules into the unsaturated oil (Figure 6.3). Within the densely-packed droplet regions, the high water-to-oil volume ratio rendered the volume loss of single droplets resulting from saturation of the oil phase negligible small. Hence, for all experiments described in the following sections, images were taken within the middle of a widespread droplet monolayer.

6.2 Size change of droplets driven by osmosis

Having confirmed the droplets' stability in the absence of osmotic pressure, size change of droplets in the presence of osmotic pressure was investigated. Non-equilibrium states (see Figure 5.1) were prepared by mixing two droplet types comprising different concentrations of sucrose. Initial concentrations of sucrose typically ranged from 100 to 800 mM, furthermore one experiment with smaller concentrations was performed in order to address the sensitivity of the system (Table 6.1). To easily distinguish between the two droplet populations, dissimilar initial radii were chosen in the majority of cases (Figure 6.4). As expected, droplets of higher initial osmolarity (type a) grew in size, whereas droplets of lower osmolarity (type b) shrank until equilibrium was reached (Figure 6.4 and Figure 6.5).

The emulsion was defined to be in equilibrium state as soon as mean droplet radii were apparently stable with time for the rest of the experiment. This "practical" definition does not necessarily imply that all droplets comprise the same solute concentration but that volume change rates are too small to be observed with the set-up used in this thesis. Consequently, non-vanishing concentration differences in the observed final state may simply result from the equilibrium state not having been reached yet.

As was shown in the previous chapter, the equilibrium state only depends on the set of initial parameters $(N_i, c_{i,0}, V_{i,0})$ of both droplet types a and b and is independent of the mechanism of water transfer as well as droplet arrangement. However, the latter play a crucial role for the dynamics of the system. Hence, in the following two sections, droplet sizes in equilibrium state and intermediate, non-equilibrium states will be analyzed separately.

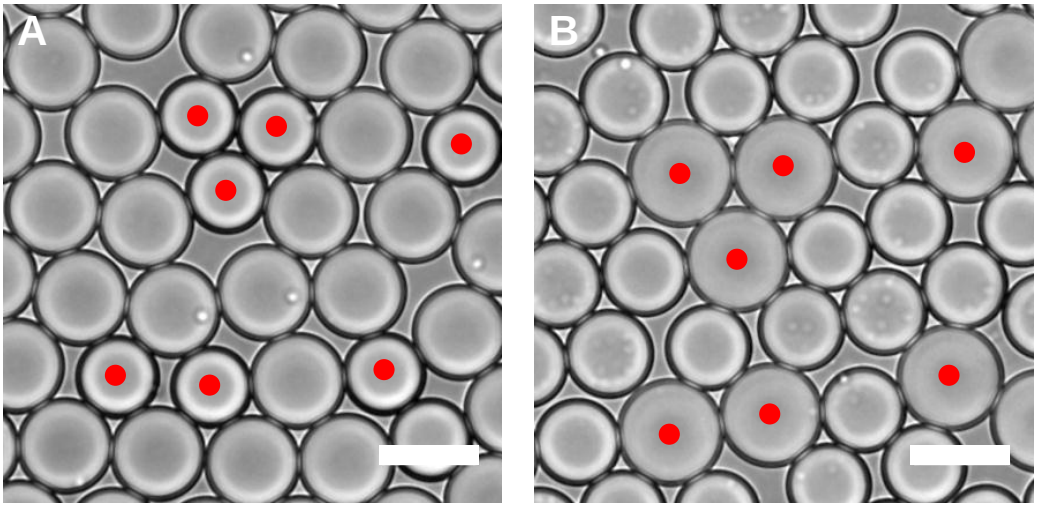

Figure 6.4: *Size change of droplets within a droplet monolayer in the presence of osmotic pressure. The micrographs show a droplet ensemble composed of two droplet types with initial concentrations of 300 mM (red in micrograph) and 100 mM sucrose in the initial (A) and equilibrated state (B, t = 26 h). Scale is 30 µm.*

6.2.1 Analysis of the equilibrium state

Usually, volume change of type a droplets was enhanced at the expense of the one of type b droplets by preparing droplet ensembles with an excess of droplets of type b (according to (5.5) and (5.6)). Consequently, in all experiments in which equilibrium state was reached, droplets of type a showed distinct size changes, whereas size changes of type b droplets were less pronounced (Table 6.1 and Figure 6.4). If initial radii were chosen equal, the size change unambiguously separated the two droplet types (Table 6.1 and Figure 6.6).

The experimentally obtained equilibrium radii agreed well with their theoretical predictions (Table 6.1). Consequently, the calculated equivalence (5.4) was also verified (Figure 6.7). In particular, in case only one droplet type contained sucrose and the other consisted of pure water, the former grew in size until the latter type vanished completely (Figure 6.8). Taken these results together, it was inferred that sucrose remains inside the droplets and neither partitions into the oil nor diffuses into other droplets (on the time-scale of the experiment).

The large errors of calculated equilibrium radii and concentrations are mainly attributable to the errors of the droplet numbers of the droplet types (10 - 15%) and a high uncertainty of initial droplet sizes, from which all concentrations $c(t)$ as well as the equilibrium radii were deduced (see section 4.3). The latter resulted from the fact, that the set-up didn't allow for the measurement of droplet sizes right after droplet production (see section 3.2). Droplet radii were first determined after a certain dead time needed to collect and transfer the droplets, seal the incubation chamber, and start

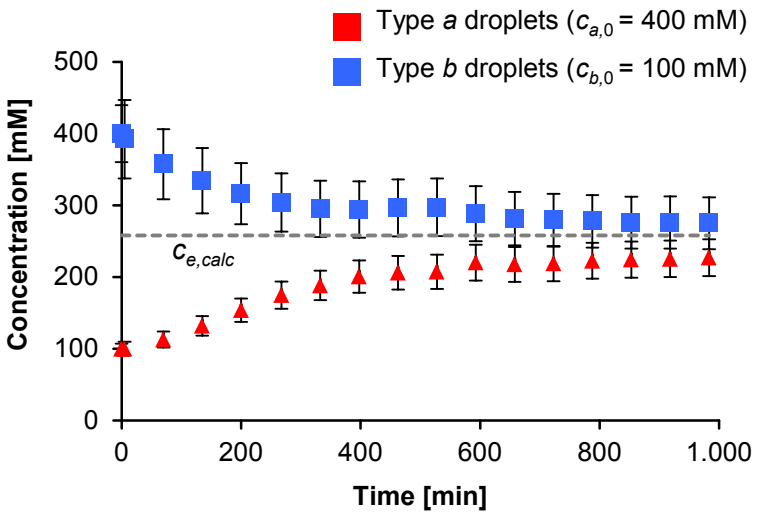

Figure 6.5: *Example for the time development of mean sucrose concentrations in both droplet ensembles due to the droplets' volume changes ($c_{a,0} = 400\ mM, c_{b,0} = 100\ mM$). The size change compensates for the osmotic pressure until equilibrium state is reached. The calculated equilibrium concentration is $c_e = 258 \pm 40\ mM$. (Figure as published in Ref. [10])*

observation. During this time, particular type a droplets already changed sizes by a few microns. Based on the size change of droplet volumes $V_a(t)$ within the first minutes of observation, a linear extrapolation was applied to estimate the initial radii of type a droplets at droplet production (see section 4.3). The calculated initial radii provided an upper boundary for the real initial radii of type a droplets for two reasons.

First, inferring from the work of Wen and Papadopoulos[96] and others[122, 92, 104], all types of water transfer mechanisms exhibit constant or decreasing water transfer rates for decreasing concentration differences. As the concentration difference between the droplet types decreased with time, volume change rates during the dead time were equal to or higher than the later observed rate used for the extrapolation.

Second, in analogy to the results presented by Gruner et al. [32] for diffusion-driven solute transport between droplets, the three-dimensional arrangement of droplets during collection in the pipette tip enhanced the size change of the droplets compared to the two-dimensional arrangement in the incubation chamber.

Hence, the extrapolation underestimated the unobserved size change and, accordingly, overestimated the initial volume of type a droplets. Since the volume $V_{a,e}(V_{a,0})$ (as a function of $V_{a,0}$) is strictly increasing and $V_{b,e}(V_{a,0})$ strictly decreasing for $V_{a,0} > 0$ and $c_a > c_b$ (see Appendix A.2), an overestimation of $V_{a,0}$ results in the experimental equilibrium volume $V_{a,e}$ being smaller than theoretically predicted, whereas $V_{b,e}$ tends to be larger than calculated. Indeed, the experimental data presented in Table 6.1 shows those very deviations from theory.

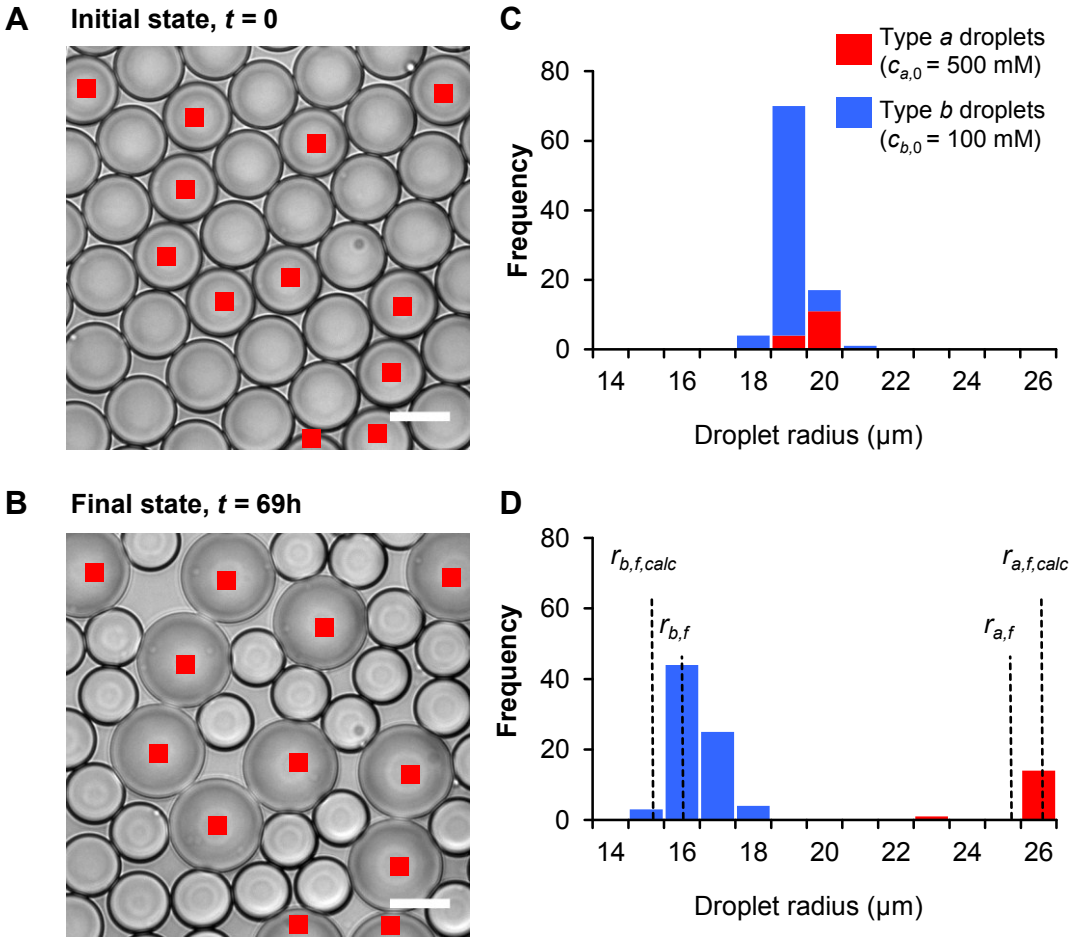

Figure 6.6: *The osmotically driven size change separates the two droplet types a ($c_{a,0}$ = 500 mM sucrose) and b ($c_{b,0}$ = 100 mM sucrose), if initial radii are chosen equal. Micrographs of the ensemble at the beginning (A) and at equilibrium (B). Scale is 30 µm.*
(C and D) Histograms show the measured distribution of the radii at both time points (mean values $r_{a,f} = 25.4 \pm 0.2$ µm and $r_{b,f} = 16.0 \pm 0.1$ µm) along with the calculated radii for the final state ($r_{a,f,calc} = 26.4 \pm 2.6$ µm, $r_{b,f,calc} = 15.3 \pm 1.5$ µm). (Figure as published in Ref. [10])

Moreover, deviations are found to increase with increasing initial concentration difference (see also Figure 6.7), which corresponds to an increasing overestimation of initial sizes of type *a* droplets with increasing concentration difference.

In addition to the previously described reasons, this effect may originate from the increase of the refractive index of sucrose solutions with concentration[175]. The higher the sucrose concentration and the refractive index of the dispersed phase, the broader (and blurrier) is the appearance of the interfaces of droplets in micrographs (Figure 6.9), and the larger are the detected radii. This effect could not be eliminated computationally, since the level of the focal plane influences the width of the borders as well. Detection of radii for sucrose concentrations higher than 400 mM was noticeably

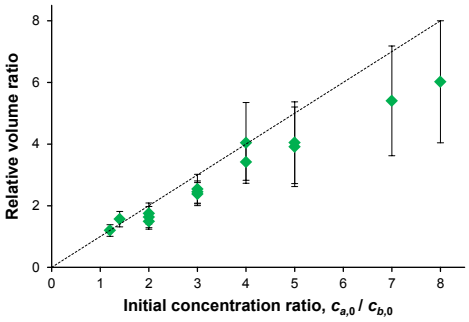

Figure 6.7: *The ratio of the relative volumes shows the predicted equivalence to the ratio of the initial concentrations (see equation (5.4)) in 15 experiments (see Table 6.1), demonstrating the good agreement of experimental results with theory.*

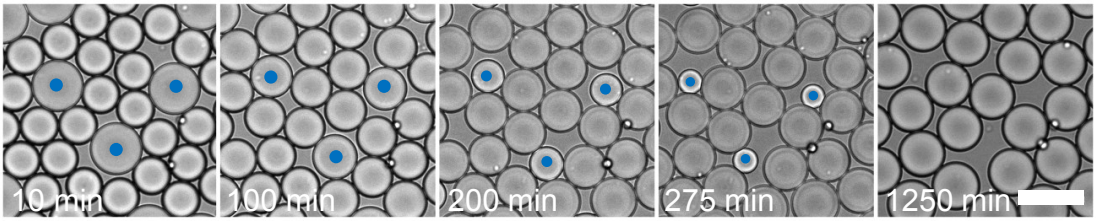

Figure 6.8: *Size change of droplets initially comprising 400 mM sucrose (type a) and pure water (type b, blue) with time. The droplets without sucrose shrink rapidly and finally dissolve completely, proving that sucrose remains inside of the type a droplets. Scale is 50* µm.

impaired by this thickening, entailing an overestimation of the droplets' radii (by up to 1 micron) at the beginning of experiments. As type *a* droplets grew in size and the comprised concentration decreased, the interfaces became sharper, partly compensating for the droplets growth and decreasing the apparent volume change rate. Therefore, for higher solute concentrations, initial type *a* radii calculated by extrapolation increasingly differ from the actual initial radii. It is noteworthy, that for sucrose concentrations equal to or higher than 400 mM (in droplet type *a*), differentiation between droplet types based on the width of droplet borders was possible (see Figure 6.6 A).

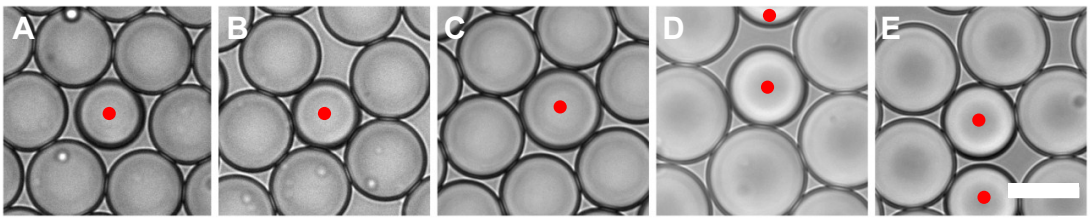

Figure 6.9: *Sucrose concentrations of droplets affect the width of the droplet borders in micrographs, and thus the detection of droplet sizes. The micrographs show type a droplets comprising 800(A), 700(B), 500(C), 400(D) and 300(E) mM sucrose (marked red) in between type b droplets (100 mM). Scale is 30* µm.

Table 6.1: *Experimentally obtained and theoretically predicted final radii, $r_{i,f}$ and $r_{i,f,calc}$ respectively, for the initial conditions used in experiments with droplets comprising sucrose. $c_{i,0}$ is the initial concentration of sucrose, N_i the number of droplets, and $r_{i,0}$ the initial radius of the droplet types a and b, respectively. The relative error of the calculated final radii is 10 %. * : $r_{a,0}$ is estimated via extrapolation, as described in section 4.3, and exhibits a relative error $\Delta r_{a,0}/r_{a,0} = 10$ %. **: Equilibrium state was not reached after 43 h of incubation.*

$c_{a,0}$ [mM]	$c_{b,0}$ [mM]	N_a [1]	N_b [1]	$r_{a,0}$* [µm]	$r_{b,0}$ [µm]	$r_{a,f}$ [µm]	$r_{a,f,\mathrm{calc}}$ [µm]	$r_{b,f}$ [µm]	$r_{b,f,\mathrm{calc}}$ [µm]
2.5	0.01	14	86	15.7±0.3	20.0±0.1	15.9±0.3**	37.0**	19.0**	7.5**
120	100	13	77	17.0±0.1	21.2±0.1	18.0±0.1	18.0	21.0±0.1	21.1
140	100	16	78	16.7±0.1	20.9±0.1	18.2±0.1	18.5	19.6±0.1	20.6
200	100	76	59	16.2±0.1	19.7±0.1	17.3±0.1	18.2	18.4±0.1	17.6
200	100	127	59	13.1±0.1	18.4±0.1	14.4±0.1	14.6	16.8±0.1	16.3
200	100	36	135	12.4±0.1	15.5±0.1	14.2±0.1	15.0	15.1±0.1	14.9
300	100	41	70	17.2±0.1	20.5±0.1	20.5±0.1	21.6	18.2±0.1	17.9
300	100	61	38	19.1±0.2	22.7±0.1	21.5±0.1	21.9	18.8±0.1	18.0
300	100	56	117	14.5±0.1	16.7±0.1	17.8±0.1	18.4	14.9±0.1	14.7
300	100	13	122	12.9±0.1	17.4±0.1	17.6±0.1	18.2	16.6±0.1	16.9
400	100	115	34	15.3±0.1	22.2±0.1	17.3±0.1	17.7	16.7±0.1	16.2
400	100	15	66	17.7±0.2	20.9±0.1	25.4±0.1	25.3	18.8±0.1	18.8
500	100	15	115	15.4±0.1	18.0±0.1	22.2±0.2	24.1	16.8±0.1	16.4
500	100	25	110	18.6±0.1	18.5±0.1	25.4±0.2	26.4	16.0±0.1	15.3
700	100	14	119	15.7±0.1	18.2±0.1	24.2±0.1	26.7	16.8±0.1	16.2
800	100	8	129	15.4±0.3	17.8±0.1	26.7±0.2	28.4	17.0±0.3	16.4

6.2.2 Non-equilibrium dynamics

In all experiments the droplets' size change compensated for the osmotic pressure until eventually, after 10 to 40 hours, equilibrium state was reached. However, the dynamics of equilibration differed considerably. In this section, intermediate states will be analyzed to provide insight into the underlying molecular mechanism of water transport and the impact of droplet arrangement on the equilibration process.

Water transport mechanism

In contrast to equilibrium state, the predominating molecular water transfer mechanism plays a crucial role for the size of droplets in intermediate states, affecting speed and course of the droplets' size change. To narrow down the prevailing transport mechanisms (see subsection 2.1.2), the imperative of contact of droplets to induce a size change was subjected to investigation. In most experiments, the contact pattern

among droplets changed continuously during the experiment due to the droplets' volume changes or motion of the droplets (see section 3.3). Thus, it was difficult to separately analyze size changes of contacting droplets, and non-contacting but neighboured droplets.

In one single experiment, however, few isolated droplets of high sucrose concentra-

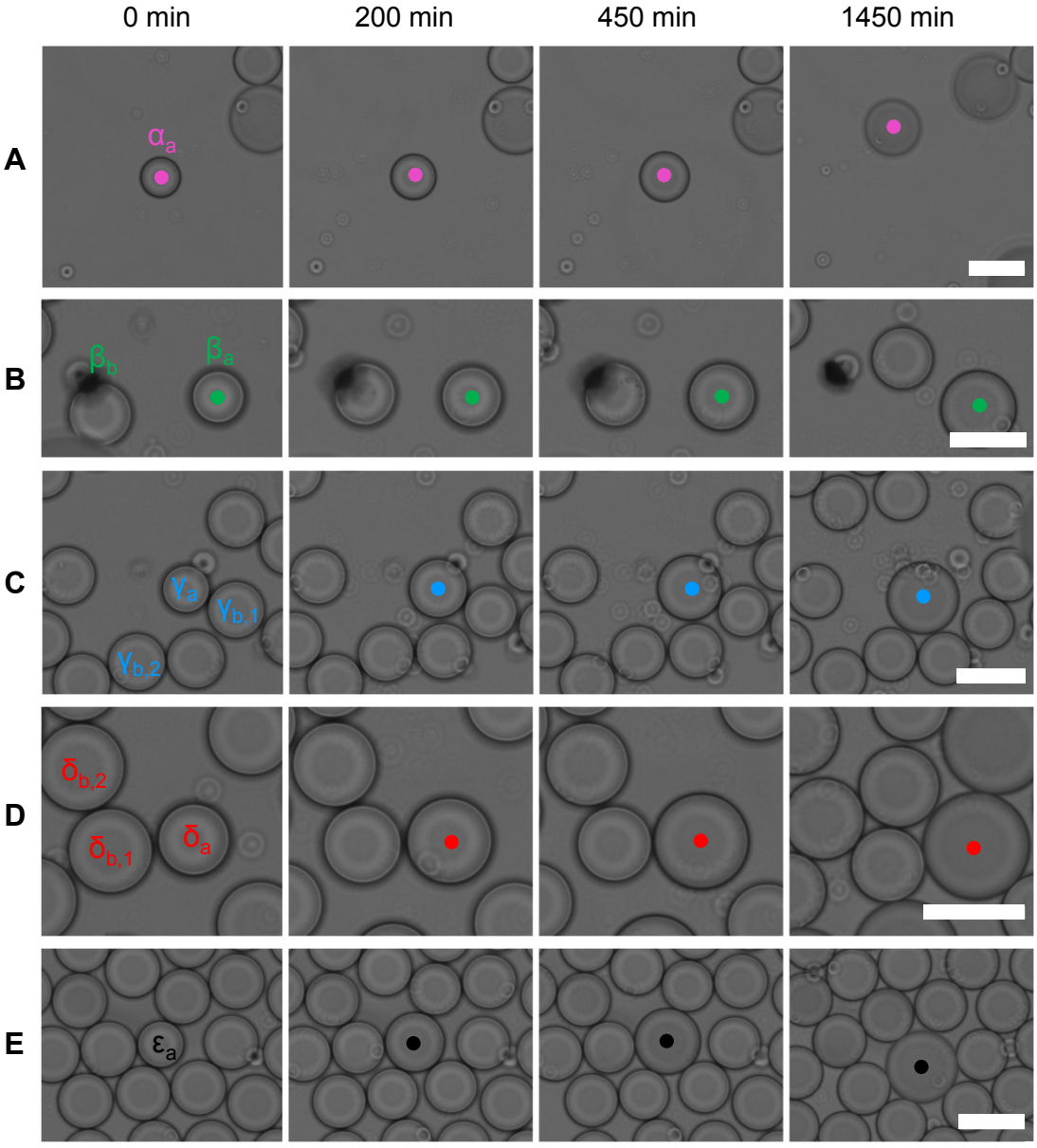

Figure 6.10: *(A-E) Series of micrographs showing the size change of contacting and non-contacting droplets of dissimilar concentrations with time. (A) and (B) give evidence for water transport by reverse micelles or single molecule diffusion. Droplets comprising 500 mM sucrose (type a) are marked and named α_a, β_a, γ_a, δ_a, and η_a, respectively. Selected droplets comprising 100 mM sucrose (type b) are named β_b, $\gamma_{b,1}$, $\gamma_{b,2}$, $\delta_{b,1}$, and $\delta_{b,2}$. Scale is 30 µm. Note the differing scale lengths.*

tion (500 mM, type a) were situated in gaps within a large droplet cluster. Although no contacts to other droplets were present during the whole experiment those droplets grew considerably in size (Figure 6.10 A, B and Figure 6.11 A). Isolated droplets of lower solute concentration (100 mM, type b) and those at the borders of a droplet cluster shrank slightly (Figure 6.10 B and Figure 6.11 B, droplet β_b). The volume decrease of such a single type b droplet over the period of observation was about ten times smaller than the volume increase of the high concentration droplets ($\Delta V_{\beta_b} = -3.4 \pm 1.5$ pl *versus* $\Delta V_{\beta_a} = 46 \pm 3$ pl, see Figure 6.11). Consequently, water transfer was mediated by diffusion of either reverse micelles or single water molecules from multiple type b droplets. Type b droplets which were only surrounded by droplets of the same type remained stable in size, suggesting that they were shielded by their neighbours.

When a pair of droplets of high and low solute concentration was in visual contact, shrinkage rates of type b droplets during the first 200 minutes were approximately ten times larger than those of the isolated droplet $\beta_{b,1}$ (Figures 6.10 C, D and 6.11 B). This was revealed by a linear fit of the radii of the droplets $\gamma_{b,1}$, $\delta_{b,1}$, and β_b within the first 200 minutes, which resulted in a slope of $s(\gamma_{b,1}) = 0.005 \pm 0.001$ µm/min and $s(\delta_{b,1}) = 0.006 \pm 0.001$ µm/min (contacting case, Figure 6.11 A), and a slope of $s(\beta_b) = 0.0006 \pm 0.0002$ µm/min (separated case, Figure 6.11 B).

On the other hand, initial growth rates of the type a droplets did not increase significantly on visual contact (Figure 6.11 C, D) compared to the droplet β_a and by about a factor of two compared to the droplet α_a, which was situated in a larger gap of the droplet cluster. Growth rates were maximal when several type b droplets contacted a type a droplet (Figure 6.10 E and 6.11 A).

One possible explanation for those enhanced rates of size change is a dependence of water transport by reverse micelles on the droplets' separation distance, that is, the thickness of the oil membrane. Alternatively, they are evidence for a new water transfer mechanism, the diffusion of hydrated surfactants (see section 2.1.2).

The time-scale of water transport *via* hydrated surfactants was reported to be much shorter compared to transport by reverse micelles[96, 94, 95] (see section 2.1.2). Thus, if the water transfer between contacting droplets was predominantly mediated by the diffusion of hydrated surfactants, the absolute rates of size change of droplets were expected to be significantly higher than in the non-contacting case. However, even when a type a droplet only had contact to a single type b droplet, a mere 15% of the total volume change of the type a droplet was compensated by the volume change of the type b droplet (Figure 6.11 γ_a and $\gamma_{b,1}$, and δ_a and $\delta_{b,1}$). This implied that other, non-contacting droplets also contributed to the growth and time-scales of the processes didn't significantly differ. Thus, transfer in reverse micelles or single molecule diffusion are likely to be the prevailing mechanisms for both, contacting and non-contacting case.

In case diffusion in the oil was the process limiting the water transfer rates, these results could be explained by means of a solution-diffusion mechanism. According to this model, the flux of water through the oil membrane is exclusively driven by a concentration gradient ($J \propto \Delta c/l$, membrane thickness l, see section 2.1.2). With decreasing separation distance between the droplets, i.e. a thinning of the membrane, the concentration gradient steepens and thus, water flux increases[92]. Accordingly, droplets in proximity of a high concentration droplet were expected to exhibit larger shrinkage rates than droplets in larger distance.

However, recent work of Wen and Papadopoulos[96, 95] and Pena[110] suggest that both transport mechanisms, reverse micelles and hydrated surfactants, are not diffusion-limited but controlled by processes at the droplet interfaces. As a consequence, transport may not be modeled accurately by the solution-diffusion mechanism. Indeed, Wen and Papadopoulos reported shrinkage rates of isolated, non-contacting water droplets to be constant and independent on the droplets' distance[95]. Due to the lack of data of isolated droplet pairs separated by various distances, no definite conclusion can be drawn at this point.

For the few isolated droplets and droplet pairs observed, a sound investigation of the dependence of water transfer rate on the difference in solute concentration was not possible, since various concentration differences prevailed between the type a droplet and diverse non-contacting droplets. Thus, a droplet arrangement allowing for the deduc-

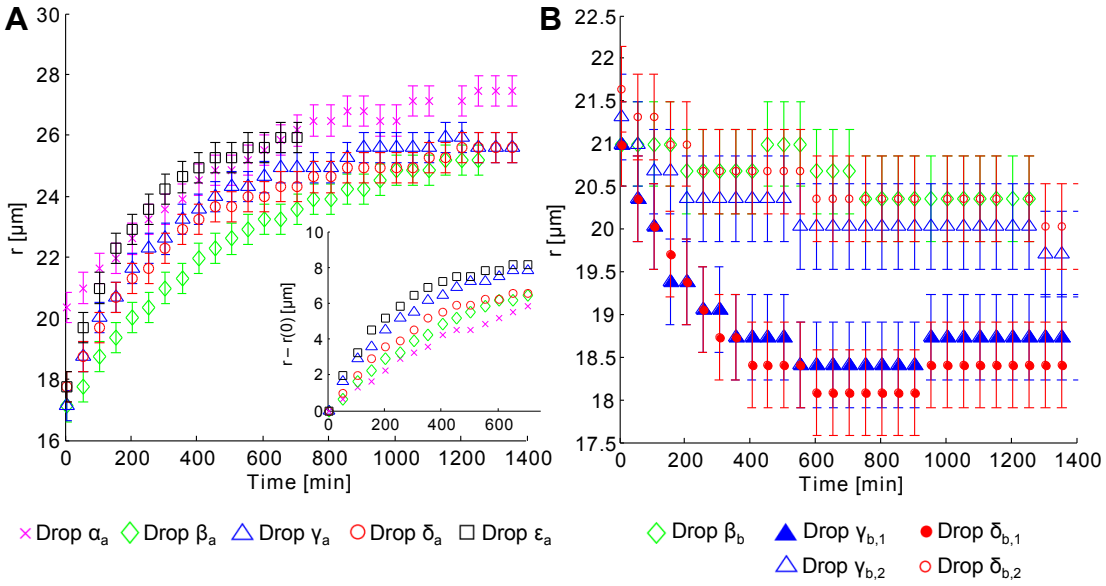

Figure 6.11: *(A) Increase of sizes of type a droplets shown in Figure 6.10 with time. Inlay: Absolute increase of the respective radii with time. (B) Shrinkage of type b droplets shown in Figure 6.10 with time. Non-contacting droplets (empty markers) exhibit smaller shrinkage rates than contacting droplets (filled markers). Errors are errors of a single measurement,* $\Delta r = 0.5$ *µm.*

tion of a well-defined osmotic pressure is a crucial prerequisite for further investigations on the relationship between water transfer rates and solute concentration differences. As will be seen in the following sections, this condition is met by certain conformations of droplets in a densely-packed droplet monolayer.

Impact of droplet arrangement

In densely-packed droplet monolayers, the direct neighbourhood of a single droplet was observed to play a crucial role for the change of its volume: Droplets which were surrounded only by droplets of the opposing type changed sizes rapidly, whereas a droplet among droplets of the same type grew or shrank slowly and growth rates of droplets in a mixed arrangement lay in between those extremes (Figure 6.12). Thus, discrepancies in the time course of mean concentrations of one droplet type between different experiments resulted not only from dissimilar droplet numbers, volumes, and concentrations, but also from the arrangement of droplets.

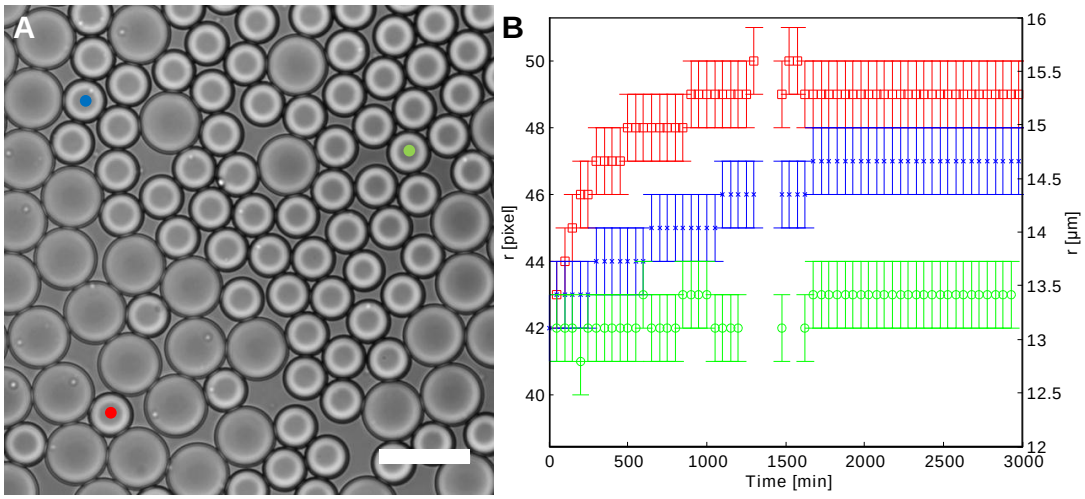

Figure 6.12: *Impact of droplet arrangement on the size change of individual droplets. (A) In initial state, the droplet ensemble is composed of droplets comprising 200 mM (type a) and 100 mM (type b) sucrose. Scale is 50 µm. (B) Size change of three individual type a droplets differing in the amount of directly neighbouring droplets of type b. Errors are errors of a single measurement, $\Delta r = 0.5$ µm.*

To follow the flux of water in a densely-packed droplet layer, size changes of droplets in regions in which one single droplet of type a was surrounded by multiple layers of droplets of type b were analyzed (Figure 6.13 A, B). Because of its high symmetry and no or few further interfering type a droplets, this arrangement allowed for the classification of type b droplets into directly contacting neighbours (type I), second next neighbours (type II, contact to two type I droplets), third next neighbours (type III, contact to one type I droplet) and droplets farther away from any type a droplets

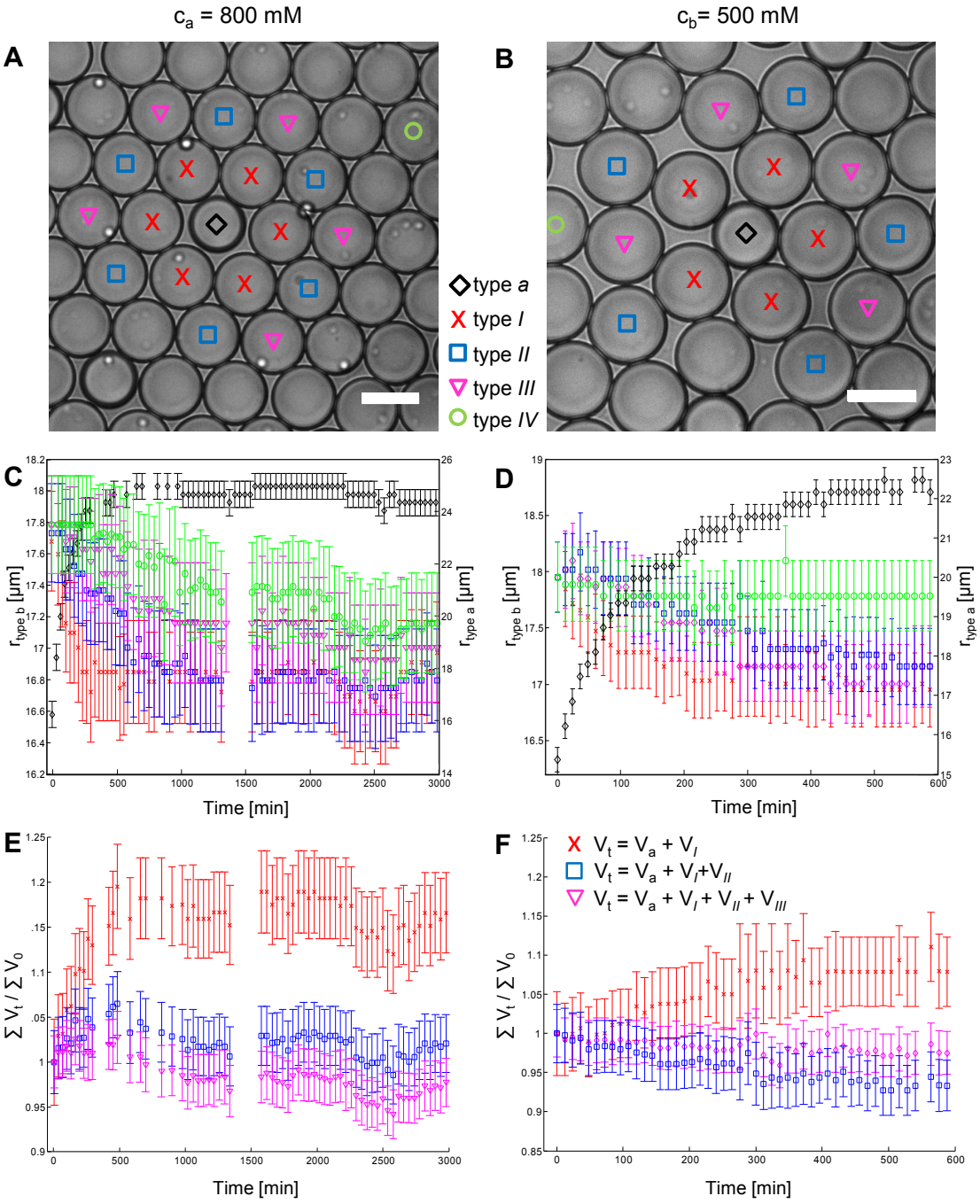

Figure 6.13: *In a densely-packed droplet arrangement, water is primarily transferred between contacting droplets. (A and B) Micrographs of two type a droplets with c_a = 800 mM (A, left column) and c_a = 500 mM (B, right column) surrounded by two layers of type b droplets (100 mM) in the initial state. Neighbouring type b droplets are assigned to classes (I,II,III,IV) according to their distance to the central type a droplet. Some type IV droplets are situated outside of the field of view. Scale is 30 µm. (C and D) Development of the sizes of the type a droplets and the neighbouring droplets with time. (E and F) Total volumes of a type a droplet and all typeI droplets, (red), additionally all type II droplets (blue), and additionally all type III droplets (magenta) normalized by the respective initial sum of total droplet volumes versus time.*

(type IV) (Figure 6.13 A, B). Within a class, all droplets behaved almost similar, despite the droplets' size change altering the organization of the neighbours slightly during the course of the experiments.

Mean radii and corresponding concentrations developed as expected, presuming droplets predominantly interact with their direct neighbours and water transport rates increase with increasing concentration differences: In the beginning, droplets in direct contact (type I), which were subjected to a high osmotic pressure, shrank immediately and most rapidly, whereas droplets of the other classes with initially similar solute concentrations decreased more slowly in size (Figure 6.13 C, D). As a consequence of the shrinkage of type I droplets, solute concentrations of type I droplets and type II droplets differed, and the latter started to shrink as well, which in turn caused shrinkage of droplets of type III. The droplets of type IV, which were farthest away from the central droplet, didn't show any size change within the first few hundreds of minutes. When the concentration difference between type a droplet and direct neighbours (type I) became smaller, their shrinkage rate decreased, while the size change of the other droplet classes persisted. In the end, concentration differences between contacting droplets gradually vanished as the radii of droplets of type I, II, and III converged to the equilibrium radius[3] (Figure 6.13 C, D). The graded size change of the droplet classes confirms water being predominantly transferred between very next neighbours. Long ranged transport of water plays a negligible role in densely-packed droplet layers. This is a consequence of the very dense packing, since diffusing reverse micelles or single molecules are likely to be absorbed or at least hindered by the direct neighbours.

As water transport is mediated by the diffusion of reverse micelles or single molecules, distant droplets may also contribute to the growth of the type a droplet (see section 6.2.2). To investigate to which extend the growth of the type a droplet is compensated by the shrinkage of droplets in its direct vicinity, the total volume of the type a droplet and all type I droplets (normalized by the initial total volume) was calculated for each point in time (Figure 6.13 E, F). In case of the 500 mM droplet, the total volume was conserved during the first 100 minutes and then increased, suggesting that other droplets also contributed to the growth of the type a droplet (Figure 6.13 F). In the 800 mM case, the total volume increased immediately (deviating from one by 5% after 50 minutes) (Figure 6.13 E). When the volumes of second next and third next neighbours were considered as well, the normalized sum of the considered droplet volumes was in good approximation equivalent to unity (Figure 6.13 E and F). As a consequence of other type a droplets in vicinity being also supplied by some of the type b droplets,

[3] In the case of $c_a = 500$ mM (Figure 6.13 D), equilibrium state had not been reached yet after 600 minutes, as the radii of droplets of type IV and droplets of the types I,II and III still differed.

the total volumes continuously decreased slightly. Stability of total volumes implied that the type a droplet's growth was almost completely fueled by shrinkage of its direct neighbours (type I) (Figure 6.13 E, F). Consequently, the uptake of water from the continuous phase, which was supplied by droplets farther away (as observed in section 6.2.2) plays a negligible role in densely-packed droplet arrangements. Therefore, for very early points in time, growth dynamics of droplets in good approximation solely depend on the arrangement of direct neighbours (i.e. type and number of droplets). In particular, the initial growth rates of different type a droplets surrounded exclusively by type b droplets are rendered comparable, independent of droplet organization at longer distances. On a longer time-scale, long-range organization of droplets has to be considered.

As reported by Skhiri and Gruner et al. [32], the spatial organization of droplets determines the equilibration time-scale of solutes in an emulsion which contains droplets with two initially differing concentrations. Deviations from a perfectly alternating droplet pattern, for which relaxation is the fastest, may prolong the equilibration process by several orders of magnitude.

Some minor modifications taking the droplets' size changes into account would be necessary to quantitatively simulate the equilibration by water transfer. Thus, the unmodified model here provides only qualitative insight into relaxation kinetics. Since frequencies of type a and b droplets varied from experiment to experiment, the dependence of the time-scale of equilibration on droplet arrangement was only qualitatively verified within this work. For example, two experiments with $c_a = 500, c_b = 100$, and approximately the same droplet frequency ratio differed considerably in the period after which equilibrium state was reached (1000 minutes, and 2500 minutes).

While the arrangement of droplets controls the dynamics of water transfer on the population (mesoscopic) level, water transfer on microscopic level is dictated by the predominating transfer mechanism (see section 2.1.2). Of particular importance for the equilibration process is the dependence of water transfer rates on concentration differences, which will be quantified in the next section.

Dependence of water transport rates on differences in solute concentration

To determine the dependence of water transport rates on differences in solute concentration between droplets within a densely-packed monolayer, the size changes of the droplets of type a and I (Figure 6.13 A, B) were further analyzed.

Since all direct neighbours (type I) showed the same growth behaviour and comprised a similar concentration of sucrose at every point in time, the concentration gradient driving the size change of the type a droplet is well-defined as $\Delta c(t) = c_{a,t} - c_{I,t}$. Figure 6.14 shows the development of $\Delta c(t)$ for both type a droplets shown in Figure 6.13.

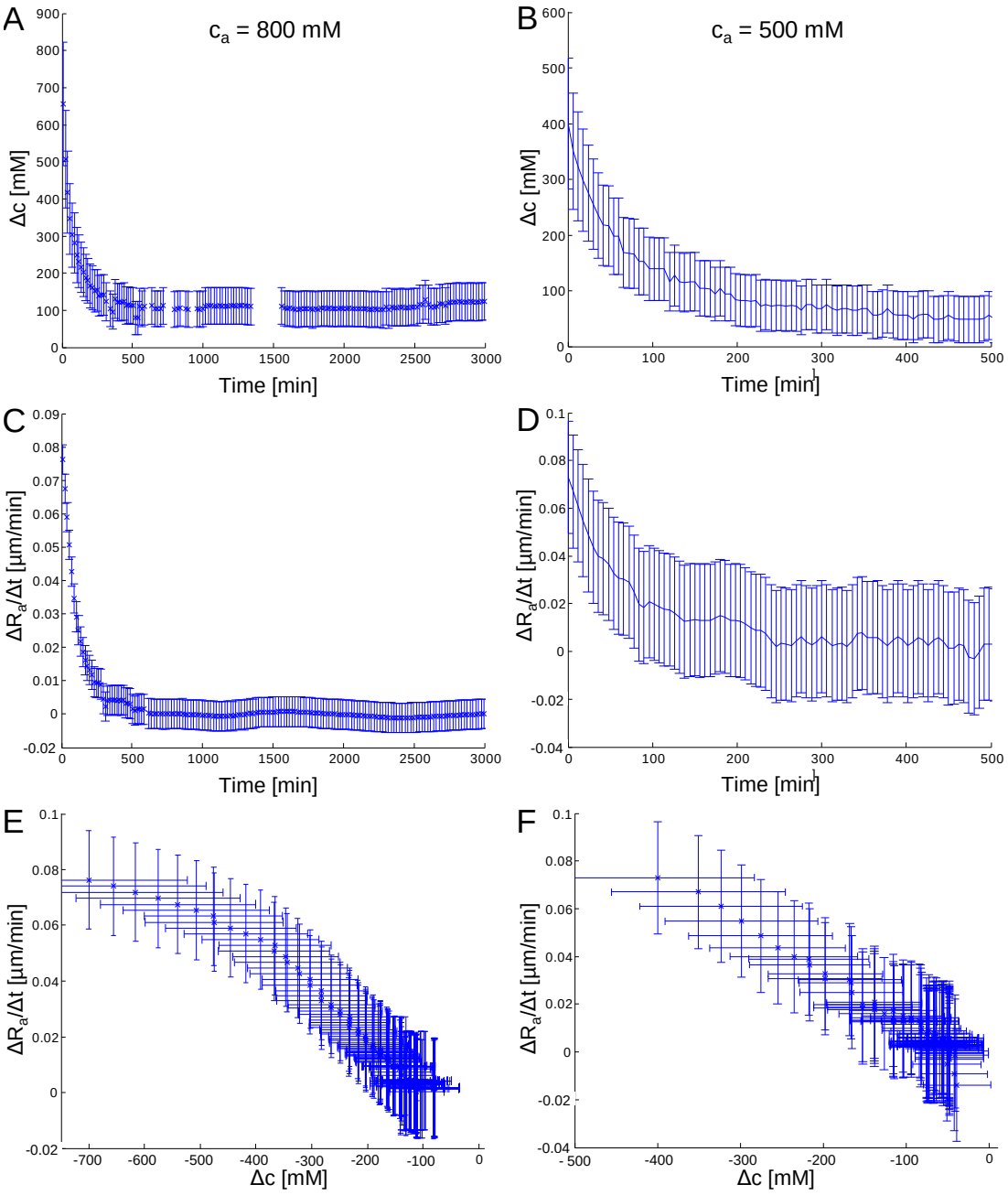

Figure 6.14: *Dependence of the droplets' rate of size change on the concentration difference, based on the experiments presented in Figure 6.13 (left column: c_a = 800 mM experiment; right column: c_a = 500 mM experiment). (A and B) Mean concentration difference Δc between type a droplet and direct neighbours (type I) versus time. For clarity, the amount of data-points shown in (B) and (D) has been reduced. (C and D) Size change rate of type a droplet $\Delta R_a/\Delta t$ versus time. (E and F) Size change rates of type a droplets $\Delta R_a/\Delta t$ versus the prevailing concentration difference Δc. Errors are those from (A) and (C) or (B) and (D), respectively.*

Rates of size change $\Delta R_a/\Delta t$ (Figure 6.14 C and D) of the type a droplets were obtained by smoothing the discrete data points[4] and calculating the differential quotient between consecutive points (t/R_a).

Plotting the size changes rate $\Delta R_a/\Delta t$ *versus* the respectively prevailing concentration differences $\Delta c(t)$[5] reveals an increasing flux for increasing concentration differences (Figure 6.14 E and F). The data supports a linear relationship between concentration difference and transfer rate over the entire range of concentration differences, with linear factors $k_{\mathrm{Os},800} = 0.16 \pm 0.12$ µm/(min mM) and $k_{\mathrm{Os},500} = 0.18 \pm 0.10$ µm/(min mM) for the 800 mM and 500 mM experiment, respectively.

This linear dependence can be explained by a proportionality of water flux $J_a(t)$ and solute concentration difference $\Delta c(t)$, as provided by the Kedem-Katchalsky equation (see section 2.1.1) or the solution-diffusion model (for constant membrane thickness; see section 2.1.2, page 23): for water transport by reverse micelles (or single molecules), the surface of the high concentration droplet is assumed to equal the membrane area $S(t) = 4\pi R_a(t)^2$. Then, the flux is $J_a(t) = dV_a/dt 1/S(t) = dR_a/dt$, and consequently, dR_a/dt and Δc are linearly dependent.

However, due to the large errors, other dependencies cannot be excluded and, even in case of a linear relationship between water transfer rates and concentration differences, the data might show nonlinearities (like the bend in Figure 6.14 F) for several reasons. The bias in radius detection discussed in section 6.2.1, for example, leads to a flattening of the curve for higher concentration differences. Additionally, a non-linear dependence may be interpreted in terms of a temporal variation of the membrane thickness or the membrane area not being proportional to the surface of the type a droplet, as assumed previously. Both might directly result from the droplets' size changes which alter the arrangement of droplets. For instance, the number of type b droplets in visual contact to a type a droplet increases with time, due to its growth. Finally, the bend in Figure 6.14 F may result from deviations of the linear relationship between osmotic pressure and concentration difference for higher sucrose concentrations, as van't Hoff's law only holds for dilute solutions (see section 2.1.1). For instance, the actual osmotic pressure between a 800 mM sucrose solution and pure water deviates from the osmotic pressure calculated from van't Hoff's law by approximately 8 % [176]. Hence, the relationship between water transfer rates and osmotic pressure might be linear, despite a nonlinear dependence of water transfer rates on concentration differences.

Summing up, the dependence of water transfer rates on concentration differences between contacting droplets, which determine the osmotic pressure, may be described by the linear relationship suggested by the Kedem-Katchalsky equation or the solution-

[4] A moving average filter with a span of 11 ($c_a = 500mM$) and 41 ($c_a = 800mM$) was used for smoothing.

[5] In fact, $-\Delta c(t)$ is plotted, for consistency with the time axes in Figure 6.14 A, B, C, and D.

diffusion mechanism (see section 2.1.1). This linear dependence differs from the non-linear dependence found by Wen and Papadopoulos[96]. However, their experimental system (oil and surfactant) differed from the one used in this work, and water transfer between contacting droplets was mediated by diffusion of hydrated surfactants. As diffusion of reverse micelles is suggested to be the prevailing water transport mechanism in this work (see section 6.2.2), the dependences of water transfer rates on concentration differences might differ.

Albeit being irrelevant for the equilibrium state, knowledge of the concentration difference-flow rate response allows for the simulation of non-equilibrium states, which is useful for the quantification of reaction kinetics inside of droplets.

6.3 Sensitivity of the droplet sensors

An inevitable prerequisite for the successful application of the droplet sensor method is that a significant size change (in statistical terms) of the droplets is induced. Since the dynamics of each droplet's volume change strongly depend on the arrangement of droplet populations (see section 6.2.2), drawing definite conclusions from droplet sizes to their contents is by implication only permitted in equilibrium state. However, if all droplets of one type show similar growth dynamics, for example because of similar organization of the neighbouring droplets (or a highly symmetric droplet arrangement), intermediate droplet sizes may quantitatively be evaluated. The sensitivity of the sensor system as defined by the minimal osmotic pressure which induces a significant change between initial and equilibrium radius of a droplet type, is contributed to by three components.

First, sensitivity is directly affected by the time-scale of the volume change of the equilibration process. As previously shown, the magnitude of the osmotic pressure dictates the rate of water transfer between contacting droplets (6.2.2) and consequently, combined with the droplet arrangement, also the time-scale of equilibration. If only a small initial osmotic pressure prevails and thus water transport is very slow, the effects of other emulsion destabilizing processes which also alter the droplets' sizes, like Ostwald ripening, have to be taken into account. Since Ostwald ripening and osmosis are mediated by the same water transfer mechanisms (see section 2.1.3), droplet arrangement as well as the choice of oil and surfactant affect the time-scale of both processes. Consequently, increasing the overall rates of water transfer, e.g. by choosing an oil with a higher water solubility, does not necessarily improve the sensitivity of the system, as Ostwald ripening and other destabilizing processes are accelerated as well.

In many practical cases, the lower bound of the detectable osmotic pressure difference will be simply set by the time available for an experiment: for an initial sucrose

concentration difference of 2.49 mM between the droplets, the observed size changes were very small (barely measurable) and equilibrium state wasn't reached after 40 hours of incubation (see Table 6.1). If the encapsulated compounds, e.g. cells, have to remain viable over a longer period, technical problems arise, like the CO_2 supply of cells in droplets, which cannot easily be accomplished without subjecting the droplets to enhanced evaporation or dissolution.

Second, a crucial question for determining the sensitivity, is whether and under which conditions a significant size change will eventually occur. Several aspects contribute to this problem: the degree of monodispersity of initial droplet populations[6], the magnitude of the droplets' size change, and the accuracy of the size measurement or sorting of the droplets. Generation of highly monodisperse droplets (dispersities of 1-3 %) is easily accomplished and, in most cases, won't be a limiting issue. Thus, significance of a size change comes down to whether the resolution of the applied detection method is sufficiently high to detect a certain size change. The 20x objective used in the experiments provided a good tradeoff between resolution and field of view, resolving the droplets radius to 0.5 µm accuracy. Both, the relative magnitude of the size change of one droplet type

$$\frac{V_{i,f} - V_{i,0}}{V_{i,0}} = \frac{1 - \frac{c_{b,0}}{c_{a,0}}}{\frac{N_a V_a}{N_b V_b} + \frac{c_{b,0}}{c_{a,0}}}$$

and, if initial volumes for both droplet subpopulations were equal, the difference of final droplet volumes $|V_{a,e} - V_{b,e}|$ are functions of the ratio of droplet numbers, the initial droplet volumes, and, in particular, the ratio of the initial concentrations (as can be derived from equations (5.5) and (5.4)). So while the difference in concentrations affects water transport rate and equilibration time-scale, the ratio dictates the absolute magnitude of the droplets' size change. Hence, reactions inside of droplets which cause only small changes in osmolarity compared to the total osmolarity won't induce a measurable size change, even if the absolute value of the change is rather large. Also, as intuitively expected, a small ratio of the total volumes of the droplet types $(N_a V_a)/(N_b V_b)$ enhances the size change of type *a* droplets (and *vice versa* for droplet type b). Therefore, initial volume and frequency ratios of droplet should be chosen carefully. The frequency and volume ratios could be rendered irrelevant by adding a dedicated reservoir of "infinite" volume (several orders of magnitude larger than the total droplet volumes) comprising one of the initial concentrations to the incubation chamber. This could be accomplished by a multilayer PDMS device similar to the one presented by Shim and coworkers[177].

[6] Provided that droplets are not tracked individually, which is not practical for very large droplet numbers.

Third, functionality and consequently also sensitivity of the droplet sensors is affected by the nature of compounds (educts and products of reactions) inside the droplets. Permeation of molecules into the oil phase or even into another droplet, as well as dissociation and interaction of molecules may alter the osmolarities of the droplet populations in a way that renders a comparison of droplet size changes, and thus, application of the sensor method, impossible.

To conclude, for the experimental system and typical initial conditions used in this thesis, concentration differences down to few millimolars, or, more generally, few milliosmoles per liter, can be detected in a reasonable amount of time. This threshold may not seem particularly low, however, because of the small droplet volumes of about 10 - 100 pl, only very small changes of the amount of solutes in the order of few picomoles are needed to build up detectable concentration differences, as will be shown in the next chapter.

7 Application of the droplet sensors to dynamic systems

The method of droplet sensors is of particular interest for screening dynamic systems, where an osmotic pressure is built up by catalytic activity of enzymes or cells inside the droplets. Since single cells can be encapsulated in an individual droplet, monitoring the size change of a droplet in principle allows to follow metabolic activity at the single cell level.

As hypothesized by Schmitz et al. [30] (and more recently by Joensson et al. [53]), the metabolic activity of encapsulated yeast might induce an osmotically driven size change of droplets. Hence, and because of its high robustness, yeast was chosen as a model system for the application of the droplet sensor method to a dynamic system. In the following chapter, the size change of droplets comprising yeast cells is analyzed and finally, the suitability of the sensor method to perform a live/dead screening is demonstrated.

7.1 Detection of metabolic activity in droplets

Monodisperse droplets containing yeast cells were classified into droplets comprising solely YPD growth medium[1] (type a), one cell (type b), or more than one yeast cells (type b'). Time-lapse studies revealed that droplets containing any amount of yeast cells shrank over time, whereas droplets containing only medium grew in size (Figure 7.1 A, B and C). Thus, metabolic activity of yeast, manifesting itself in cell growth or cell division (Figure 7.1 A and B), decreased the total amount of osmotically active solutes inside the droplets.

For the growth medium used, the prevalent metabolic process of yeast is fermentation, converting glucose to ethanol and carbon dioxide[178]. Both ethanol and CO_2 rapidly permeate into the continuous phase and other droplets[179, 180] (at least orders of magnitude faster than water). Substances inside of cells and cells themselves do not contribute to osmotic pressure. Thus, provided that solely water and no nutrients permeate through the oil membrane, the osmotic pressure results from differences in concentration of glucose and other nutrients.

[1] Yeast extract Peptone Dextrose medium (comprising 20 g/l (111 mM) glucose)

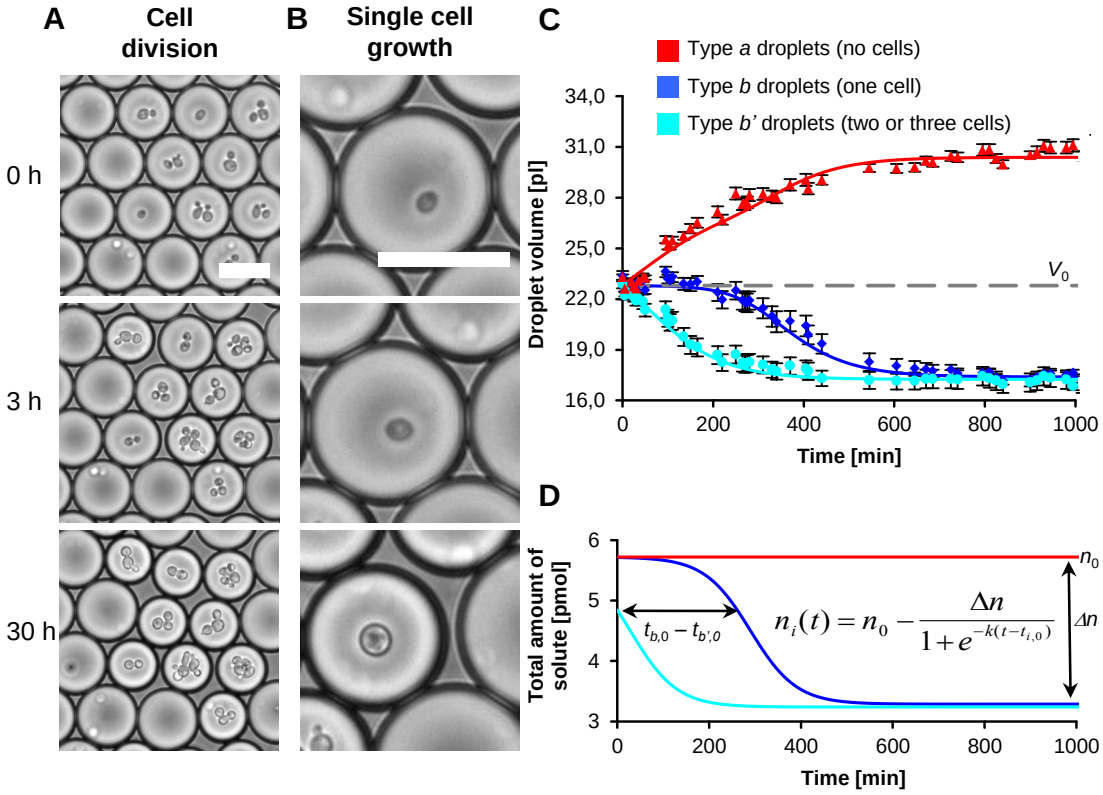

Figure 7.1: *Osmotically driven size change of droplets in dynamic systems comprising droplets with living yeast as a biological active compound. Cell activity inside the droplets manifests itself in the form of cell division (A) and cell growth (B), both leading to a decrease in droplet size. Scale is 30* µm. *(C) Measured volume change of droplets containing no (type a), one (type b) or more than one (type b′) cell as well as the respective simulation of the development of droplet volumes (solid lines). Error bars, s.e.m. (D) Quantifying the kinetics of the metabolic activity: Assuming a sigmoid function for solute decrease, the corresponding kinetic constants are* $k = 0.020 \pm 0.005$ *min*$^{-1}$, $t_{b,0} = 290$ *min and* $t_{b',0} = 30$ *min. (Figure as published in Ref. [10])*

Indeed, a control experiment with two droplet types comprising YPD medium and a 1:1 aqueous dilution of YPD, respectively, resulted in size changes of droplets according to theory[2], which only considers transfer of water (see section 5.2). Consequently, the effect of solute transport between droplets is negligible in this case and shrinkage of droplets reflects the nutrient consumption of yeast.

After about 17 hours, size change of droplets stopped, suggesting that all nutrients were metabolized and the yeast cells rendered inactive (Figure 7.1 B). In fact, no growth or proliferation of yeast was observed beyond that point. According to the hypothesis that all nutrients were metabolized and thus, total osmolarities in type b and b' drops

[2]Mean initial radii: $r_{a,0} = 11.4 \pm 0.4$ µm, $r_{b,0} = 13.8 \pm 0.4$ µm; Mean equilibrium radii: $r_{a,e} = 13.1 \pm 0.3$ µm, $r_{b,e} = 12.3 \pm 0.4$ µm; Calculated equilibrium radii: $r_{a,e} = 13.2 \pm 0.3$ µm, $r_{b,e} = 12.7 \pm 0.4$ µm ($N_a = 73$, $N_b = 97$).

Table 7.1: *Experimental and calculated data for yeast experiments. The kinetic values were calculated by numerically fitting the experimental data. The input parameters for the model were c_0, $V_{i,0}$, N_i, and $k_{Os} = 0.18$ µm/(mM min) (see subsection 6.2.2). Fitting parameters were the reaction constant of the yeast's metabolism k as well as a time offset t_0.*

Quantity	Data origin	Droplet type a	Droplet type b	Droplet type b'
Number of droplets	Measured[a]	39	24	30
Average number of cells (t = 0)	Measured	0	1	2.7 ± 0.2
V_0 [pl]	Measured[a]	23.2 ± 0.2	23.4 ± 0.2	22.9 ± 0.2
c_0 [mM]	Measured[a]	251 ± 2	251 ± 2	251 ± 2
V_e [pl]	Measured (model output)	29.9 ± 0.2 (30.3)	16.9 ± 0.2 (17.4)	17.0 ± 0.2 (17.3)
c_e[b] [mM]	Calculated (model output)	(188 ± 22)	195 ± 2 (188 ± 22)	195 ± 2 (188 ± 22)
Apparent c_0[c] [mM]	Calculated (bulk measurement)	—	141 ± 2 (133 ± 1)	145 ± 2 (133 ± 1)
n_0[d] [pmol]	Calculated	—	5.9 ± 0.1	5.7 ± 0.1
Δn_0[e] [pmol]	Calculated[a]	—	2.6 ± 0.1	2.4 ± 0.1
k [1/min]	Model output	—	0.020 ± 0.005	0.020 ± 0.005
t_0 [min]	Model output	—	290	30

[a] Data used as input for model. [b] The equilibrium concentration c_e is calculated from $V_{a,0}$, $c_{a,0}$, and $V_{a,f}$. [c] Apparent c_0 is the concentration calculated from the final volumes and equilibrium concentration. It reflects the total solute consumption due to the cell activity without taking into account its time development; bulk measurements refer to the experimentally determined osmolarity of depleted medium, which was used for yeast culture. [d] n_0 is calculated from c_0 and V_0. [e] $\Delta n = n_0 - n_f$ is calculated from n_0, V_f, and c_e.

were equal once equilibrium state was reached, the final volume of droplets containing yeast was independent of the initial number of encapsulated cells ($V_{f,b} = V_{f,b'}$). Final volumes as well as initial volumes and other measured and calculated parameters are summarized in Table 7.1.

The volume change of type b and type b' droplets corresponded to a net decrease of the total amount of solutes by $\Delta n = 2.5 \pm 0.1$ pmol (mean of type b and b' droplets), from initially

$$\langle n_0 \rangle = \langle c_{i,0} V_{i,0} \rangle = 5.8 \pm 0.1 \text{ pmol to}$$
$$\langle n_e \rangle = \langle c_e V_{i,e} \rangle = 3.3 \pm 0.1 \text{ pmol } (i = b, b') \ .$$

$c_{i,t}$ denotes the total concentration of osmotically active solutes in the droplet type i. For calculation, the measured initial osmolarity $c_0 = 251 \pm 2$ mOsm/l and the final osmolarity $c_e = c_{a,0} V_{a,0} / V_{a,e} = 196 \pm 2$ mOsm/l were used. The latter was derived from droplet type a, since conservation of the amount of solutes only holds for this

droplet type (see 5.3). Control experiments with droplets containing no yeast cells, but either fresh (type a) or depleted YPD medium (type b, $c_d = 133 \pm 1$ mOsm/l), which was used before for yeast cell culture, led to the same volume changes. Thus, volume change may be interpreted as driven by an apparent difference in initial total osmolarity of $\Delta c = c_e - c_d = 118 \pm 2$ mOsm/l, which is in good agreement with the calculated value $\Delta c = c_{a,0} - c'_{b,0} = 108 \pm 5$ mOsm/l, with $c'_{b,0} = V_{b,f}/V_{a,f} c_{a,0} = 141 \pm 3$ mOsm/l (from equation (5.4) and $V_{a,0} = V_{b,0}$, conservation of solutes is assumed).

When yeast was encapsulated in droplets comprising PBS without any supplements instead of YPD medium, yeast cells were rendered inactive and no size change of droplets was observed.

Despite the rather slow kinetics of the osmotic process and an asymmetric droplet arrangement, dynamics of shrinking clearly differentiated between droplets containing one or more than one cell initially (Figure 7.1 C): if a droplet comprised more than one cell, it shrank more rapidly compared to droplets comprising only one cell at the beginning of the experiment. This is due to the increase in total rate of nutrient consumption with the number of encapsulated cells, corresponding to a faster decrease in total osmolarity. Consequently, after a short amount of time, droplets comprising more than one cell (type b') exhibited the least total osmolarity and shrank rapidly, at the expense of neighbouring droplets. As rates of water transfer scale with the concentration difference between neighbouring droplets (section 6.2.2), water was primarily transferred to droplets containing only medium (type a). However, the slow shrinkage of type b droplets, comprising only one cell initially, was additionally retarded by water uptake from neighbouring droplets of type b' (Figure 7.1 C).

The kinetics of metabolic activity of encapsulated yeast could be quantified by a simple[3] numerical simulation (see Figure 7.1 C and D), in which water transfer due to osmosis was modeled by the proportionality found in section 6.2.2, $dR/dt = k_{\mathrm{Os}} \Delta c$. As yeast cultures typically show a sigmoid growth[181, 182], solute decrease in type b and b' droplets was modeled by sigmoid curves

$$n_i(t) = n_0 - \frac{\Delta n}{1 + \exp -k(t - t_{i,0})} \ .$$

Here, n_0 is the total amount of osmotically active solute, Δn the difference between final and initial total amount of solute (see Table 7.1), and k and $t_{i,0}$ fitting parameters of the model. For $k = 0.020 \pm 0.005$ min^{-1}, $t_{b,0} = 290$ min and $t_{b',0} = 30$ min, the model was in very good agreement with the measured radii (see Figure 7.1 C). Consequently, the droplet sensors can be used to not only draw conclusions from the final state, but also to quantitatively analyze reaction kinetics of single cells. For more precise investigation

[3] Water transfer between droplets of type b and type b' was neglected.

of reaction kinetics, each droplet comprising any amount of cells should be surrounded by at least one layer of droplets of type *a*. This way, interactions between droplets comprising cells could be minimized (see section 6.2.2).

Most recently, Boitard et al. [180] used the sensor method to further investigate the size change of droplets comprising yeast cells, focusing on the consumption of glucose of single yeast cells. Despite the choice of an adhesive surfactant which facilitated formation of adhesive bilayers between the droplets shrinkage rates of droplets were in the same order of magnitude as those observed in this work. From the size change of droplets in which glucose was not the growth limiting nutrient and from droplets containing non-proliferating yeast mutants, they were able to estimate the glucose consumption of single yeast cells to 0.1 - 0.2 pg(glucose)/(min cell)[180]. Moreover, they reported on shrinkage of droplets containing *E. coli*, and growth of droplets comprising BSA (Bovine serum albumin) and a digestive enzyme (proteinase K), proving the broad applicability of the sensor method.

Prior to Boitard's publication, both of these systems had been tested in the course of this work, but unfortunately, they only induced very little size changes (BSA/proteinase K) or no size changes at all (*E. coli*) (see Appendix A.1). In case of *E. coli*, measurements showed that the osmolarity of the growth medium used in this work was not altered by the rapidly proliferating bacteria, even after several days of incubation. Therefore, no change in the droplet sizes was expected. Boitard et al. used a different growth medium, a minimal medium supplemented with glucose, in which activity of *E. coli* lead to a change in osmolarity.

In the experiments with droplets comprising BSA with and without proteinase K, stability of droplets was severely impaired by addition of BSA and droplets deformed heavily, adhering to the walls of the incubation chamber. Consequently, the passivating function of the surfactant was adversely affected, probably due to the adhesion of BSA to the droplets' interfaces. Moreover, partitioning of reaction products or the enzyme out of the droplet into the oil phase could not be excluded, which would alter the total osmolarity inside the droplet.

7.2 Live/dead screening using droplet sensors

For further demonstration of the value of the droplet sensor method for biological applications a live/dead assay was performed. Viable and dead yeast cells were mixed and encapsulated in initially monodisperse droplets of fresh YPD-medium (Figure 7.2 A and C). Prior to mixing, dead yeast were fluorescently labelled.

After incubation for 33 hours, droplets containing only dead yeast had grown in size, whereas droplets containing any amount of living cells had shrunk in radius by

2-3 microns (Figure 7.2 B and D). The size distribution of droplet populations showed very little overlap and thus allowed for reliable separation of droplets containing living yeast from droplets containing no or exclusively dead cells by means of optical video microscopy (Figure 7.2 B and D).

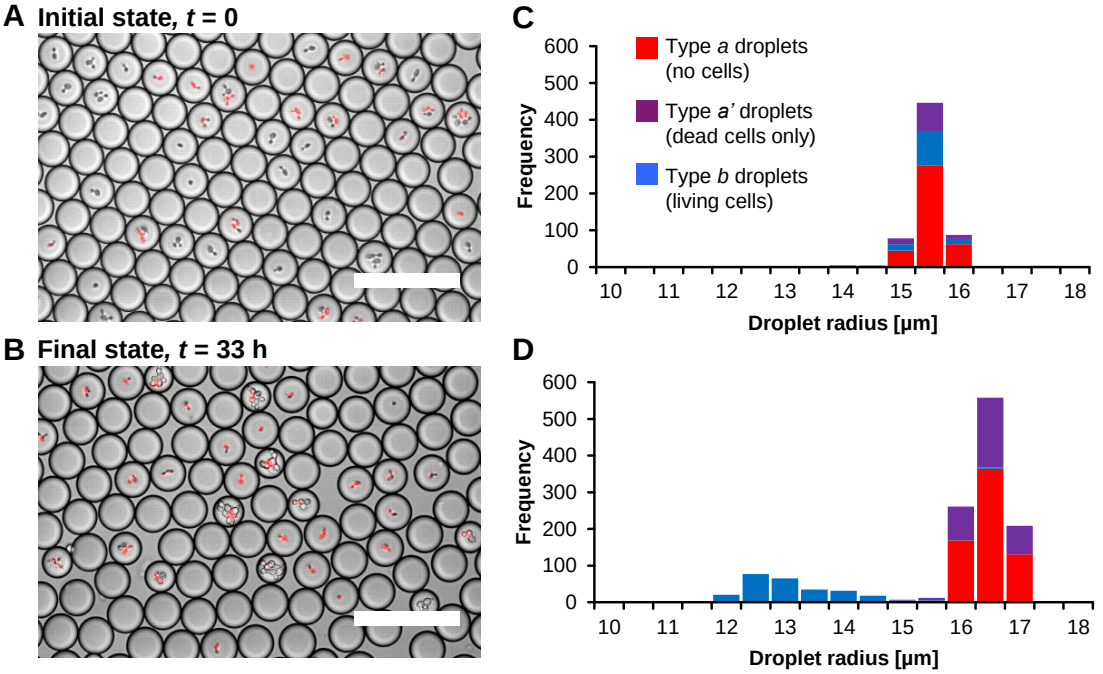

Figure 7.2: *Overlays of bright field and fluorescence micrographs of initially mono-disperse droplets ($r_0 = 15.92 \pm 0.03$ µm) with living and dead cells encapsulated at $t = 0$ (A) and at equilibrium after 33 h (B). Dead cells are stained with potassium iodide. Scale is 100* µm. *(C and D) Histograms show the size distribution of empty droplets (type a) and droplets containing living (type b) or exclusively dead (type a′) cells at both time points ($N_0 = 626$; $N_e = 1320$ with 672 empty droplets, 258 with living and 368 with dead yeast cells). While empty droplets and droplets with solely dead cells behave similarly and grow slightly in size ($r_{a,f} = 16.42 \pm 0.01$ µm, $r_{a',f} = 16.44 \pm 0.02$ µm), droplets comprising any amounts of living cells show a significant volume decrease ($r_{b,f} = 13.15 \pm 0.05$ µm). All errors are standard errors of the mean. (Figure as published in Ref. [10])*

Part IV

Conclusion and Outlook

8 Conclusion

HTS (High-throughput screening) has become an invaluable tool in pharmaceutical science as well as modern biology. The transition to droplet microfluidics represents a significant evolution of high-throughput technology in terms of minimization of both, volume of reagents and time consumed. In spite of its enormous potential, widespread applications of droplet microfluidics have been limited by the reliance of most methods for analyzing the droplets' contents on specific markers.

The novel sensor method invented within this thesis avoids this obstacle and provides a simple and elegant means for analysis of the contents of droplets. By exploiting the osmotically driven change in droplet size as a novel marker, the activity of analytes and changes in solute concentration in droplets can be measured directly and label-free. Both the total and the rate of size change can be utilized for quantification of chemical reactions and metabolic activity of cells inside droplets.

Despite the rather slow kinetics of the osmotic process, the total size change unambiguously distinguished between live and dead or one and more cells, detecting changes in the total amount of solutes of few picomoles (section 7.1 and 7.2). Moreover, the size change allowed one to monitor the time course of metabolic activity quantitatively (section 7.1). Investigation of non-equilibrium dynamics yielded diffusion of either single molecules or reverse micelles to be the predominant mechanisms of water transfer (section 6.2.2). As a consequence of the densely-packed arrangement of droplets, however, water transport occurred primarily between adjacent droplets, showing a linear relationship between water flux and solute concentration difference. Providing insight into the underlying mechanisms, those information may prove useful for further optimization and application of the sensor system.

The key strength of the sensor method is its general and simple principle, granting immediate access to changes in solute concentrations down to few millimolars (section 6.3), and hence facilitating diverse screening applications, notably at the single-cell level. As thousands of droplets can be analyzed in a very short amount of time by means of simple image analysis, the method is well-suited for high-throughput applications. For analysis, only a bright-field microscope is needed. Alternatively, in combination with microfluidic methods for the separation of droplets by size (see section 1.4), the droplet sensor method provides a simple way for the "on-chip" detection of biochemical

reactions inside of droplets, rendering even the microscope obsolete.

A particular advantage of the sensor method is that no calibration of the system is required, as the equilibrium state is independent of the dynamics of the size change (section 6.2.1 and 5.2).

Limitations of the sensor method are the slow kinetics of the osmotic process, and the risk to affect cell viability or functioning of enzymes by the size change adversely. For example, cells might not tolerate the potential pH change and the change of buffer concentration associated with the shrinkage and growth of droplet volumes. Moreover, only the total amount of osmotically active solutes in droplets can be detected and not the individual contributions of a compound. This lack of specificity complicates or completely prevents the detection of changes in the concentration of a certain solute if the total osmolarity is several factors higher, e.g. due to the buffer used. Hence, although detection of PCR (Polymerase Chain Reaction) in droplets seems to be ideal for application of the sensor method due to synthesis of few macromolecules from thousands of small molecules, it can not be detected, at least when using conventional buffers: the osmolarity of the reaction buffer is too high to detect the small changes in osmolarity of few µOsm/l caused by synthesis of DNA.

Aside from being used as a sensor system, the osmotically driven size change of droplets has to be considered in common screening applications as well. Depending on experimental design and incubation time volume changes could, for instance, alter the fluorescence intensities of specific markers inside the droplets and therefore decrease the screening accuracy - even if the fluorescent marker itself remains inside the droplets.

Finally, the sensor method extends the droplet capabilities into a novel functional dimension, which opens a promising avenue for an “on-chip” processing integrating chemistry and computation as proposed by Prakash and Gershenfeld[183]. While acting as a reaction container, a droplet traveling in a channel represents a bit which allows logical control operations to be performed. By linking chemistry inside the droplets to a physical property of the droplets, the sensor method provides a unique approach to integrate the application of droplets as passive containers and logical information units.

9 Outlook

Within this thesis, the proof of principle of exploiting the osmotically driven size change of droplets as an intrinsic, label-free marker for cellular activity was provided. Recently, Boitard et al. [180] showed that the sensor method developed in this work can also be applied to detect microbial and enzymatic activity in microdroplets. Having verified the applicability of the sensor method to cellular and enzymatic systems, the next step will be the implementation of the technique in high-throughput systems.

To this end, the experimental set-up, in particular the incubation chamber, has to be optimized. First, nozzle and incubation chamber should be implemented in one microfluidic device, eliminating sources of error like the coalescence of droplets during the transfer to the incubation chamber, and maximizing speed. To avoid dissolution of droplets, the chamber should either consist of pure glass or glass and thin layers of PDMS saturated with water.

Second, the addition of a dedicated reservoir of predefined total osmolarity (e.g. equivalent to those of the empty droplets in chapter 7) to which all droplets have contact would shorten the time-scale of equilibration and render the dynamics of the growth of individual droplets comparable. This could be accomplished by a multilayer PDMS device, in which two layers are separated by a thin PDMS membrane. One layer comprises the nozzle, an incubation chamber, and, potentially, pillar fields for DLD, and another layer above comprises meandering channels filled with an aqueous solution which serves as reservoir. As all droplets are in close contact to this reservoir of constant osmolarity[1], size change of individual droplets is accelerated and should be decoupled from type and growth of neighbouring droplets.

In case droplets comprising single cells are needed, one can make use of channel geometries promoting deterministic encapsulation of one cell per droplet[38, 39].

The optimized design of the microfluidic device will allow for HTS of selected biological systems. Basic compatibility of specific cellular or enzymatic systems with the sensor method (a change in total osmolarity has to be induced) can be tested by measurement of buffer osmolarities prior to and after the reaction or a certain period.

Main fields of application are growth assays of cells, e.g. bacterial persistence screens, allowing not only to separate between live and dead cells, but also between cells of high

[1] As the volume of the reservoir is several orders of magnitude larger than the combined volume of the droplets, the variation in osmolarity due to water exchange with the droplets is negligible small.

and low metabolic activity. Furthermore, the sensor method may be applied for the optimization of the yield of enzymes by directed evolution and the measurement of dose-response curves of bioactive compounds.

Bibliography

[1] Sunitha Nagrath, Lecia V Sequist, Shyamala Maheswaran, Daphne W Bell, Daniel Irimia, Lindsey Ulkus, Matthew R Smith, Eunice L Kwak, Subba Digumarthy, Alona Muzikansky, Paula Ryan, Ulysses J Balis, Ronald G Tompkins, Daniel A Haber, and Mehmet Toner. Isolation of rare circulating tumour cells in cancer patients by microchip technology. *Nature*, 450(7173):1235–9, December 2007.

[2] Piyush B Gupta, Tamer T Onder, Guozhi Jiang, Kai Tao, Charlotte Kuperwasser, Robert A Weinberg, and Eric S Lander. Identification of selective inhibitors of cancer stem cells by high-throughput screening. *Cell*, 138(4):645–59, August 2009.

[3] Salvatore Pece, Daniela Tosoni, Stefano Confalonieri, Giovanni Mazzarol, Manuela Vecchi, Simona Ronzoni, Loris Bernard, Giuseppe Viale, Pier Giuseppe Pelicci, and Pier Paolo Di Fiore. Biological and molecular heterogeneity of breast cancers correlates with their cancer stem cell content. *Cell*, 140(1):62–73, January 2010.

[4] Analysis of the genome sequence of the flowering plant Arabidopsis thaliana. *Nature*, 408(6814):796–815, December 2000.

[5] Konrad H Bleicher, Hans-Joachim Böhm, Klaus Müller, and Alexander I Alanine. Hit and lead generation: beyond high-throughput screening. *Nature reviews. Drug discovery*, 2(5):369–78, May 2003.

[6] Lorenz M Mayr and Dejan Bojanic. Novel trends in high-throughput screening. *Current opinion in pharmacology*, 9(5):580–8, October 2009.

[7] Mira T Guo, Assaf Rotem, John A Heyman, and David A Weitz. Droplet microfluidics for high-throughput biological assays. *Lab on a chip*, 12(12):2146–55, June 2012.

[8] Jeremy J Agresti, Eugene Antipov, Adam R Abate, Keunho Ahn, Amy C Rowat, Jean-christophe Baret, Manuel Marquez, Alexander M Klibanov, Andrew D Griffiths, and David A Weitz. Ultrahigh-throughput screening in drop-based microflu-

idics for directed evolution. *Proceedings of the National Academy of Sciences of the United States of America*, 107(9):4004–9, March 2010.

[9] Oliver J Miller, Abdeslam El Harrak, Thomas Mangeat, Jean-christophe Baret, Lucas Frenz, Bachir El Debs, Estelle Mayot, Michael L Samuels, Eamonn K Rooney, Pierre Dieu, Martin Galvan, Darren R Link, and Andrew D Griffiths. High-resolution dose-response screening using droplet-based microfluidics. *Proceedings of the National Academy of Sciences of the United States of America*, 109(2):378–83, January 2012.

[10] Tobias W Hofmann, Siegfried Haenselmann, Jan-Willi Janiesch, Anne Rademacher, and Christian H J Boehm. Applying microdroplets as sensors for label-free detection of chemical reactions. *Lab on a chip*, 12(5):916–22, March 2012.

[11] Todd Thorsen, Richard W. Roberts, Frances H. Arnold, and Stephen R. Quake. Dynamic Pattern Formation in a Vesicle-Generating Microfluidic Device. *Physical Review Letters*, 86(18):4163–4166, April 2001.

[12] Shia-Yen Teh, Robert Lin, Lung-Hsin Hung, and Abraham P Lee. Droplet microfluidics. *Lab on a chip*, 8(2):198–220, February 2008.

[13] Jean-Christophe Baret. Surfactants in droplet-based microfluidics. *Lab on a chip*, 12(3):422–33, February 2012.

[14] Dominic Eicher and Christoph A Merten. Microfluidic devices for diagnostic applications. *Expert review of molecular diagnostics*, 11(5):505–19, June 2011.

[15] Ansgar Huebner, Sanjiv Sharma, Monpichar Srisa-Art, Florian Hollfelder, Joshua B Edel, and Andrew J Demello. Microdroplets: a sea of applications? *Lab on a chip*, 8(8):1244–54, August 2008.

[16] Xavier Casadevall i Solvas and Andrew DeMello. Droplet microfluidics: recent developments and future applications. *Chemical communications (Cambridge, England)*, 47(7):1936–42, February 2011.

[17] Ralf Seemann, Martin Brinkmann, Thomas Pfohl, and Stephan Herminghaus. Droplet based microfluidics. *Reports on progress in physics. Physical Society (Great Britain)*, 75(1):016601, January 2012.

[18] Ashleigh B Theberge, Fabienne Courtois, Yolanda Schaerli, Martin Fischlechner, Chris Abell, Florian Hollfelder, and Wilhelm T S Huck. Microdroplets in microfluidics: an evolving platform for discoveries in chemistry and biology. *Angewandte Chemie (International ed. in English)*, 49(34):5846–68, August 2010.

[19] Todd Squires and Stephen Quake. Microfluidics: Fluid physics at the nanoliter scale. *Reviews of Modern Physics*, 77(3):977–1026, October 2005.

[20] A S Utada, E Lorenceau, D R Link, P D Kaplan, H A Stone, and D A Weitz. Monodisperse double emulsions generated from a microcapillary device. *Science (New York, N.Y.)*, 308(5721):537–41, April 2005.

[21] Chantal Khan Malek, Laurent Robert, Jean-Jacques Boy, and Pascal Blind. Deep microstructuring in glass for microfluidic applications. *Microsystem Technologies*, 13(5-6):447–453, May 2006.

[22] M G Pollack, A D Shenderov, and R B Fair. Electrowetting-based actuation of droplets for integrated microfluidics. *Lab on a chip*, 2(2):96–101, May 2002.

[23] Jason P Rolland, R Michael Van Dam, Derek A Schorzman, Stephen R Quake, and Joseph M DeSimone. Solvent-resistant photocurable liquid fluoropolymers for microfluidic device fabrication [corrected]. *Journal of the American Chemical Society*, 126(8):2322–3, March 2004.

[24] M A Unger, H P Chou, T Thorsen, A Scherer, and S R Quake. Monolithic microfabricated valves and pumps by multilayer soft lithography. *Science (New York, N.Y.)*, 288(5463):113–6, April 2000.

[25] Dong Qin, Younan Xia, John A. Rogers, Rebecca J. Jackman, Xiao-Mei Zhao, and George M. Whitesides. *Microfabrication, Microstructures and Microsystems*, volume 194 of *Topics in Current Chemistry*. Springer Berlin Heidelberg, 1998.

[26] Valessa Barbier, Michaël Tatoulian, Hong Li, Farzaneh Arefi-Khonsari, Armand Ajdari, and Patrick Tabeling. Stable modification of PDMS surface properties by plasma polymerization: application to the formation of double emulsions in microfluidic systems. *Langmuir : the ACS journal of surfaces and colloids*, 22(12):5230–2, June 2006.

[27] T. C. Merkel, V. I. Bondar, K. Nagai, B. D. Freeman, and I. Pinnau. Gas sorption, diffusion, and permeation in poly(dimethylsiloxane). *Journal of Polymer Science Part B: Polymer Physics*, 38(3):415–434, February 2000.

[28] Greg C Randall and Patrick S Doyle. Permeation-driven flow in poly(dimethylsiloxane) microfluidic devices. *Proceedings of the National Academy of Sciences of the United States of America*, 102(31):10813–8, August 2005.

[29] Jessamine Ng Lee, Cheolmin Park, and George M Whitesides. Solvent compatibility of poly(dimethylsiloxane)-based microfluidic devices. *Analytical chemistry*, 75(23):6544–54, December 2003.

[30] Christian H J Schmitz, Amy C Rowat, Sarah Köster, and David A Weitz. Dropspots: a picoliter array in a microfluidic device. *Lab on a chip*, 9(1):44–9, January 2009.

[31] A Studer, S Hadida, R Ferritto, S Y Kim, P Jeger, P Wipf, and D P Curran. Fluorous synthesis: a fluorous-phase strategy for improving separation efficiency in organic synthesis. *Science (New York, N.Y.)*, 275(5301):823–6, February 1997.

[32] Yousr Skhiri, Philipp Gruner, Benoît Semin, Quentin Brosseau, Deniz Pekin, Linas Mazutis, Victoire Goust, Felix Kleinschmidt, Abdeslam El Harrak, J. Brian Hutchison, Estelle Mayot, Jean-François Bartolo, Andrew D. Griffiths, Valérie Taly, and Jean-Christophe Baret. Dynamics of molecular transport by surfactants in emulsions. *Soft Matter*, 8(41):10618, 2012.

[33] Yunpeng Bai, Ximin He, Dingsheng Liu, Santoshkumar N Patil, Dan Bratton, Ansgar Huebner, Florian Hollfelder, Chris Abell, and Wilhelm T S Huck. A double droplet trap system for studying mass transport across a droplet-droplet interface. *Lab on a chip*, 10(10):1281–5, May 2010.

[34] Fabienne Courtois, Luis F Olguin, Graeme Whyte, Ashleigh B Theberge, Wilhelm T S Huck, Florian Hollfelder, and Chris Abell. Controlling the retention of small molecules in emulsion microdroplets for use in cell-based assays. *Analytical chemistry*, 81(8):3008–16, April 2009.

[35] Gabrielle Woronoff, Abdeslam El Harrak, Estelle Mayot, Olivier Schicke, Oliver J Miller, Patrice Soumillion, Andrew D Griffiths, and Michael Ryckelynck. New generation of amino coumarin methyl sulfonate-based fluorogenic substrates for amidase assays in droplet-based microfluidic applications. *Analytical chemistry*, 83(8):2852–7, April 2011.

[36] Shelley L. Anna, Nathalie Bontoux, and Howard A. Stone. Formation of dispersions using "flow focusing" in microchannels. *Applied Physics Letters*, 82(3):364, 2003.

[37] Piotr Garstecki, Michael J Fuerstman, Howard A Stone, and George M Whitesides. Formation of droplets and bubbles in a microfluidic T-junction-scaling and mechanism of break-up. *Lab on a chip*, 6(3):437–46, March 2006.

[38] Evelien W M Kemna, Rogier M Schoeman, Floor Wolbers, Istvan Vermes, David A Weitz, and Albert van den Berg. High-yield cell ordering and deterministic cell-in-droplet encapsulation using Dean flow in a curved microchannel. *Lab on a chip*, 12(16):2881–7, August 2012.

[39] Jon F Edd, Dino Di Carlo, Katherine J Humphry, Sarah Köster, Daniel Irimia, David A Weitz, and Mehmet Toner. Controlled encapsulation of single-cells into monodisperse picolitre drops. *Lab on a chip*, 8(8):1262–4, August 2008.

[40] Remi Dreyfus, Patrick Tabeling, and Herve Willaime. Ordered and Disordered Patterns in Two-Phase Flows in Microchannels. *Physical Review Letters*, 90(14), April 2003.

[41] Venkatachalam Chokkalingam, Stephan Herminghaus, and Ralf Seemann. Self-synchronizing pairwise production of monodisperse droplets by microfluidic step emulsification. *Applied Physics Letters*, 93(25):254101, 2008.

[42] Sung-Yong Park, Ting-Hsiang Wu, Yue Chen, Michael A Teitell, and Pei-Yu Chiou. High-speed droplet generation on demand driven by pulse laser-induced cavitation. *Lab on a chip*, 11(6):1010–2, March 2011.

[43] Shaojiang Zeng, Bowei Li, Xiao'ou Su, Jianhua Qin, and Bingcheng Lin. Microvalve-actuated precise control of individual droplets in microfluidic devices. *Lab on a chip*, 9(10):1340–3, May 2009.

[44] Shashi Thutupalli, Stephan Herminghaus, and Ralf Seemann. Bilayer membranes in micro-fluidics: from gel emulsions to soft functional devices. *Soft Matter*, 7(4):1312, 2011.

[45] Abdou R Thiam, Nicolas Bremond, and Jérôme Bibette. From stability to permeability of adhesive emulsion bilayers. *Langmuir : the ACS journal of surfaces and colloids*, 28(15):6291–8, April 2012.

[46] Natalia L Sitnikova, Rudolf Sprik, Gerard Wegdam, and Erika Eiser. Spontaneously formed trans-anethol/water/alcohol emulsions: mechanism of formation and stability. *Langmuir : the ACS journal of surfaces and colloids*, 21(16):7083–9, August 2005.

[47] C Holtze, A C Rowat, J J Agresti, J B Hutchison, F E Angilè, C H J Schmitz, S Köster, H Duan, K J Humphry, R A Scanga, J S Johnson, D Pisignano, and D A Weitz. Biocompatible surfactants for water-in-fluorocarbon emulsions. *Lab on a chip*, 8(10):1632–9, October 2008.

[48] Jenifer Clausell-Tormos, Diana Lieber, Jean-Christophe Baret, Abdeslam El-Harrak, Oliver J Miller, Lucas Frenz, Joshua Blouwolff, Katherine J Humphry, Sarah Köster, Honey Duan, Christian Holtze, David A Weitz, Andrew D Griffiths,

and Christoph A Merten. Droplet-based microfluidic platforms for the encapsulation and screening of Mammalian cells and multicellular organisms. *Chemistry & biology*, 15(5):427–37, May 2008.

[49] G F Christopher, J Bergstein, N B End, M Poon, C Nguyen, and S L Anna. Coalescence and splitting of confined droplets at microfluidic junctions. *Lab on a chip*, 9(8):1102–9, April 2009.

[50] Keunho Ahn, Jeremy Agresti, Henry Chong, Manuel Marquez, and D. A. Weitz. Electrocoalescence of drops synchronized by size-dependent flow in microfluidic channels. *Applied Physics Letters*, 88(26):264105, 2006.

[51] Adam R Abate, Tony Hung, Pascaline Mary, Jeremy J Agresti, and David A Weitz. High-throughput injection with microfluidics using picoinjectors. *Proceedings of the National Academy of Sciences of the United States of America*, 107(45):19163–6, November 2010.

[52] Jean-Christophe Baret, Oliver J Miller, Valerie Taly, Michaël Ryckelynck, Abdeslam El-Harrak, Lucas Frenz, Christian Rick, Michael L Samuels, J Brian Hutchison, Jeremy J Agresti, Darren R Link, David A Weitz, and Andrew D Griffiths. Fluorescence-activated droplet sorting (FADS): efficient microfluidic cell sorting based on enzymatic activity. *Lab on a chip*, 9(13):1850–8, July 2009.

[53] Haakan N Joensson, Mathias Uhlén, and Helene Andersson Svahn. Droplet size based separation by deterministic lateral displacement-separating droplets by cell–induced shrinking. *Lab on a chip*, 11(7):1305–10, April 2011.

[54] Timothy Bowman, Joelle Frechette, and German Drazer. Force driven separation of drops by deterministic lateral displacement. *Lab on a chip*, 12(16):2903–8, August 2012.

[55] Yung-Chieh Tan, Jeffrey S Fisher, Alan I Lee, Vittorio Cristini, and Abraham Phillip Lee. Design of microfluidic channel geometries for the control of droplet volume, chemical concentration, and sorting. *Lab on a chip*, 4(4):292–8, August 2004.

[56] Michelle R Bringer, Cory J Gerdts, Helen Song, Joshua D Tice, and Rustem F Ismagilov. Microfluidic systems for chemical kinetics that rely on chaotic mixing in droplets. *Philosophical transactions. Series A, Mathematical, physical, and engineering sciences*, 362(1818):1087–104, May 2004.

[57] Luis M Fidalgo, Graeme Whyte, Daniel Bratton, Clemens F Kaminski, Chris Abell, and Wilhelm T S Huck. From microdroplets to microfluidics: selective

emulsion separation in microfluidic devices. *Angewandte Chemie (International ed. in English)*, 47(11):2042–5, January 2008.

[58] SKY Tang, Ratmir Derda, Qimin Quan, Marko Loncar, and GM Whitesides. Microdroplet optical cavity sensors. In *15th International Conference on Miniaturized Systems for Chemistry and Life Sciences*, pages 702–703, Seattle, 2011.

[59] Xize Niu, Mengying Zhang, Suili Peng, Weijia Wen, and Ping Sheng. Real-time detection, control, and sorting of microfluidic droplets. *Biomicrofluidics*, 1(4):44101, January 2007.

[60] Luis M Fidalgo, Graeme Whyte, Brandon T Ruotolo, Justin L P Benesch, Florian Stengel, Chris Abell, Carol V Robinson, and Wilhelm T S Huck. Coupling microdroplet microreactors with mass spectrometry: reading the contents of single droplets online. *Angewandte Chemie (International ed. in English)*, 48(20):3665–8, January 2009.

[61] Shaojiang Zeng, Xiaoyan Pan, Qingquan Zhang, Bingcheng Lin, and Jianhua Qin. Electrical control of individual droplet breaking and droplet contents extraction. *Analytical chemistry*, 83(6):2083–9, March 2011.

[62] Yunhan Chen, Adi Wijaya Gani, and Sindy K Y Tang. Characterization of sensitivity and specificity in leaky droplet-based assays. *Lab on a chip*, 12(23):5093–103, October 2012.

[63] Abraham Aserin, editor. *Multiple Emulsions*. John Wiley & Sons, Inc., Hoboken, NJ, USA, October 2007.

[64] Eric Brouzes, Martina Medkova, Neal Savenelli, Dave Marran, Mariusz Twardowski, J Brian Hutchison, Jonathan M Rothberg, Darren R Link, Norbert Perrimon, and Michael L Samuels. Droplet microfluidic technology for single-cell high-throughput screening. *Proceedings of the National Academy of Sciences of the United States of America*, 106(34):14195–200, August 2009.

[65] Nicolas Bremond and Jérôme Bibette. Exploring emulsion science with microfluidics. *Soft Matter*, 2012.

[66] Wilhelm Ostwald. Über die vermeintliche Isomerie des roten und gelben Quecksilberoxyds und die Oberflächenspannung fester Körper. *Zeitschrift für Physikalische Chemie*, 34:495–503, 1901.

[67] P W Voorhees. The Theory of Ostwald Ripening. *Journal of Statistical Physics*, 38:231–252, 1985.

[68] Lorin J. Mullins. Osmotic Regulation in Fish as Studied with Radiosotopes. *Acta Physiologica Scandinavica*, 21(4):303–314, December 1950.

[69] D. Powers. Fish as model systems. *Science*, 246(4928):352–358, October 1989.

[70] K. G. Denbigh and G. Raumann. The Thermo-Osmosis of Gases through a Membrane. II. Experimental. *Proceedings of the Royal Society A: Mathematical, Physical and Engineering Sciences*, 210(1103):518–533, January 1952.

[71] F P Chinard and T Enns. Osmotic pressure. *Science (New York, N.Y.)*, 124(3220):472–4, September 1956.

[72] Henri L Rosano, François G. Gandolfo, and Jean-denis P Hidrot. Stability of W1/O/W2 multiple emulsions. *Colloids and Surfaces A: Physicochemical and Engineering Aspects*, 138(1):109–121, June 1998.

[73] Winson C L Lay, Tzyy Haur Chong, Chuyang Y Tang, Anthony G Fane, Jinsong Zhang, and Yu Liu. Fouling propensity of forward osmosis: investigation of the slower flux decline phenomenon. *Water science and technology : a journal of the International Association on Water Pollution Research*, 61(4):927–36, January 2010.

[74] Jing Cheng, Jian-Feng Chen, and Li-Xiong Wen. Visual Study for Producing Zirconia Precursors with Two Reverse-Emulsion Precipitation Method. *Industrial & Engineering Chemistry Research*, 46(19):6259–6263, September 2007.

[75] J. H. van't Hoff. The role of osmotic pressure in the analogy between solution and gases. *Zeitschrift fur Physikalische Chemie*, 1:481–508, 1887.

[76] Wilhelm Pfeffer. *Osmotische Untersuchungen*. Wilh. Engelmann, Leipzig, 1877.

[77] A. MAURO. Nature of Solvent Transfer in Osmosis. *Science*, 126(3267):252–3, August 1957.

[78] A. Raghunathan and N. Aluru. Molecular Understanding of Osmosis in Semipermeable Membranes. *Physical Review Letters*, 97(2):1–4, July 2006.

[79] S. A. Ben-Sasson and N. B. Grover. Osmosis: a macroscopic phenomenon, a microscopic view. *AJP: Advances in Physiology Education*, 27(1):15–19, March 2003.

[80] Frank G. Borg. What is osmosis? Explanation and understanding of a physical phenomenon. *arXiv:physics/0305011 [physics.gen-ph]*, May 2003.

[81] D.C. Guell. *The Physical Mechanism of Osmosis and Osmotic Pressure: A Hydrodynamic Theory for Calculating The Osmotic Reflection Coefficient .* PhD thesis, Massachusetts Institute of Technology, 1991.

[82] H T Hammel. Evolving ideas about osmosis and capillary fluid exchange. *FASEB journal : official publication of the Federation of American Societies for Experimental Biology*, 13(2):213–31, February 1999.

[83] Fredrik Kiil. Mechanism of osmosis. *Kidney International*, 21(2):303–308, February 1982.

[84] Fredrik Kiil. Molecular mechanisms of osmosis. *The American journal of physiology*, 256(4 Pt 2):R801–8, April 1989.

[85] J. W. Gibbs. On the Equilibrium of Heterogeneous Substances. *Trans. Conn. Acad. Arts Sci. 3*, 108:343, 1878.

[86] G. Czihak, H. Langer, and H. Ziegler. *Biologie - ein Lehrbuch*, volume 24. Springer-Verlag Berlin, 2 edition, 1978.

[87] Walter J. Hamer and Yung-Chi Wu. Osmotic Coefficients and Mean Activity Coefficients of Uni-univalent Electrolytes in Water at 25 C. *Journal of Physical and Chemical Reference Data*, 1(4):1047, 1972.

[88] Kenneth S. Pitzer, J. Christopher Peiper, and R. H. Busey. Thermodynamic Properties of Aqueous Sodium Chloride Solutions. *Journal of Physical and Chemical Reference Data*, 13(1):1, 1984.

[89] O Kedem and A Katchalsky. Thermodynamic analysis of the permeability of biological membranes to non-electrolytes. *Biochimica et biophysica acta*, 27(2):229–46, February 1958.

[90] J. Dickson. Reverse Osmosis Technology. In B. Parekh, editor, *Reverse Osmosis Technology*, chapter Fundamenta, pages 1–51. Marcel Dekker, Inc., New York, 1988.

[91] G Suchanek. Mechanistic equations for membrane transport of multicomponent solutions. *General physiology and biophysics*, 25(1):53–63, March 2006.

[92] J.G. Wijmans and R.W. Baker. The solution-diffusion model: a review. *Journal of Membrane Science*, 107(1-2):1–21, November 1995.

[93] Amrit Kalra, Shekhar Garde, and Gerhard Hummer. Osmotic water transport through carbon nanotube membranes. *Proceedings of the National Academy of Sciences of the United States of America*, 100(18):10175–80, September 2003.

[94] Lixiong Wen and Kyriakos D. Papadopoulos. Effects of Surfactants on Water Transport in W1/O/W2 Emulsions. *Langmuir*, 16(20):7612–7617, October 2000.

[95] Lixiong Wen and Kyriakos D Papadopoulos. Visualization of water transport in W1/O/W2 emulsions. *Colloids and Surfaces A: Physicochemical and Engineering Aspects*, 174(1-2):159–167, November 2000.

[96] Lixiong Wen and Kyriakos D. Papadopoulos. Effects of Osmotic Pressure on Water Transport in W1/O/W2 Emulsions. *Journal of colloid and interface science*, 235(2):398–404, March 2001.

[97] Jing Cheng, Jian-Feng Chen, Min Zhao, Qing Luo, Li-Xiong Wen, and Kyriakos D Papadopoulos. Transport of ions through the oil phase of W1-O-W2 double emulsions. *Journal of colloid and interface science*, 305(1):175–82, January 2007.

[98] Ansgar Huebner, Dan Bratton, Graeme Whyte, Min Yang, Andrew J Demello, Chris Abell, and Florian Hollfelder. Static microdroplet arrays: a microfluidic device for droplet trapping, incubation and release for enzymatic and cell-based assays. *Lab on a chip*, 9(5):692–8, March 2009.

[99] Jung-Uk Shim, Galder Cristobal, Darren R Link, Todd Thorsen, Yanwei Jia, Katie Piattelli, and Seth Fraden. Control and measurement of the phase behavior of aqueous solutions using microfluidics. *Journal of the American Chemical Society*, 129(28):8825–35, July 2007.

[100] Sachio Matsumoto, Takeshi Inoue, Masanori Kohda, and Keiko Ikura. Water permeability of oil layers in W/O/W emulsions under osmotic pressure gradients. *Journal of Colloid and Interface Science*, 77(2):555–563, October 1980.

[101] N. Garti, A. Romano-Pariente, and A. Aserin. The effect of additives on release from w/o/w emulsions. *Colloids and Surfaces*, 24(1):83–94, May 1987.

[102] Takumi Kinugasa, Kunio Watanabe, and Hiroshi Takeuchi. Stability of (W/O) Emulsion Drops and Water Permeation through a Liquid Membrane. *Journal of Chemical Engineering of Japan*, 25(2):128–133, 1992.

[103] Sachio Matsumoto and Masanori Kohda. The viscosity of W/O/W emulsions: An attempt to estimate the water permeation coefficient of the oil layer from the viscosity changes in diluted systems on aging under osmotic pressure gradients. *Journal of Colloid and Interface Science*, 73(1):13–20, January 1980.

[104] P Colinart, S Delepine, G Trouve, and H Renon. Water transfer in emulsified liquid membrane processes. *Journal of Membrane Science*, 20(2):167–187, August 1984.

[105] Jun Yan and Rajinder Pal. Osmotic swelling behavior of globules of W/O/W emulsion liquid membranes. *Journal of Membrane Science*, 190(1):79–91, August 2001.

[106] Yoshiko Kita, Sachio Matsumoto, and Daizo Yonezawa. Viscometric method for estimating the stability of W/O/W-type multiple-phase emulsions. *Journal of Colloid and Interface Science*, 62(1):87–94, October 1977.

[107] Alexey Kabalnov and Jeffry Weers. Kinetics of Mass Transfer in Micellar Systems: Surfactant Adsorption, Solubilization Kinetics, and Ripening. *Langmuir*, 12(14):3442–3448, January 1996.

[108] Jochen Weiss and D. Julian McClements. Mass Transport Phenomena in Oil-in-Water Emulsions Containing Surfactant Micelles: Solubilization. *Langmuir*, 16(14):5879–5883, July 2000.

[109] Alexey S. Kabalnov. Can Micelles Mediate a Mass Transfer between Oil Droplets? *Langmuir*, 10(3):680–684, March 1994.

[110] Alejandro a. Peña and Clarence a. Miller. Kinetics of Compositional Ripening in Emulsions Stabilized with Nonionic Surfactants. *Journal of Colloid and Interface Science*, 244(1):154–163, December 2001.

[111] P. Taylor. Ostwald ripening in emulsions. *Advances in Colloid and Interface Science*, 75(2):107–163, April 1998.

[112] Maria Minakova, Alexey Savelyev, and Garegin a Papoian. Nonequilibrium water transport in a nonionic microemulsion system. *The journal of physical chemistry. B*, 115(20):6503–8, May 2011.

[113] S. Magdassi, M. Frenkel, and N. Garti. Correlation Between Nature of Emulsifier and Multiple Emulsion Stability. *Drug Development and Industrial Pharmacy*, 11(4):791–798, January 1985.

[114] Nissim Garti. Double emulsions - scope, limitations and new achievements. *Colloids and Surfaces A: Physicochemical and Engineering Aspects*, 123-124:233–246, May 1997.

[115] Brendan Joseph Carroll. The kinetics of solubilization of nonpolar oils by nonionic surfactant solutions. *Journal of Colloid and Interface Science*, 79(1):126–135, January 1981.

[116] Bing-Hung Chen, Clarence A. Miller, and Peter R. Garrett. Rates of solubilization of triolein into nonionic surfactant solutions. *Colloids and Surfaces A: Physicochemical and Engineering Aspects*, 128(1-3):129–143, August 1997.

[117] Y. Sela, S. Magdassi, and N. Garti. Release of markers from the inner water phase of W / O / W emulsions stabilized by silicone based polymeric surfactants. *Journal of Controlled Release*, 33(1):1–12, January 1995.

[118] Sanhita S Dixit, Alexandra Pincus, Bin Guo, and Gregory W Faris. Droplet shape analysis and permeability studies in droplet lipid bilayers. *Langmuir : the ACS journal of surfaces and colloids*, 28(19):7442–51, May 2012.

[119] M B Lande, J M Donovan, and M L Zeidel. The relationship between membrane fluidity and permeabilities to water, solutes, ammonia, and protons. *The Journal of general physiology*, 106(1):67–84, July 1995.

[120] Keiichi Kato, Peter Walde, Norio Koine, Sosaku Ichikawa, Takashi Ishikawa, Ryo Nagahama, Takehiko Ishihara, Tetsuya Tsujii, Masachika Shudou, Yousuke Omokawa, and Takashi Kuroiwa. Temperature-sensitive nonionic vesicles prepared from Span 80 (sorbitan monooleate). *Langmuir : the ACS journal of surfaces and colloids*, 24(19):10762–70, October 2008.

[121] BJ Bruno J Zwolinski, Henry Eyring, and Cecil E Reese. Diffusion and Membrane Permeability. *The Journal of Physical and Colloid Chemistry*, 53(9):1426–1453, September 1949.

[122] A. Finkelstein. *Water movement through lipid bilayers, pores and plasma membranes: Theory and reality.*, volume 6. John Wiley and Sons Ltd, New York, July 1987.

[123] John F Nagle, John C Mathai, Mark L Zeidel, and Stephanie Tristram-Nagle. Theory of passive permeability through lipid bilayers. *The Journal of general physiology*, 131(1):77–85, January 2008.

[124] D. Clausse, A. Drelich, and B. Fouconnier. Thermal behaviour of emulsions studied by differential scanning calorimetry. In Hironori Nakajima, editor, *Mass Transfer - Advanced Aspects*, volume 51, chapter 33, pages 743–778. Intech, January 2011.

[125] Danièle Clausse, Isabelle Pezron, and Amélie Behaeghel. Water Transfer Between Water And Water+NaCl Droplets In Emulsions. *Journal of Dispersion Science and Technology*, 20(1-2):315–326, January 1999.

[126] Bo Zheng, Joshua D Tice, and Rustem F Ismagilov. Formation of Arrayed Droplets by Soft Lithography and Two-Phase Fluid Flow, and Application in Protein Crystallization. *Advanced materials (Deerfield Beach, Fla.)*, 16(15):1365–1368, August 2004.

[127] Zuzanna Michalak, Darius Fartash, Nousin Haque, and Sunghee Lee. Tunable crystallization via osmosis-driven transport across a droplet interface bilayer. *CrystEngComm*, 14(23):7865, 2012.

[128] B. P. Binks, J. H. Clint, P. D. I. Fletcher, S. Rippon, S. D. Lubetkin, and P. J. Mulqueen. Kinetics of Swelling of Oil-in-Water Emulsions. *Langmuir*, 14(19):5402–5411, September 1998.

[129] Marina Yu Koroleva and Evgeny V Yurtov. Water mass transfer in W/O emulsions. *Journal of colloid and interface science*, 297(2):778–84, May 2006.

[130] Alexey S. Kabalnov and Eugene D. Shchukin. Ostwald ripening theory: applications to fluorocarbon emulsion stability. *Advances in Colloid and Interface Science*, 38:69–97, March 1992.

[131] W. Thomson. Hydrokinetic Solutions and Observations. *(Lord Kelvin), Proceedings of the Royal Society*, 7:63, 1871.

[132] L.M Skinner and J.R Sambles. The Kelvin equation - a review. *Journal of Aerosol Science*, 3(3):199–210, January 1972.

[133] Hans-Jürgen Butt, Karlheinz Graf, and Michael Kappl. *Physics and Chemistry of Interfaces*. Wiley-VCH Verlag GmbH & Co. KGaA, Weinheim, FRG, September 2003.

[134] M. Porras, C. Solans, C. González, and J.M. Gutiérrez. Properties of water-in-oil (W/O) nano-emulsions prepared by a low-energy emulsification method. *Colloids and Surfaces A: Physicochemical and Engineering Aspects*, 324(1-3):181–188, July 2008.

[135] Suwimon Ariyaprakai and Stephanie R Dungan. Influence of surfactant structure on the contribution of micelles to Ostwald ripening in oil-in-water emulsions. *Journal of colloid and interface science*, 343(1):102–8, March 2010.

[136] I.M. Lifshitz and V.V. Slyozov. The kinetics of precipitation from supersaturated solid solutions. *Journal of Physics and Chemistry of Solids*, 19(1-2):35–50, April 1961.

[137] Carl Wagner. Theorie der Alterung von Niederschlägen durch Umlösen (Ostwald-Reifung). *Zeitschrift für Elektrochemie, Berichte der Bunsengesellschaft für physikalische Chemie*, 65(7-8):581–591, 1961.

[138] Eva M. Wong, John E. Bonevich, and Peter C. Searson. Growth Kinetics of Nanocrystalline ZnO Particles from Colloidal Suspensions. *The Journal of Physical Chemistry B*, 102(40):7770–7775, October 1998.

[139] Ibon Aranberri, Kate J. Beverley, Bernard P. Binks, John H. Clint, and Paul D. I. Fletcher. How Do Emulsions Evaporate? *Langmuir*, 18(9):3471–3475, April 2002.

[140] Mingyan He, Chenhang Sun, and Daniel T Chiu. Concentrating solutes and nanoparticles within individual aqueous microdroplets. *Analytical chemistry*, 76(5):1222–7, March 2004.

[141] Xavier Casadevall I Solvas, Vladimir Turek, Themistoklis Prodromakis, and Joshua B Edel. Microfluidic evaporator for on-chip sample concentration. *Lab on a chip*, 12(20):4049–54, September 2012.

[142] Bo Zheng, L Spencer Roach, and Rustem F Ismagilov. Screening of protein crystallization conditions on a microfluidic chip using nanoliter-size droplets. *Journal of the American Chemical Society*, 125(37):11170–1, September 2003.

[143] Ramsey I Zeitoun, Marcus J Goudie, Jacob Zwier, David Mahawilli, and Mark a Burns. Active control of nanolitre droplet contents with convective concentration gradients across permeable walls. *Lab on a chip*, 11(23):4022–8, December 2011.

[144] Jung-uk Shim, Santoshkumar N Patil, James T Hodgkinson, Steven D Bowden, David R Spring, Martin Welch, Wilhelm T S Huck, Florian Hollfelder, and Chris Abell. Controlling the contents of microdroplets by exploiting the permeability of PDMS. *Lab on a chip*, 11(6):1132–7, March 2011.

[145] N Chidambaram and D J Burgess. Effect of nonionic surfactant on transport of surface-active and non-surface-active model drugs and emulsion stability in triphasic systems. *AAPS pharmSci*, 2(3):E30, January 2000.

[146] David J. McClements and Stephanie R. Dungan. Factors that affect the rate of oil exchange between oil-in-water emulsion droplets stabilized by a nonionic surfactant: droplet size, surfactant concentration, and ionic strength. *The Journal of Physical Chemistry*, 97(28):7304–7308, July 1993.

[147] S Paula, a G Volkov, and D W Deamer. Permeation of halide anions through phospholipid bilayers occurs by the solubility-diffusion mechanism. *Biophysical journal*, 74(1):319–27, January 1998.

[148] H Mathies. [Differential indications in rheumatism therapy on the basis of well-known drug side effects]. *Acta medica Austriaca*, 2(4):156–60, January 1975.

[149] Marie Bonnet, Maud Cansell, Frédéric Placin, Marc Anton, and Fernando Leal-Calderon. Impact of sodium caseinate concentration and location on magnesium release from multiple W/O/W emulsions. *Langmuir : the ACS journal of surfaces and colloids*, 26(12):9250–60, June 2010.

[150] Brahma Prakash Gupta, Navneet Thakur, Nishi P Jain, Jitendra Banweer, and Surendra Jain. Osmotically controlled drug delivery system with associated drugs. *Journal of pharmacy & pharmaceutical sciences : a publication of the Canadian Society for Pharmaceutical Sciences, Société canadienne des sciences pharmaceutiques*, 13(4):571–88, January 2010.

[151] R. P. Cahn and N. N. Li. Separation of Phenol from Waste Water by the Liquid Membrane Technique. *Separation Science*, 9(6):505–519, December 1974.

[152] N Othman, H Mat, and M Goto. Separation of silver from photographic wastes by emulsion liquid membrane system. *Journal of Membrane Science*, 282(1-2):171–177, October 2006.

[153] D C Duffy, J C McDonald, O J Schueller, and G M Whitesides. Rapid Prototyping of Microfluidic Systems in Poly(dimethylsiloxane). *Analytical chemistry*, 70(23):4974–84, December 1998.

[154] Dong Qin, Younan Xia, and George M. Whitesides. Rapid prototyping of complex structures with feature sizes larger than 20 micron. *Advanced Materials*, 8(11):917–919, November 1996.

[155] J C McDonald, D C Duffy, J R Anderson, D T Chiu, H Wu, O J Schueller, and G M Whitesides. Fabrication of microfluidic systems in poly(dimethylsiloxane). *Electrophoresis*, 21(1):27–40, January 2000.

[156] J. Cooper McDonald and George M. Whitesides. Poly(dimethylsiloxane) as a Material for Fabricating Microfluidic Devices. *Accounts of Chemical Research*, 35(7):491–499, July 2002.

[157] Adam R Abate, Chia-Hung Chen, Jeremy J Agresti, and David A Weitz. Beating Poisson encapsulation statistics using close-packed ordering. *Lab on a chip*, 9(18):2628–31, September 2009.

[158] Sarah Köster, Francesco E Angilè, Honey Duan, Jeremy J Agresti, Anton Wintner, Christian Schmitz, Amy C Rowat, Christoph A Merten, Dario Pisignano, Andrew D Griffiths, and David A Weitz. Drop-based microfluidic devices for encapsulation of single cells. *Lab on a chip*, 8(7):1110–5, July 2008.

[159] M R Wilkins, E Gasteiger, A Bairoch, J C Sanchez, K L Williams, R D Appel, and D F Hochstrasser. Protein identification and analysis tools in the ExPASy server. *Methods in molecular biology (Clifton, N.J.)*, 112:531–52, January 1999.

[160] Tao Peng. Detect circles with various radii in grayscale image via Hough Transform, 2005.

[161] PVC Paul Hough. Method and Means for Recognizing Complex Patterns, December 1962.

[162] Azriel Rosenfeld. Picture Processing by Computer. *ACM Computing Surveys*, 1(3):147–176, September 1969.

[163] Richard O. Duda and Peter E Hart. Use of the Hough transformation to detect lines and curves in pictures. *Communications of the ACM*, 15(1):11–15, January 1972.

[164] F. O'Gorman and M. B. Clowes. Finding Picture Edges Through Collinearity of Feature Points. *IEEE Transactions on Computers*, C-25(4):449–456, April 1976.

[165] Carolyn Kimme, Dana Ballard, and Jack Sklansky. Finding circles by an array of accumulators. *Communications of the ACM*, 18(2):120–122, February 1975.

[166] D.H. Ballard. Generalizing the Hough transform to detect arbitrary shapes. *Pattern Recognition*, 13(2):111–122, January 1981.

[167] Leandro A.F. Fernandes and Manuel M. Oliveira. Real-time line detection through an improved Hough transform voting scheme. *Pattern Recognition*, 41(1):299–314, January 2008.

[168] George Vosselman, Er Dijkman, Key Words Building Reconstruction, Laser Altimetry, and Hough Transform. 3D building model reconstruction from point clouds and ground plans. *Int. Arch. of Photogrammetry and Remote Sensing*, pages 37–43, 2001.

[169] Caroline A Schneider, Wayne S Rasband, and Kevin W Eliceiri. NIH Image to ImageJ: 25 years of image analysis. *Nature Methods*, 9(7):671–675, June 2012.

[170] Yung-Chieh Tan, Yao Li Ho, and Abraham Phillip Lee. Microfluidic sorting of droplets by size. *Microfluidics and Nanofluidics*, 4(4):343–348, June 2007.

[171] Carl L Hansen, Scott Classen, James M Berger, and Stephen R Quake. A microfluidic device for kinetic optimization of protein crystallization and in situ structure determination. *Journal of the American Chemical Society*, 128(10):3142–3, March 2006.

[172] E Verneuil, A Buguin, and P Silberzan. Permeation-induced flows: Consequences for silicone-based microfluidics. *Europhysics Letters (EPL)*, 68(3):412–418, November 2004.

[173] Michael P. Aronson. The role of free surfactant in destabilizing oil-in-water emulsions. *Langmuir*, 5(2):494–501, March 1989.

[174] David Julian McClements. Ultrasonic determination of depletion flocculation in oil-in-water emulsions containing a non-ionic surfactant. *Colloids and Surfaces A: Physicochemical and Engineering Aspects*, 90(1):25–35, September 1994.

[175] W M Yunus and A B Rahman. Refractive index of solutions at high concentrations. *Applied optics*, 27(16):3341–3, August 1988.

[176] R. A. Robinson and R. H. Stokes. Tables of osmotic and activity coefficients of electrolytes in aqueous solution at 25 C. *Transactions of the Faraday Society*, 45:612, 1949.

[177] Jung-uk Shim, Luis F Olguin, Graeme Whyte, Duncan Scott, Ann Babtie, Chris Abell, Wilhelm T S Huck, and Florian Hollfelder. Simultaneous determination of gene expression and enzymatic activity in individual bacterial cells in microdroplet compartments. *Journal of the American Chemical Society*, 131(42):15251–6, October 2009.

[178] T Bauchop and S R Elsden. The growth of micro-organisms in relation to their energy supply. *Journal of general microbiology*, 23:457–69, December 1960.

[179] Lu Kwang Ju, Jaw F. Lee, and William B. Armiger. Enhancing oxygen transfer in bioreactors by perfluorocarbon emulsions. *Biotechnology Progress*, 7(4):323–329, July 1991.

[180] L Boitard, D Cottinet, C Kleinschmitt, N Bremond, J Baudry, G Yvert, and J Bibette. Monitoring single-cell bioenergetics via the coarsening of emulsion droplets. *Proceedings of the National Academy of Sciences of the United States of America*, 109(19):7181–6, May 2012.

[181] Raymond Pearl. The Growth of Populations. *The Quarterly Review of Biology*, 2(4):532–548, 1927.

[182] A Tsoularis and J Wallace. Analysis of logistic growth models. *Mathematical biosciences*, 179(1):21–55, 2002.

[183] Manu Prakash and Neil Gershenfeld. Microfluidic bubble logic. *Science (New York, N.Y.)*, 315(5813):832–5, February 2007.

Acknowledgements

An erster Stelle gilt mein Dank meinem Doktorvater, Professor Joachim Spatz, für die Möglichkeit, in diesem interdisziplinären und spannenden Bereich der Wissenschaft forschen zu dürfen. Einen besonderen Dank auch für die Möglichkeit, meine Forschungsergebnisse auf verschiedenen nationalen und internationalen Konferenzen zu präsentieren und diskutieren.

Professor Rainer Fink danke ich herzlich für die Übernahme des Zweitgutachtens. Ihm und meinen anderen Prüfern, Professor Jörg Hüfner und Privatdozent Dr. Klaus Reygers, danke ich ausserdem für die Bereitschaft, sich in die teilweise sehr fachfremde Materie einzuarbeiten.

Ein sehr großer Dank gebührt Christian Böhm, und zwar schlicht für zwei Jahre hervorragende Betreuung und Zusammenarbeit. Ich wünsche Dir viel Erfolg abseits der akademischen Pfade!

Heike Böhm danke ich herzlich für die Aufnahme in ihre Arbeitsgruppe, in der ich mich sehr gut aufgehoben gefühlt habe, und für zahlreiche hilfreiche Anmerkungen und Diskussionen.

Ein besonderer Dank gilt Siegfried Hänselmann, meinem ehemaligen Hiwi, der sich zu jeder Tageszeit für die (bzw meine) Wissenschaft opferte und viel zum Erfolg der Experimente beigetragen hat.

Ebenso ein großer Dank an Jan-Willi Janiesch für das Durchführen verschiedenster Experimente, die Synthese der Surfactants und die generelle Hilfe bei chemischen Fragen.

Bei den Mitgliedern der neuen und meiner alten Böhm-Gruppe bedanke ich mich für fruchtvolle Diskussionen und viele Ideen und Anregungen.

Konrad Schade, Sebastian Rausch, Siegfried Hänselmann, Jan-Willi Janiesch, Heike Böhm, und Christian Böhm danke ich vielmals für das teilweise kurzfristige, aber trotzdem gründliche Korrekturlesen dieser Arbeit.

Frau Ulshöfer und Frau Schleehauf möchte ich für die sehr freundliche Unterstützung in Sachen Bürokratie danken.

Der gesamten Spatz Gruppe, insbesondere den Heidelberger Spatzen, danke ich für das freundschaftliche Miteinander und das angenehme Arbeitsklima am Institut!

Sigi, Jan, Seba, Martin, Sabri, und Janosch danke ich darüber hinaus für die vielen

sportlichen und spaßigen Unternehmungen über den Institutsalltag hinaus. Shanti, Marco, Tobinal, Konni, Marc, und Fabi danke ich für die gute gemeinsame Zeit seit vielen Jahren und hoffe, dass wir uns nicht aus den Augen verlieren. Ein großer Dank geht an meine Eltern und meine Schwester, für den Rückhalt während meiner gesamten Studienzeit.

Zu guter Letzt ein großes Dankeschön an meine Freundin Eva für die permanente Unterstützung, die Geduld mit mir gegen Ende der Promotion, und die vielen schönen gemeinsamen Momente.

A Appendix

A.1 Experiments with enzymatic systems and E. coli

Figure A.1 shows typical size changes of droplets in experiments with the enzymatic system proteinase K/BSA (Figure A.1 A), and encapsulated *E. coli* bacteria (Figure A.1 B).

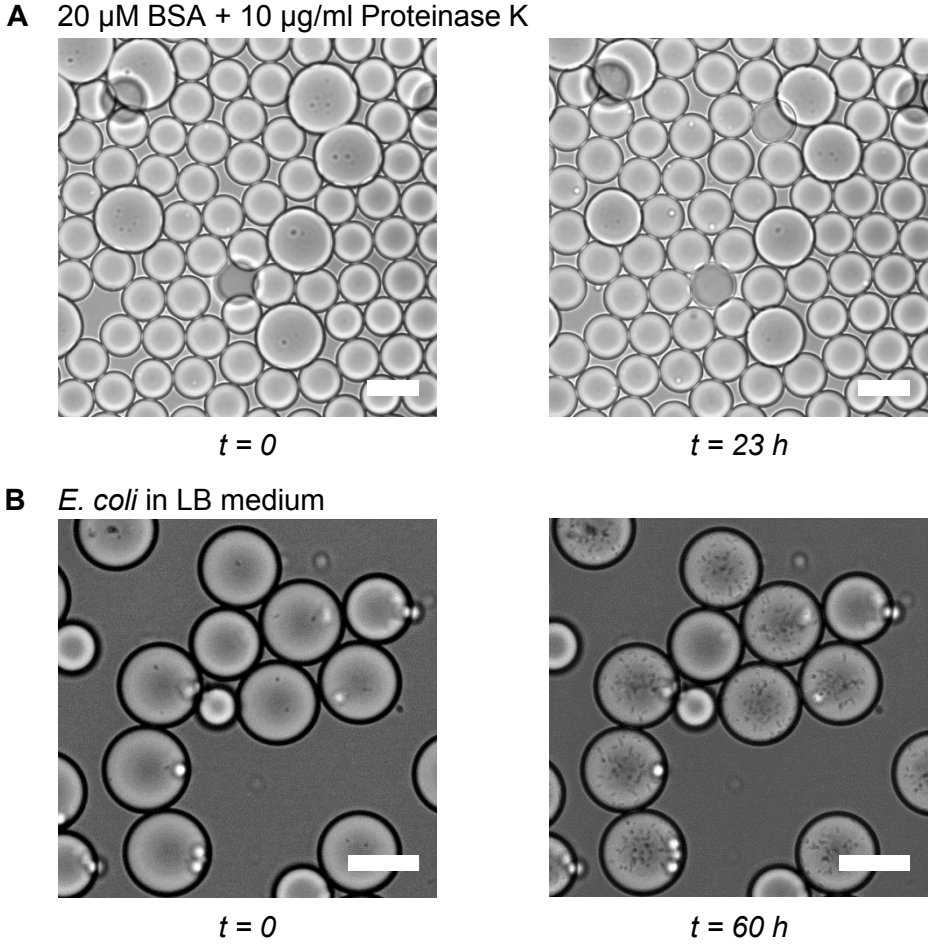

Figure A.1: *(A) A small size change of droplets containing BSA (large droplets) and droplets containing BSA and Proteinase K (small droplets) can be observed, which is considerably smaller than expected (see section 3.5.3) Droplets with only BSA deform heavily. (B) No size change of droplets is visible when incubating E. coli, despite of almost 3 days of incubation and rapid proliferation of the bacteria. Scales are 30* µm.

A.2 Proof of Monotonicity

Defining $k = N_a/N_b$, $c = c_b/c_a$, and $v = V_{b,0}$, the equations 5.5 and 5.6 can be written as

$$V_{a,e}(V_{a,0}) = \frac{kV_{a,0} + v}{k + \frac{v}{V_{a,0}}c} \text{ , and} \tag{A.1}$$

$$V_{b,e}(V_{a,0}) = \frac{V_{a,0} + \frac{v}{k}}{\frac{V_{a,0}}{vc} + \frac{1}{k}} \tag{A.2}$$

As all variables are non-negative, and, for all experiments conducted, $c_b < c_a$ and thus $c < 1$, the monotonicities of the functions $V_{a,e}(V_{a,0})$ and $V_{b,e}(V_{a,0})$ follow directly from the quotient rule. Both proofs are trivial, which is why the proof that $V_{a,e}$ is strictly increasing with $V_{a,0}$, i.e. $\frac{dV_{a,e}}{dV_{a,0}} > 0$, will be omitted.
Proof that $V_{b,e}$ is strictly decreasing with $V_{a,0}$, i.e. $\frac{dV_{a,e}}{dV_{a,0}} < 0$:

$$\frac{dV_{b,e}}{dV_{a,0}} = \frac{(\frac{V_{a,0}}{cv} + \frac{1}{k}) - \frac{1}{cv}(V_{a,0} + \frac{v}{k})}{(\frac{V_{a,0}}{vc} + \frac{1}{k})^2} \tag{A.3}$$

$$= \frac{1}{k} - \frac{1}{ck} < 0 \text{ for } c < 1. \tag{A.4}$$

A.3 List of publications

Journal articles

- **Tobias W. Hofmann**, Siegfried Hänselmann, Jan-Willi Janiesch, Anne Rademacher, and Christian H J Böhm. Applying microdroplets as sensors for label-free detection of chemical reactions. *Lab on a chip*, 12(5):916-22, 2012.

Conference proceedings

- **Tobias W. Hofmann**, Siegfried Hänselmann, Jan-Willi Janiesch, Christian H.J. Böhm. Impact of osmosis on micro-droplets - a new route to novel sensors. *Proceedings of the 15th International Conference on Miniaturized Systems for Chemistry and Life Sciences (μTAS 2011)*, Seattle, Washington, USA, pp. 260-262, 2011.

- **Tobias W. Hofmann**, Sebastian Rausch, Siegfried Hänselmann, Jan-Willi Janiesch, Chi Nguyen, Christian H.J. Böhm and Heike Böhm. Applying microdroplets as sensors. *Proceedings of the 16th International Conference on Miniaturized Systems for Chemistry and Life Sciences (μTAS 2012)*, Okinawa, Japan, 2012 (in process of publication).

Erklärung:

Ich versichere, dass ich die vorgelegte Dissertation selbst verfasst und mich keiner anderen als der von mir ausdrücklich bezeichneten Quellen und Hilfen bedient habe.

Heidelberg, den 10.12.2012

Tobias Hofmann